THE DEVELOPMENT AND UTILIZATION OF SOME EQUIPMENT FOR LOW REYNOLDS NUMBER SUPERSONIC FLOW RESEARCH

Thesis by

Raymond L. Chuan

In Partial Fulfillment of the Requirements

For the Degree of

Doctor of Philosophy

California Institute of Technology

Pasadena, California

1953

ACKNOWLEDGMENTS

The writer wishes to thank his adviser, Professor H. W. Liepmann, for initiating the research program which led eventually to the present work, and for his continued interest, helpful advice and enlightening criticism in the course of the execution of the investigation.

The construction and successful operation of the equipment could not have been possible without the assistance of Mr. R. J. Magnus, who designed and built many of the components of the tunnel and associated instruments.

The friendly and patient assistance of other members of the GALCIT staff, and particularly of Mrs. E. Fox, Mrs. B. Cottingham, and Mrs. B. Wood in the preparation of the thesis, is gratefully acknowledged.

ABSTRACT

A low Reynolds number supersonic wind tunnel is a useful tool for the investigation of viscous effects in a high-speed flow. In order to avoid some of the difficulties inherent in a conventional wind tunnel system when operating at low Reynolds numbers, a two-phase cycle is proposed. By examining the thermodynamics of the wind tunnel the relative merits of two methods of operation -- the one-phase cycle and the two-phase cycle -- are compared, indicating certain advantages the two-phase cycle possesses over the conventional one-phase cycle when the tunnel is operated at high-speed and low Reynolds number. The design, construction and operation of a small (about 5 $cm.^2$ test section area) supersonic ($M \cong 2$) wind tunnel using a two-phase cycle with water (in liquid and vapor phases) as the working medium are described.

Difficulties in pressure measurement and flow visualization, due to the nature of the working medium and the low density of the flow, are encountered. Means of meeting these difficulties are proposed, including a critical analysis of the schlieren technique, from which is evolved a workable arrangement for visualizing the low Reynolds number flow.

As an example of the possible utilizations of the tunnel, the curvature, due to viscosity, of the attached shock wave on a wedge in uniform supersonic flow is investigated, using schlieren photography. The effective shape of the wedge is deduced from the shape of the shock wave, and is compared to theory with satisfactory qualitative agreement.

TABLE OF CONTENTS

NOMENCLATURE

			Units
a	sonic velocity		cm./sec.
a^*	critical sonic velocity		cm./sec.
B	boundary layer coefficient, defined in Section 10		
C	radius of curvature		cm.
c_p	specific heat of a gas at constant pressure		cal./gm. ^oC
c_v	specific heat of a gas at constant volume		cal./gm. ^oC
L	latent heat of transition		cal./gm.
M	Mach number		
Mf	mass flow per unit test section area		gm./sec. $cm.^2$
m	molecular weight		
P	power		watts
Pr	Prandtl number, $\mu c_p / K$		
p	pressure	or	dynes/$cm.^2$ cm. Hg mm. Hg atmospheres
p_{cr}	critical pressure		atmospheres
p_{tr}	triple-point pressure		mm. Hg
p_s	saturation pressure		mm. Hg
q	heat		calories
R	gas constant		ergs/^oC gm.
R_o	universal gas constant		ergs/^oC mole
Re	Reynolds number		
Re_o	Reynolds number per unit length		1/cm.

S	specific entropy	cal./^{o}C gm.
T	temperature	deg. Centigrade or deg. Kelvin
T_{cr}	critical temperature	^{o}C or ^{o}K
T_{tr}	triple-point temperature	^{o}C or ^{o}K
T_{s}	saturation temperature	^{o}C or ^{o}K
u	velocity in the direction of the undisturbed flow	cm./sec.
Vf	volume flow per unit test section area	cm.^{3}/sec. cm.^{2}
v	specific volume	cm.^{3}/gm.
w	specific work	ergs/gm.
x	direction of undisturbed flow	
β	shock wave angle measured from direction of undisturbed flow	degrees
β^{*}	Mach angle	degrees
γ	ratio of specific heats	
δ	displacement boundary layer thickness in compressible flow	cm.
δ^{*}	displacement boundary layer thickness in incompressible flow	cm.
ϵ	specific internal energy of a gas	ergs/gm.
η	efficiency	
θ	flow deflection angle	degrees
κ	coefficient of thermal conductivity	cal./sec.^{o}C cm.
λ	molecular mean free path	cm.
μ	coefficient of viscosity	dynes sec./cm.^{2}
μf	microfarad (capacity)	
ν	kinematic viscosity	cm.^{2}/sec.

ν^*	critical kinematic viscosity	$cm.^2/sec.$
ρ	density	$gm./cm.^3$
τ	shock wave thickness	cm.
χ	specific enthalpy	cal./gm.

Where there are several units for one quantity the one used is specified in the text. Other quantities not listed here are defined separately when their use arises.

INTRODUCTION

This dissertation describes the design and construction of a low Reynolds number, supersonic wind tunnel, and its application to the investigation of a particular problem in viscous compressible flow. The tunnel uses a new type of driving mechanism (a two-phase cycle) especially suited to operation at high speed and low density.

In order to facilitate certain experimental studies on the effects of viscosity in compressible flow it is desirable to enhance viscous effects by a reduction in Reynolds number, but without decreasing the Mach number. One way of providing these conditions is to use a low density, supersonic wind tunnel, which, however, raises certain problems in the driving mechanism. To avoid some of the difficulties a new wind tunnel has been designed and built, utilizing a two-phase water vapor cycle. Some instrumentation problems also arise from the low density in the flow, and the nature of the working fluid. Part I of this presentation, therefore, deals with the development of the equipment for low Reynolds number, supersonic flow research. To demonstrate the usefulness of the new tunnel, the problem of the curvature due to viscosity of an attached shockwave on a straight wedge in uniform supersonic flow is investigated, and is presented in Part II.

PART I

THE DEVELOPMENT OF SOME EQUIPMENT FOR LOW REYNOLDS NUMBER SUPERSONIC FLOW RESEARCH

1. Basic Considerations

In choosing the proper flow characteristics for the study of viscous, compressible fluid motion, not only must the effects of the Reynolds number and the Mach number be considered individually, but also, depending on the particular phenomenon under investigation, the effects of a parameter made up of some combination of these two dimensionless quantities.

If, for example, the phenomenon of interest is the interaction of a laminar boundary layer and a shockwave, one may wish to treat the shockwave as a discontinuity while regarding the boundary layer as a finite region of viscous flow. Such a situation implies the condition $\tau/\delta << 1$, where τ is the thickness of the shockwave and δ the boundary-layer thickness. This condition in turn implies that some parameter $f(M, Re)$ satisfy certain requirements. It is shown in Appendix A that for such a case the pertinent parameter and the condition it must satisfy are as follows:

$$\frac{\sqrt{M^2-1}}{M Re_\delta} << \frac{(\gamma+1)\theta}{8\gamma}$$

This expression is valid for the case of a weak shockwave caused by a small deflection, θ, of a flow at a Mach number of the order of unity. Re_δ is the Reynolds number based on the boundary-layer thickness.

Another problem of interest may be the effect of viscosity on the shape of the attached shockwave on a wedge, which is treated in

Part II of this dissertation. In this case the approach to the experimental investigation is by way of enlarging the physical extent of the region in which the shock wave exhibits appreciable, or measurable, curvature as a result of the curvature of the boundary layer. This region is so small when produced in a flow at a Reynolds number (of the order of 10^5 for 1 cm.) normally encountered in conventional supersonic tunnels that it is quite difficult to conduct any kind of measurement within it. It is shown in Part II (cf. p. 43) that in order to enlarge the region sufficiently for experimental study, the following conditions must be satisfied:

$$\frac{(M_1^2 - 1)^2}{M_1^5} Re_o \leq \frac{B^2}{8} \left(\frac{\gamma+1}{2}\right)^2 \left(\frac{C_s}{x}\right)_m \frac{1}{x_m}$$

In this expression Re_o is the Reynolds number based on unit length, (as such, Re_o has the dimension 1/cm.), M_1 the Mach number in the undisturbed flow, x_m a distance that can be measured with accuracy, and C_{sm} the maximum radius of curvature. B is a boundary layer coefficient defined in Part II. The validity of the expression depends on two restrictions: that the Mach number be of order one, and the wedge angle of order zero.

For the following assumed conditions

$$M_1 = 2$$

$$x_m = 10^{-1} \text{ cm.}$$

$$\left(\frac{C_s}{x}\right)_m = 10^3$$

the condition on Re_o is

$$Re_o \leq 16,000$$

The Reynolds number cannot be decreased indefinitely because of slip-flow conditions and conditions at the leading-edge where the shock wave and the boundary layer intersect. There is then a

lower limit on the Reynolds number. The establishment of this lower limit is discussed in Part II (cf. p. 45); and it suffices to mention here that for the same conditions as stated above the lower limit is

$$Re_o \geqslant 1,300$$

For the design of the low Reynolds number tunnel described in the present work Re_o is chosen at 5,000.

2. Problems with a Low Reynolds Number Supersonic Tunnel of Conventional Design

For a tunnel with fixed Mach number, test-section dimensions, and stagnation temperature the density and the mass flow decrease with the Reynolds number, while the volume flow remains constant. This immediately raises two problems. One is that ordinary centrifugal or axial-flow compressors do not operate effieiently at low Reynolds numbers. Second is the fact that the size and speed of the compressors remain constant, though the mass flow decreases, with the result that mechanical losses in the compressors constitute an increasing percentage of the total power consumption.

For the tunnel under consideration the Mach number, Reynolds number and stagnation temperature may be specified as follows:

$M = 2$

$Re_o = 5,000$

$T_1 = 300^\circ K.$

Then, using air as the working gas, the following quantities are determined from the above: (See Appendix B)

p_1 = 4.6 cm. Hg

$\rho_1 = 7.1 \times 10^{-5}$ gm./cm.^{3}

Mf = 0.85 gm./sec. cm.^{2} test-section area

Vf = 3.7×10^4 cm.^{3}/sec. cm.^{2} test section area (at $\rho = 2.3 \times 10^{-5}$)

The density specified above for the volume flow is based on conditions at the exit end of the diffuser. It appears that with such a low density the only suitable way of driving the tunnel (in a one-phase cycle) would be by a positive displacement pump. However, since pumps of this type depend for their operation on the movements of close-fitting parts sealed and lubricated by oil, much of the power consumed is dissipated in friction; and this frictional loss depends only on the volume flow. Therefore, the power consumption does not decrease with decreasing mass flow if the volume flow remains constant. The power efficiency (ratio of isothermal compression power to actual power) thus decreases with the density of the flow.

An alternative might be to use an induction drive, if the tunnel can operate on a non-return circuit. This method is fairly convenient where there is a readily available high-pressure steam supply. But the jets are noisy and are extremely inefficient in power consumption. The exhaust of the jets is at atmospheric pressure, resulting in overall compression ratio (from diffuser to atmosphere) much higher than necessary for the operation of a medium Mach number tunnel.

In fact, all conventional methods adaptable to wind tunnel drives for continuous operation appear unsatisfactory, and some new scheme has to be devised.

2.1 The Two-Phase Wind Tunnel Cycle

Since the difficulties mentioned above can be traced to the use

of a one-phase cycle, one possible solution is to use a two-phase cycle similar to that of a steam engine or a diffusion pump. The possibility of applying a two-phase cycle to a wind tunnel was suggested by Prof. Liepmann in 1950, after considering use of the diffusion pump for driving a low density tunnel. In the diffusion pump the vapor from an evaporated liquid expands in a nozzle, and the resulting high-speed, low-pressure jet is used as an induction pump; the vapor is finally condensed and returned to the evaporating chamber. (See, for example, Refs. 1 and 2). The new idea was that instead of using the vapor of a diffusion pump to drive the flow in a tunnel, the pump itself could be the wind tunnel*.

Before embarking on a detailed discussion of the two-phase wind tunnel it is useful to consider first the basic thermodynamic characteristics of a wind tunnel, and develop some general relationships governing the performance of a tunnel. With these as background the two-phase tunnel cycle can then be treated in detail.

3. Thermodynamics of the Wind Tunnel

Consider an idealized wind tunnel system, adiabatically enclosed from the stagnation chamber to the exit reservoir, and containing a thermodynamically perfect gas. By perfect gas in the thermodynamic sense we mean a gas obeying the simple equation

---

*In a later literature survey it was discovered that the two-phase cycle was considered in part by Hawthorne, et al, in 1947. (See Ref. 3). However, the full advantage of the cycle was apparently not brought out by Ref. 3, as will be seen in Section 3.121.

of state

$$pv = \mathcal{R} T \tag{1}$$

where R is the gas constant for a unit mass, and whose internal energy is a function only of the temperature,

$$\varepsilon = c_v T \tag{2}$$

where c_v, the specific heat at constant volume, is constant.

This gas starts from rest in the stagnation chamber at the pressure p_1, specific volume v_1 and stagnation temperature T_1, expands through the nozzle, where it does no external work and exchanges no heat with the exterior, and comes to rest again in the exit reservoir at the state p_2, v_2, T_2. It is evident that no energy is gained or lost by the gas in going from state 1 to state 2. Therefore it is important to note that "dissipation of energy" (a term commonly referred to in wind tunnel nomenclature) in a wind tunnel (between stagnation chamber and exit reservoir) does not imply transfer of energy to the exterior, or loss of energy in any way. A more appropriate way of stating this would be that there is a degradation of the energy. By virtue of the Second Law of Thermodynamics the degraded energy in the gas cannot be used to perform anything, whether it be doing mechanical work or moving itself in directed motion, without either some change in the environment (in this case a lowering of the pressure in another exit reservoir, that is, $p_3 < p_2$), or the expenditure of energy (in this case the use of a pump to return the gas to p_1). Since the wind tunnel is a cyclic process in which the gas must be returned to the initial state, the second choice, that of energy expenditure, must be adopted.

Since the degradation of energy is measured by the increase of entropy, the external energy required to return the gas to the initial

state depends on the irreversible entropy increase during the cycle through the tunnel circuit. However, the knowledge of the increase of entropy alone does not define the energy required because a temperature must be defined in order to relate entropy to energy. Conversely, describing the dissipation in terms of energy does not give a unique answer, unless one tacitly assumes some temperature. Ackeret (Ref. 4) brings out this point in defining the diffuser efficiency in two ways: in terms of pressure and in terms of energy which involves a temperature. It is felt, however, that the significance of the temperature has not been sufficiently brought out, particularly in the light of present developments toward higher Mach numbers and higher temperatures.

Consider the First Law of Thermodynamics

$$q = \Delta\varepsilon + w \tag{3}$$

where q is the heat added to the system, $\Delta\varepsilon$ the change in internal energy of the system, and w the work performed by the system, during a given interval.

Equation (3) may be written in another form,

$$\Delta\varepsilon = \sum_n q_n - w \tag{4}$$

where q_n are the quantities of heat added to or removed from the system during the chosen interval, the summation being the net amount of heat transferred, and w is the work done by the system during the interval, all the work being considered concentrated in one single process.

The second law of thermodynamics may be written in the form adopted by Tolman (Ref. 5)

$$\Delta S = \sum_n \frac{q_n}{T_n} + \Delta S_{irr} \tag{5}$$

where q_n/T_n represents the entropy change during the transfer of heat q_n at temperature T_n, and ΔS_{irr} is the entropy produced by irreversible processes during the interval.

If (4) and (5) are applied to a cyclic process in which the initial and final states are identical,

$$\Delta \varepsilon = 0, \qquad \Delta S = 0$$

they become

$$\sum_n q_n - w = 0 \tag{6}$$

$$\sum_n \frac{q_n}{T_n} + \Delta S_{irr} = 0 \tag{7}$$

Let T_e be the temperature of the environment, or that of an infinite heat reservoir into which heat can be added, and from which heat can be extracted without changing its temperature. Multiplying (7) by T_e and subtracting from (6)

$$\sum_n q_n \frac{T_n - T_e}{T_n} - w - T_e \Delta S_{irr} = 0 \tag{8}$$

Now for a cycle in which heat transfers take place only at T_e, the first term in (8) vanishes, leaving

$$w = - T_e \Delta S_{irr} \tag{9}$$

Since w is work done by the gas, (9) expresses the work done on the gas. In reality the transfer of heat to or from the environment cannot be accomplished at T_e so that there is always some entropy increase from heat exchange over finite temperature differences. However, it will be shown later that for a wind tunnel cycle the net heat exchange is a removal to the environment so that the entropy increase is charged

to the environment rather than to the tunnel system. Hence (9) represents the externally applied work necessary to maintain the flow in the tunnel.

The next step in the analysis is to determine ΔS_{irr}, the irreversible entropy rise. Most of this will arise out of dissipative processes in the tunnel nozzle and the diffuser. The remainder, which is much smaller than the above because of much lower flow speeds, is attributed to dissipative processes in the return circuit. The entropy increase during the flow through the tunnel is due to the irreversible conversion of kinetic energy of directed motion to kinetic energy of thermal motion through shockwaves, boundary layers and boundary-layer separations. It is, in general, difficult to express in simple relationships the entropy rise due to these processes by parameters directly involved in them. However, since in this analysis we are concerned only with the total difference in entropy between the gas in the stagnation chamber and in the exit reservoir, it is sufficient just to relate the entropy difference to the pressures and temperatures of the gas in the two equilibrium states. The entropy can be expressed in terms of the state of the gas by the relation

$$S = c_p \log T - R \log p + S_o \tag{10}$$

Hence,

$$\Delta S_{irr} = S_2 - S_1 = c_p \log \frac{T_2}{T_1} - R \log \frac{p_2}{p_1} \tag{11}$$

Applying the First Law to the interval 1-2, we have, since $q = 0$, $w = 0$,

$$\Delta \varepsilon = 0$$

Since, for a perfect gas, the internal energy depends only on the temperature, this means that

$$\Delta T = 0$$

or

$$T_2 = T_1$$

Therefore Equation (11) becomes

$$\Delta S_{irr} = -R \log \frac{p_2}{p_1} \tag{12}$$

Equation (9) then becomes

$$w = +R T_e \log \frac{p_2}{p_1} \tag{13}$$

That the work should depend on the temperature is apparent when we consider that S, being a function of state, does not depend on the path for its value in going from one state to another, but that w, not being a function of state, depends on the path. This is illustrated in Fig. 1 where it is seen that S_1 and S_2 are uniquely defined but that w, being the area under the curve in the p-v plane, depends on the path; path (a) requiring more work than (b).

Again applying the First Law of Thermodynamics, Equation (3), this time to the cyclic process from stagnation chamber back to stagnation chamber, the following relation is obtained

$$w = q \tag{14}$$

In other words, the work done on the gas equals the heat removed from the gas to the environment in the return circuit. Thus, instead of the area in the p-v plane, that under the curve in the T-S plane, representing heat, can be used to represent the work done on the gas. If the flow from 2 to 1 consists of two reversible adiabatic processes and one reversible isothermal process, the area under the curve in

the T-S plane is just

$$T_e (S_2 - S_1)$$

which, as is shown in Equation (9), is the work required to return the gas from state 2 to state 1.

It becomes apparent at this point, that with a given value of ΔS, the work is directly proportional to the environment temperature, or the temperature of the heat sink.

The work as expressed in Equation (13) is for a unit weight of the gas, and depends, aside from the sink temperature, on the gas constant (which is inversely proportional to the molecular weight) and the compression ratio. The total power required is w times the mass flow, Mf, through the nozzle, which may be expressed as

$$Mf = \sqrt{\frac{\gamma}{R}} \frac{p_1 M}{\sqrt{T_1}} \left(1 + \frac{\gamma - 1}{2} M^2\right)^{-\frac{\gamma+1}{2(\gamma-1)}} \qquad (15)$$

(mass flow per second per unit test-section area)

Therefore, $w \sim \sqrt{R}$, and, in this respect, a gas with a large molecular weight is preferable to a lighter one. The ratio p_2/p_1 is determined by the geometry of the nozzle, flow conditions, and the kinematic viscosity of the gas.

The work thus determined for a given gas and given values of T_e, p_1, p_2, T_1, and test-section area is the ideal minimum. In practice, the work required is larger than the ideal, the amount depending on numerous factors about whose effects no general rules can be stated. The most important factors are the thermodynamic processes used in the return circuit from 2 to 1, the range of pressures and temperatures covered in the cycle, and the kind of gas used. To see what effects these

may have on the actual power consumption, it will be best to see what combinations of thermodynamic processes may be used.

3.1 Thermodynamic Processes Adaptable to a Wind Tunnel Circuit

In most conventional wind tunnels the return circuit from the exit reservoir to the stagnation chamber consists of one or more compressors with suitable provision for cooling the gas. The compressors may in some applications be replaced by some kind of induction drive, usually with steam ejectors. Discussions on compressor drives and steam ejector drives are well covered in the literature, from the early works of Crocco (Ref. 6) and Ackeret (Ref. 4), to the more recent works of which a good survey may be found in the work of Ruptash (Ref. 7). If phase changes are admitted, methods other than the conventional ones just mentioned may be adapted to wind tunnel drives.

3.11 The One-phase Cycle

Consider the conventional one-phase cycle as represented in the T-S and p-v planes in Fig. 2. The irreversible process 1 - 2 represents the flow from the stagnation chamber through the nozzle and diffuser into the exit reservoir with an entropy rise of ΔS. In the return circuit the isothermal compression should be conducted at the lowest possible temperature, say the temperature of the atmosphere T_a. Reversible adiabatic or isobaric processes can be used to move the gas to and from T_a. These are the paths 2-3, or 2-3', and 4-1, or 4'-1, in the T-S and p-v planes in the figure. Since, by Equation (14), the net work done on the gas equals the net heat removed, it is seen from the T-S diagram that the net work is the area under 3-4,

or 3'-4'. Since 2-3 is parallel to 4-1 and 2-3' to 4'-1, the area under 3-4 or 3'-4' is equal to $T_a \Delta S$, which is, of course, the work given by Equation (9) with T_e replaced by T_a. So the work required in the one-phase cycle for unit mass flow is, by Equation (13)

$$w_g = R T_a \log \frac{p_2}{p_1} \tag{16}$$

3.12 The Two-phase Cycle

Figure 3 shows the T-S and p-v diagrams of a two-phase system. A-B is the liquid saturation line and C-B the vapor saturation line. The one-phase cycle described in the preceding section operates entirely above the vapor saturation line C-B. In the two-phase cycle the gas goes through the tunnel (1 to 2) with a gain in entropy of ΔS as before. From 2 the gas is cooled isobarically or adiabatically all the way to saturation at 3. (The adiabatic cooling process reaches saturation at a temperature below that reached by an isobaric cooling. In practice it is preferable to operate at a higher temperature; therefore only the isobaric process is considered). From 3 to 4 the saturated vapor is condensed by further heat removal at constant temperature and pressure. The saturated liquid at 4 is compressed adiabatically to a pressure equal to that of the stagnation chamber p_1. The liquid is now heated isobarically from 5 to 6, where it reaches saturation, and is then evaporated from 6 to 7. The saturated vapor at 7 is superheated isobarically to stagnation temperature T_1, thus completing the cycle.

From 2 to 8 along the isobar (where $T_8 = T_7$) the heat removed can be transferred to the isobaric heating from 7 to 1, since $T_1 = T_2$

and $T_7 = T_8$, (remembering that these processes are all considered as ideal equilibrium thermodynamic processes). From 8 through 3 to 4 heat is taken out of the system. From 4 to 5 work is done on it. Heat is added to the system from 5 through 6 to 7. This heat can come from the process 8-3-4 if a refrigerator is used to transfer heat over a temperature rise. The work required to transfer a quantity of heat q from a temperature T_ℓ to a higher temperature T_h by a reverse Carnot cycle is:

$$w_r = q\left(\frac{T_h}{T_\ell} - 1\right) \tag{17}$$

In our case the process from 8 to 3 is not at constant temperature, but we can place the heat receiver of the refrigerator at T_3 and remove heat from 8 to 4, q_{84}. The heat rejector is placed at T_7. The work required to transfer q_{84} from T_3 to T_7 is then, by Equation (17):

$$w_{r_1} = q_{84}\left(\frac{T_7}{T_3} - 1\right) \tag{18}$$

The total heat to be rejected at T_7 is q_{84} plus the heat equivalent to the refrigeration work,

$$q_r = q_{84} + w_{r_1} = q_{84}\,\frac{T_7}{T_3}$$

The system in the tunnel return circuit is not an infinite heat reservoir, so that not all of q_r can be rejected at T_7. All that the refrigerator can reject at T_7 is the amount q_{57}. The remainder must be rejected into a sink at atmospheric temperature T_a. The work required to do this is:

$$w_{r_2} = \left(q_{84}\,\frac{T_7}{T_3} - q_{57}\right)\left(\frac{T_a}{T_7} - 1\right) \tag{19}$$

The adiabatic compression of the liquid from 4 to 5 requires

$$w_c = \frac{1}{\gamma_\ell - 1} (p_5 v_5 - p_4 v_4) \tag{20}$$

where v_4 and v_5 are the specific volumes of the liquid at 4 and 5, and γ_ℓ is the adiabatic constant of the liquid.

To satisfy Equation (14) this work must be rejected as heat. This heat can be rejected only at T_a, to perform which the work required is:

$$w_{r_3} = w_c \left(\frac{T_a}{T_3} - 1\right) \tag{21}$$

Adding Equations (18), (19), (20) and (21), we have, for the total work required in the two-phase cycle, for unit mass flow,

$$w_\ell = q_{84} \left(\frac{T_a}{T_3} - 1\right) - q_{57} \left(\frac{T_a}{T_7} - 1\right) + w_c \left(\frac{T_a}{T_3}\right) \tag{22}$$

In practice q_{84} is nearly equal to the latent heat of condensation, L_3, at T_3, and q_{57} to the latent heat of vaporization, L_6, at T_6. The reason for this is that the saturation temperature has a logarithmic dependence on the saturation pressure, so that for saturation pressures of the same order the saturation temperatures are nearly equal. (For example, the saturation temperature of water vapor at 4 mm. Hg. is 271°K., and at 40 mm. it is 307°K.) In our case, then, $(T_8 - T_3)c_p$, (which is q_{83}), is usually very small compared to L_3, if p_2 and p_1 are of the same order. The same reasoning applies to replacing q_{57} by L_6. Again, if the saturation temperatures are nearly equal, so are the corresponding latent heats.

Furthermore, γ_ℓ, the adiabatic constant of the liquid, is very large, so that w_c is very small, and the third term of Equation (22) is

therefore negligible compared to the others. With this and the other simplifications justifiable under the condition that p_1/p_2 is less than 10, Equation (22) may be written in the approximate form

$$w_\ell = \angle \left(\frac{T_7}{T_3} - 1\right) \frac{T_a}{T_7} \tag{23}$$

It should be emphasized that Equation (16) represents the minimum possible energy required with a given T_a, and that w_ℓ from Equation (22) is equal to or greater than w_g. We will show, by applying perfect gas thermodynamics to both the gas and liquid phases, that w_ℓ is in the ideal case exactly equal to w_g. To do so we introduce a fictitious substance whose specific heats in the gas and liquid phases are equal and whose liquid saturation line coincides with the adiabatic line of the saturated liquid. This is represented in Fig. 4 where (3)-(7) is the vapor saturation line and (4)-(6) the liquid saturation line. Let the lowest temperature be T_3, and the sink temperature, T_a. If now the gas is allowed to condense at T_3 to a saturated liquid at (4), and compressed and evaporated to (7), the adiabatic expansion work from (2) to (3) is equal to the adiabatic compression work from (4) to (6) and (7) to (1), because of the properties just ascribed to the fictitious fluid. All the external work required will be in refrigeration, removing heat $T_3\Delta S_2$ at T_3, rejecting $T_7\Delta S_1$ at T_7 and the remainder at T_a. Since all the other processes in the cycle are adiabatic, $T_3\Delta S_2$ must be equal to $T_7\Delta S_1$. Therefore, the total refrigeration work is

$$\begin{aligned} w_\ell &= T_3\,\Delta S_2\left(\frac{T_7}{T_3} - 1\right) + (T_7\,\Delta S_2 - T_7\,\Delta S_1)\left(\frac{T_a}{T_7} - 1\right) \\ &= T_a\,(\Delta S_2 - \Delta S_1) + T_7\,\Delta S_1 - T_3\,\Delta S_2 \\ &= T_a\,\Delta S \end{aligned}$$

This, as has been shown in Section 3.11, is just the work required

in a one-phase cycle with the same heat sink temperature T_a.

3.121 The Simplified Two-phase Cycle

If the saturation temperature, T_3, is above T_a, the cooling and condensation can be done without a refrigerator by rejecting the heat directly to the atmosphere or running water. The equipment in this case is simplified, but heat from an external source will have to be used to evaporate and superheat the working medium. The energy consumption (in the form of heat) in this method of operation is then

$$q_a = q_{57} + c_p (T_1 - T_7)$$

Or, approximating q_{57} with L, the latent heat,

$$q_a = L + c_p (T_1 - T_7) \qquad (24)$$

This energy consumption q_a is higher than w_ℓ as computed from Equation (23), because in Equation (23) both T_a/T_3 and T_a/T_7 are less than unity by the assumption on temperatures made above. Therefore the simplification of equipment is achieved at the expense of added power consumption.

The method proposed in Ref. 3 (cf. p. 6) is based on this simplified two-phase cycle. Substances that can be used for such a cycle are necessarily limited to those with saturation temperatures above atmospheric.

3.13 Comparison of the One-phase and Two-phase Cycles

Equations (16) and (22) represent ideal minimums of work required for the two cycles. In actual practice there are many thermal and mechanical inefficiencies. In the one-phase cycle isothermal

compression of the gas is never realized. The compression efficiency (defined as the ratio of the isothermal work to the actual work) decreases as the compression ratio goes very high, or as the density becomes very low.

In the two-phase cycle the major factor governing its efficiency is the refrigeration efficiency (defined as the ratio of the reverse Carnot cycle work to the actual work) which decreases as the difference between operating temperature levels increases. The refrigeration efficiency is, however, not directly affected by the density of the working medium in the tunnel cycle. Indirectly it is influenced to a small extent by the density, because low density usually means low pressure which in turn results in low saturation temperature. The other factor affecting the performance of the two-phase cycle is the heat exchange between the medium in the isobaric cooling process and that in the isobaric heating process. Incomplete cooling and heating must be made up by additional refrigeration and heat addition, representing added energy expenditure.

The equipment required by the one-phase cycle is simpler than that needed to perform the several processes in the two-phase cycle. The primary advantage of the two-phase cycle is in the compression of the working medium of the tunnel in the liquid phase, which avoids the inefficient utilization of gas pumps under certain conditions of low density and high compression ratio. It should be remarked at this point that although there is only a liquid pump in the two-phase cycle, it does not mean there is no gas pump at all in the total equipment. Indeed there are gas pumps in the refrigerators. However, the pressure and density of the refrigerant need not be in such unfavorable working ranges as to cause inefficient operation of the refrigeration

cycle.

For medium Mach number and normal density operation the simplicity and fairly good compression efficiency (say 80°/o or better) of the one-phase cycle make it the better cycle to use than the more complicated two-phase cycle. For very high Mach number operation in which the compression ratio p_2/p_1 is very high (say 1000 or higher), or for very low density operation (say 10^{-5} gm/cm^3 or less) at any Mach number, the efficiency of gas compression becomes so low (say 10°/o or less) that the higher efficiency of the more complicated two-phase cycle may well be used for driving the tunnel. The two-phase cycle has the further advantage that the liquid pump in it needs no oil for sealing and lubrication, so that there is no contamination of the working medium by oil, as usually happens with compression by positive displacement pumps. In certain applications the two-phase cycle may not need any pump at all, as will become evident in the description of the application of the cycle to a low Reynolds number supersonic wind tunnel in the next section.

3.2 Application of the Two-phase Cycle to a Low Reynolds Number Supersonic Wind Tunnel

The analysis above has not been restricted to any particular working medium, so that one may choose the substance best suited to the requirements of a particular tunnel. In our case these requirements, as already stated in Sections 1 and 2, are that M = 2 and Re_o = 5,000. That these requirements, when incorporated into a conventional one-phase cycle using air, cause the air density to be so low that compression becomes a serious problem has also been mentioned in Section 2.

In applying the two-phase cycle, water has been selected as the working medium. The criteria for selecting a working medium to meet specific requirements in wind tunnel operation are discussed in Appendix B. Suffice it here to mention briefly that under the operating conditions imposed by our tunnel the temperatures involved, if water is used, are not very far from atmospheric. This simplifies the problems of refrigeration and insulation. At Mach numbers up to about 2 the γ of water vapor, which is 1.33, results in flow geometry differing negligibly from that of an air flow.

On the basis of a maximum Mach number of 2 and a Reynolds number per centimeter of 5,000, the complete design data of pressure, temperature, heat exchange (per gram of water) through the whole two-phase cycle are listed in Fig. 5, together with the T-S diagram showing the various processes. In this T-S diagram the isentropic expansion in the nozzle and the irreversible processes through the nozzle and diffuser to the exit reservoir are shown as paths 0-1 and 1-2. A positive value of q means heat added to the fluid. The sum of the q's is not zero because the mechanical work involved in moving the liquid from (5) to (6) is not included.

Since the power requirement is quite low, because of the small size of the tunnel (about 5 cm.^{2} test section area) and small mass flow, and a refrigerator is already available in the laboratory, it does not seem worthwhile to design a special refrigerator to perform the more ideal processes described in Section 3.12. Therefore, separate refrigeration and heating are employed.

The pressure difference between 0 and 2 is quite small - only

9.4 mm. Hg. (because of the low absolute pressures) so that instead of using a pump, the water in the condenser is caused to flow back to the boiler simply by keeping the condenser water level higher (by at least 9.4x13.6 mm) than that in the boiler.

4. Description of the Tunnel

The tunnel, using water in a two-phase cycle, is designed for continuous operation at a Mach number up to 2, and Reynolds number per centimeter of about 5,000 in the test-section with an area of 5.2 cm^2 (2.1 cm x 2.5 cm). A schematic diagram showing the general arrangement of the tunnel is shown in Fig. 6, while Fig. 7 shows the actual installation.

4.1 Boiler and Superheater

The boiler and superheater are housed inside a steel tank with seven 1-kw immersion heaters at the bottom to supply the heat for evaporation, the power input being controlled by an autotransformer. Electrical rod heaters, with a total capacity of 1.7 kw, constitute the superheater, also controlled by an autotransformer. Between the superheater and the water below are two baffle plates to prevent splashing water (the result of occasional explosive boiling) from reaching the superheater. The vapor, in passing through the superheater, is mixed by baffles to give uniform temperature.

The contraction section is bolted and sealed directly to the top of the boiler tank. Both this and the upper half of the boiler, where the superheater is mounted, are covered on the outside with one layer of aluminum foil, one layer of one-inch glasswool, and finally an

outside cover of corrugated cardboard.

4.2 Nozzle and Test Section

The nozzle is made of brass, with the side walls soldered to the nozzle contour blocks. Two-inch diameter windows cover the test section. The ends of the nozzle are equipped with sliding gate valves to seal the remainder of the tunnel circuit when the test section is open, and for starting the flow, for which the downstream valve is used. All moving and detachable parts are sealed with o-rings.

The nozzle contour was originally designed by the characteristics method, with an approximate linear boundary layer correction. Repeated failures to achieve shock-free flow to the test section eventually resulted in a decision to use flexible nozzle plates inserted inside the original fixed nozzle and controlled by two pairs of jacks. Fig. 8 shows the complete nozzle section.

Several static pressure orifices are placed along the side (fixed) walls and two on each nozzle plate in the test section. There are two traversing mechanisms carrying pressure probes. The use of so many pressure taps is necessitated by the fact that visualization of the flow is very difficult due to the very low density of the flow and short optical path through the flow.

Wedges or other models can be mounted in the test section on two supports which also act as pressure leads connected to pressure orifices on the surface of the wedge. These orifices are used to set the wedge at zero angle of attack. The wedge support assembly can be adjusted from the outside to vary the angle of attack.

4.3 Diffuser and Condenser

The diffuser extends from downstream of the second throat along a 5 degree total expansion angle to a point where the area is four times that at the starting end. The circuit from here to the condenser is connected by a pipe. Both the diffuser and this pipe are insulated in the same manner as the superheater. One static pressure tap is placed at each end of the diffuser.

The condenser consists of two refrigeration evaporator units arranged in tandem inside a sealed tank. Water is accumulated in the conical bottom of this tank whence it returns to the boiler through a valve and a small tubing. A refrigerating unit, capable of removing 1800 cal./sec., discharging heat to circulating water, is used with two refrigerant-evaporators inside the condenser and a third one in parallel outside acting as ballast.

4.4 Power Consumption

As mentioned in Section 3.2 the power used in this tunnel is actually more than it need be since the boiler and superheater are heated separately instead of receiving heat from the condenser. During a typical run the power consumption figures are: boiler 4.0 kw, superheat 0.9 kw, and condenser 2.2 kw, making a total of 7.1 kw. If the heat from the condenser is transferred to the boiler and superheater, probably no more than 2.5 kw is required. Some of the heat is lost to the atmosphere from all the hot parts of the tunnel. The ideal minimum power, from Equation (16), is

$$P = Mf\, R\, T_a \log \frac{p_2}{p_1}$$

Using

$T_a = 295^{\circ}K.$

$Mf = 2.1$ gm/sec.

$\frac{P_1}{P_2} = 3$

we find $P = 0.31$ kw.

If Equation (23) is used, with $T_a = T_7 = 300^{\circ}K.$ and $T_3 = 278^{\circ}K.$, $P = 0.47$ kw.

4.41 Power Consumption of an Equivalent One-phase Cycle Using Air

As a comparison, we will estimate the actual power requirement of an equivalent air one-phase cycle, with operating conditions as given in Section 2. As mentioned there, the actual power requirement depends primarily on the volume flow, if a positive displacement pump is used.

Using the volume flow per cm^2 test-section area given in Section 2 and a test-section area of 5.2 cm^2, the total volume flow for the tunnel is

$Vf = 1.83 \times 10^5$ cm^3/sec

The power requirement of a rotary positive displacement pump with this volume flow capacity ranges between 10 and 15 kw., depending on the type or model.

If an induction drive is used, a steam ejector requiring about 500 pounds of high pressure steam (150 psi. gage) is needed, and the minimum power (heat input to the boiler with perfect efficiency) is about 125 kw.

The actual power consumption and the various estimated con-

sumptions are summarized below:

Ideal minimum (isothermal)	0.31 kw
Theoretical minimum using two-phase water cycle	0.47 kw
Practically feasible minimum using readily available equipment	2.5 kw
Estimated one-phase air cycle with mechanical pump	10 - 15 kw
Estimated one-phase air cycle with steam ejector	125 kw
Actual operating	7 kw

5. Instrumentation of the Tunnel

As a result of the low density, low pressure, and the water vapor used as the working fluid, several problems arise in the instrumentation. Some of these same problems are often encountered in conventional tunnel work; but in this instance they become acute so that special treatments are deemed necessary.

5.1 Temperature

Three temperatures are measured by dial thermometers (Dillon) with thermal elements enclosed in stainless steel stems extending into the tunnel. These correspond to T_7, T_0 and T_5 in Fig. 5. T_7, the boiling temperature, is measured just under the water surface level in the boiler, and T_0, the stagnation temperature, is measured above the superheater at the beginning of the contraction section. T_5, the temperature of the condensate, is measured under the water surface in the condenser.

5.2 Pressure Measurement

The pressures encountered in the operation of this tunnel, from 5 to 40 mm. Hg., are unfortunately in the range reached neither by normal pressure (near atmospheric) techniques or by vacuum techniques (10^{-3} mm. or lower). The two vacuum gages which are useful at higher pressures are the McLeod and Pirani gages (Refs. 2 and 8), which can reach only up to 10^{-1} mm. Mechanical gages operating on the displacement of diaphragms under differential pressures are very convenient, though the accuracy is no better than 10^{-1} mm. for commercially available models. Fluid manometers are still the only practical type for use here where many pressures need be read simultaneously. With special optical reading methods and many corrections as to temperature, pressure, surface tension, a high precision mercury manometer can read to 10^{-2} mm. Hg. (Ref. 9) but this is not adaptable to rapid readings. By using a fluid lighter than mercury an accuracy of 10^{-2} mm. Hg. can be achieved by vernier-reading micromanometers. The vapor pressure of the manometer fluid must be negligibly small compared to the pressures to be measured. Therefore, the usual alcohols used for manometry of normal pressure wind tunnels cannot be used here. Maslach (Ref. 10) has developed a micromanometer using n-butyl phthalate that has an accuracy of 10^{-4} mm. Hg. in a range 0 to 4×10^{-2} mm. Hg. Silicone fluids (Ref. 11) have very low vapor pressures but are more viscous than water and alcohol.

For the present work of this tunnel the requisites of simplicity and low cost outweigh the demands of high accuracy, so that in the measurement of pressures an accuracy of 10^{-1} mm. Hg. is considered sufficient. Therefore, the pressure instrumentation consists of sili-

cone manometers with reference pressure read by an aneroid gage.

The lines connecting the pressure orifices with the manometers are filled with water vapor which condenses when the pressure is above the saturation pressure corresponding to the temperature of the lines which is room temperature. This condensed water not only tends to clog the lines, but also, when the orifice is at a pressure below the vapor pressure of the water drops, gives erroneous readings higher than the true values. By placing the manometers close to the nozzle and using as short lines as possible it is possible to keep them free of condensed water drops. Another way of meeting this difficulty is to isolate the working fluid, whatever it may be, from the measuring device, and to transmit the pressure by a transducer. Accordingly, a null-reading diaphragm transducer has been designed and built. A 0.002 cm. diaphragm is sealed in a chamber one end of which is connected directly to the pressure orifice and the other end connected to a known pressure source. Movement of the diaphragm, when the unknown and known pressures are not equal, is detected by a Schaevitz linear variable differential transformer.

A schematic drawing of the transducer and the control arrangement is shown in Fig. 9. The control valve regulates the amount of air let into or out of the air chamber of the transducer in order to balance the pressure in the vapor chamber. Voltage from the Schaevitz gage when the diaphragm is displaced is amplified and read on a vacuum-tube-voltmeter. A detailed description of the Schaevitz gage may be found in the treatise by Dhawan (Ref. 12).

A pressure difference of 0.1 mm. Hg. can be detected with

this device. However, for lack of proper electronic devices, this transducer is not used in actual operation. This discussion is only for the sake of mentioning one of the special problems faced by this tunnel.

5.3 Schlieren System

Flow visualization by schlieren technique becomes quite difficult when the density and the density gradient in the flow are very low. In our case the nature of the tunnel results in low density, and the thickness of the shockwave is greater than in a conventional tunnel because of the low Reynolds number (cf. Appendix A), resulting in low density gradient through the shockwave. The estimated density gradient in this tunnel for a normal shockwave is of the order of 10^{-3} gm/cm^4, while in a conventional tunnel at the same Mach number but with atmospheric stagnation pressure the density gradient is of the order of 10^{2} gm/cm^4. However, analysis shows that detection of the very low density gradient by the schlieren technique is possible through careful design and handling of the optical system. Detailed discussion of the schlieren technique is given in Appendix C.

The system designed and built has an estimated theoretical sensitivity of 1.4×10^{-4} radian, while the estimated deflection of the light beam in traversing the tunnel with a normal shock at M = 1.5 is 1.3×10^{-3} radian. (See Appendix C). Using this apparatus under actual operating conditions the shockwaves are barely discernible to the eye. Diffraction at the knife-edge and noise in the system are the main causes for the poor sensitivity as compared to the theoretical estimate. Photographic technique is therefore depended upon to

produce useful results. By exposing fine-grain, high contrast, blue-sensitive film to high intensity spark illumination (discharge of 1.75 μf condenser charged to 20 kv.) tolerably satisfactory results are produced, as shown in Fig. 10.

6. Sealing and Evacuation

Air must be removed from the entire interior of the tunnel circuit in order that there may be no contamination of the working fluid. As the pressures in all parts are below atmospheric, sealing becomes of prime importance. High vacuum techniques are well developed in the field of physics. The best comprehensive coverage of the techniques and equipment may be found in the work of Dushman (Ref. 1). The adaptation and modification of the physicist's techniques to wind tunnel construction in which large metal vessels are involved is given by Horning (Ref. 13) in connection with the research on slip flow and free molecule flow at the University of California.

Considerable difficulty has been encountered in the sealing and evacuation of the equipment, due mainly to lack of experience. Therefore, a few observations and conclusions may be of interest here. In general, the size and number of joints must be kept to a minimum. Careful soldering and welding of metal joints are essential, though not difficult to achieve. Movable metal-to-metal joints are best sealed by the use of O-rings held between machined surfaces, finished to an average roughness of no more than 32 microinches (Ref. 14). Rubber tubing is usually not reliable. For the low pressure levels in this tunnel (about 5 mm. Hg. minimum) Tygon tubing over metal or glass fittings are sufficient for sealing. Static joints need no sealing compound

or lubricant; while moving seals require a small amount of vacuum grease, although care must be taken to prevent the grease from flowing into the tunnel when the grease melts at high temperatures. Flared copper tubing joints are safe only when the flaring is very carefully done, and not considered safe after disassembling. The same is true of tapered thread fittings (pipe fitting). To insure sealing all flared and pipe fittings should be painted with glyptal lacquer.

Leak detection is a very annoying problem. Large leaks can be detected by noise, which can be accomplished very simply by inserting one end of a tube in the ear and probing the vessel surface with the other. Pressurizing the vessel and detecting leaks with soap solution is a simple method, but does not necessarily locate all leaks, because some of them may only be open in one direction. Standard leak detection techniques are described by Strong (Ref. 2) and Guthrie (Ref. 15). The high-potential ionization method (Ref. 2) cannot be used with conducting vessels. The tracer gas mass-spectrograph method (Ref. 15) is very expensive. Therefore, the only method that can be used now is the soap bubble test, even though there is no assurance of perfect detection.

The evacuation of the tunnel is not too difficult a problem, since the pressure level is not very low; and an ordinary mechanical vacuum pump can be used. However, there is the problem of water vapor being mixed with the air pumped out. If the amount of vapor is small, no great harm is done to the vacuum pump. But in this case as the total pressure approaches the vapor pressure of the water, the mixture entering the pump is nearly all water vapor. Therefore, some means of water removal must be used to protect the pump.

The mixture from the tunnel enters a vapor trap where the low temperature (about -40°C) causes the water vapor to freeze to ice. From here on the partial pressure of the water vapor is equal to the vapor pressure of ice at -40°C, which is very small, 0.0966 mm.Hg. This small amount of water is taken out by a desiccant ($CaSO_4$) before it reaches the pump. An indicating agent which turns from blue to red when it is saturated with water, is mixed in the calcium sulphate as a safety device.

A slow but inexpensive device can be used for the evacuation from atmospheric pressure down to the neighborhood of 50 mm.Hg. This is the water driven aspirator, which, of course, needs no protection from water contamination. The theoretical limit of vacuum attainable with such a device is the vapor pressure of the driving water. However, in practice the lowest pressure reached with the driving water at 20°C (vapor pressure 17 mm.) is 42 mm. Therefore, a vacuum pump (Cenco Hyvac) is used from about 50 mm. down to the vapor pressure of the water in the tunnel.

The total volume to be evacuated is approximately 400 liters, and the evacuation time, using the aspirator and then the pump, is about two to three hours, depending on the sealing conditions. Due to poor welding joints in the boiler, and, to much lesser extents, other undetected leaks in the system, the tunnel has an average leak rate (at nominal pressure of 30 mm.) of 2 mm. per hour, which does not affect the operation of the tunnel for short intervals. For extended operation the pump is kept on to remove the entering air. Assuming all the leakage takes place upstream from the nozzle, the rate of contamination at the above mentioned leak rate is about 10^{-4} gm./sec., which

is very small compared to the mass flow of 2 gm./sec.

7. Operation of the Tunnel

Since the tunnel operates on a cycle very unlike that of a conventional wind tunnel, it is of value to describe in some detail the procedure devised for starting and regulating the flow.

7.1 Starting the Tunnel

When the boiler is free of air the heaters are turned up to partial load in order to warm up the walls of the tunnel and to bring the boiler to the temperature corresponding to the desired stagnation pressure. This is necessary to prevent condensation of the water vapor on the cold walls during the initial period of flow when the pressure downstream of the stagnation chamber is not yet low enough to prevent condensation on encountering room temperature. A subsonic, or partially supersonic flow will result. When the desired p_o and T_o are reached, and the tunnel walls warmed up, the exit valve of the nozzle is closed to build up a pressure differential between the boiler and the condenser. When the valve is closed the refrigerator is kept on (but the boiler and superheater are turned off) to condense the water vapor and so reduce the pressure in the condenser. At the same time the vacuum pump is used to remove any of the air left in the condenser. With the condenser pressure dropping and the boiler pressure remaining constant, a difference is built up across the valve. When the pressure ratio reaches about 3, the heaters and condenser are turned up to operating levels, the valve is opened quicky and supersonic flow is established.

The stagnation pressure and temperature are regulated by the heat input of the boiler and superheater respectively. With the present arrangement of electrical heaters, the pressure control is fairly sensitive; a setting to within 1 mm. Hg. can be accomplished in a few minutes, after the operator gains some experience in manipulating the autotransformer. The temperature control shows considerable lag, but is not a serious matter as the stagnation temperature is not critical as long as there is no condensation in the test section.

7.2 Mach Number Determination

In the beginning the Mach number was determined by using Equation (B-2). However, this was soon discovered to be erroneous when the Mach number so determined did not check the angle of the shock wave far away from the nose of a wedge. Apparently there is about a 10 per cent loss in stagnation pressure between the boiler and the test section. This is not surprising when one considers that, as a result of the low Reynolds number, about 30 per cent of the area of a cross-section normal to the flow is made up of boundary layers, with the resultant dissipation of kinetic energy into heat. Further, the high stagnation temperature ($180^{o}C$) causes the walls of the nozzle to be at much higher temperatures than the surrounding atmosphere, resulting in heat loss which takes energy out of the flow, making it non-adiabatic.

By taking the local stagnation pressure behind a normal shock, and the local static pressure, the Mach number can be determined by the equation (Rayleigh Formula)

$$\frac{p_o'}{p} = \frac{\left(\frac{\gamma+1}{2} M^2\right)^{\frac{\gamma}{\gamma-1}}}{\left(\frac{2\gamma}{\gamma+1} M^2 - \frac{\gamma-1}{\gamma+1}\right)^{\frac{1}{\gamma-1}}} \tag{25}$$

This is the method used now to determine Mach numbers. Fig. 11 shows two profiles of Mach number in the test section, made by traversing the section from one nozzle plate to some point near the center line.

The accuracy of the Mach number depends on the pressure measurements. The accuracy of the absolute pressure measurement is about $\pm$ 0.2 mm. Hg, and the accuracy of the manometer readings is about $\pm$ 0.1 mm. Hg. The resulting accuracy in the Mach number is about $\pm$ 0.015. Errors due to viscous effects will be discussed in Section 12.21.

7.3 Pressure Recovery and Maximum Mach Number Attainable

As noted in Fig. 5 the design pressure in the condenser is estimated on the basis of 50 percent recovery from the test section to the exit of the diffuser, that is,

$$p_2 - p_1 / p_o - p_1 = 0.5$$

This was thought to be conservative during the design stage. Actual results show that the pressure recovery is only about 20 percent. In fact, by the time the flow reaches the downstream end of the nozzle it has as much static pressure as in the condenser, so that the diffuser is apparently ineffective.

There is a lower limit to the condenser pressure, and hence an upper limit to the maximum Mach number attainable with a given stagnation pressure. Although theoretically it is possible to descend

to the triple point, $T = 0^{\circ}C$, $p = 4.6$ mm. Hg., in practice the condenser temperature must be set a few degrees above zero in order to have some efficiency in the heat transfer to the cooling vanes without ice formation. Therefore, a practical lower limit is about $8^{\circ}C$, corresponding to 8 mm. pressure, and, with a 20 per cent pressure recovery, this would mean a maximum attainable Mach number of 2.24 at $p_o = 30$ mm. To reach higher Mach numbers it would be necessary to resort to higher stagnation pressures, which means higher mass flow and power requirement.

7.4 Typical Operating Conditions

Operating data for two typical runs are outlined below:

Mach number	1.68	1.80
Reynolds number	4800	4250
Stagnation Temperature	$180^{\circ}C$	$224^{\circ}C$
Stagnation pressure	30.3 mm. Hg.	33.2 mm. Hg.
Static pressure	5.9	6.7
Condenser pressure	11.0	10.4
Boiler power	3.8 kw	3.0 kw
Superheater power	0.9	1.7
Condenser power	2.2	2.2

The Mach number is computed from the Rayleigh formula, (Equation (25), using the static pressure measured on the wall of the test section and the total head measured by a probe. The mass flow can be estimated from the boiler power input. The temperature of the boiler being fairly close to room temperature there is not much

loss of heat to the room air, so that all the power input of the boiler heaters may be counted as having gone into the evaporation of the water. On this basis the estimated mass flow is 1.7 gm./sec. The superheater is at a temperature much higher than that of the boiler, therefore, with the way these two parts are assembled in proximity, some of the superheat heat must be transferred to the boiler by conduction of the metal vessel. Taking this effect into account the mass flow just estimated is probably too low. By using the size of the nozzle and the data on the flow conditions the mass flow is computed to be 2.0 gm./sec. This is likely to be high, as no allowance is made for the reduction due to boundary layers. The correct value of the mass flow is, therefore, taken to be between 1.7 and 2.0 gm./sec.

PART II

CURVATURE OF AN ATTACHED SHOCKWAVE NEAR THE LEADING-EDGE OF A WEDGE

8. The Curved Shockwave

When a supersonic flow is deflected by a curved boundary, convex in the direction of the initial deflection, an attached curved shockwave is formed if the initial deflection is below the detachment angle for the Mach number of the flow ahead of the deflection. The flow, after the initial deflection, expands along the convex surface through a series of expansion waves which intersect the shockwave and are reflected from it back to the surface which again reflects them. These expansion waves also intersect one another. The resulting flow field is thus seen to be quite complicated.

In the flow of a viscous fluid a boundary layer is built up along the surface of the wedge, resulting in an effectively curved surface. If the displacement boundary layer were taken literally as a solid surface replacing the flat surface of the wedge or plate, the shape of the shockwave could be determined. The justification for making such an assumption may be seen in the work of Van Dyke (Ref. 16), who shows that, to the second order, the flow field outside the boundary layer in the impulsive motion of an infinite plate in a viscous, compressible fluid is the same as that produced in an inviscid fluid by a solid piston moving according to the displacement thickness of the boundary layer. But in reality there must be interaction between the shockwave and the boundary layer. The expansion waves from the effective convex surface are reflected from the shockwave, and the subsequent changes in the pressure and velocity field behind the

shockwave affect the boundary-layer structure. Furthermore, in the immediate neighborhood of the leading-edge, where the shock-wave and the boundary layer intersect, there is an even stronger interaction effect. At Reynolds numbers normally encountered in a conventional medium Mach number tunnel the attached shockwave on a wedge is straight except for a very small portion close to the leading-edge. The dimension of this curved portion is so small compared to other characteristic lengths involved that the shock-wave is considered straight altogether. However, there must presumably prevail conditions of the flow in which the curved portion of the shock is not negligible--or, in other words, in which the influence of the initial curvature in the boundary layer as well as the interaction effects of the shock wave and the boundary layer result in non-uniform flow over an appreciable portion of the wedge surface.

For ease of treatment of the problem the interaction region is divided into two parts--an outer-region in which the reflected waves from the shockwave are assumed to have negligible effects on the boundary layer; and a sub-region in which the shockwave and the boundary layer interact very strongly, so that they cannot be treated as two distinct phenomena. These regions are illustrated in Fig. 12. The limit of the outer-region can be readily set at some point on the shockwave where its radius of curvature is very much larger than some characteristic dimension in the flow. The sub-region is rather difficult to define, because the interaction problem is not easily solved. For our considerations here, however, it will

be assumed to extend several times the thickness of the shockwave from the leading-edge. The validity of such an assumption will later be checked against the experimental results.

8.1 Limits of the Outer-region and the Sub-region

8.11 The Outer-region

The validity of the existence of the outer-region depends on the validity of the assumption that there is no effect on the boundary layer from the waves reflected from the shockwave. That such an assumption is justified can be seen from the work of Chu in Ref. 17. Chu finds that a Mach wave is reflected from a shockwave with the same sign but with diminished strength. He defines a reflection index (or a damping factor) as

$$\sigma = \frac{TAN\ \lambda - TAN\ \beta^*}{TAN\ \lambda + TAN\ \beta^*} \tag{26}$$

where

$$TAN\ \lambda = \frac{\left[1 + \frac{\gamma-1}{2} M_1^2\ SIN^2(\beta-\theta)\right] SIN^2(\beta-\theta)}{\left(1 - \frac{1}{M_1^2}\right)\left[1 + \frac{\gamma-1}{2} M_1^2\ SIN^2(\beta-\theta)\right] + \left[\gamma M_1^2\ SIN^2(\beta-\theta) - \frac{\gamma-1}{2}\right] COS^2(\beta-\theta)} \tag{27}$$

and M_1 is the Mach number of the flow ahead of the shockwave.

Equations (26) and (27), when applied to conditions prevailing in our experiments, yield values of σ which are less than 10^{-2}.

With this small value of σ our assumption of zero feed-back is valid, unless the waves from the boundary are very strong, in which case the expression for σ is no longer valid, and the strength of the reflected wave, even after being diminished, may still be large enough to affect the boundary-layer structure. It is therefore necessary

to investigate at this point the strength of the expansion waves from the convex surface of the boundary layer.

Since the slope of the boundary layer changes continuously the strength of the expansion wave (or the rapidity of the continuously increasing expansion) can only be judged relative to some other quantity. A suitable comparison is that between the radius of curvature of the boundary layer, C_b, and the distance, D, along the Mach line from the boundary layer to the shockwave, as shown in Fig. 13.

D can be computed approximately, using Fig. 13 (see also Appendix A), by the expression

$$D = \frac{4}{\gamma+1}\left(1 - \frac{1}{M_1^2}\right)\frac{x}{M_1\theta} \tag{28}$$

where x is the distance from the leading-edge measured in the direction of the undisturbed flow.

C_b can be computed by using an expression for the displacement boundary-layer thickness,

$$\delta = \frac{B\sqrt{x}}{\sqrt{Re_o}} \tag{29}$$

where B is a coefficient dependent upon the Mach number and the properties of the fluid.

Then

$$\theta = \frac{d\delta}{dx} = \frac{B}{2}\frac{1}{\sqrt{Re_o\, x}} \tag{30}$$

and

$$C_b = \frac{1}{\frac{d^2\delta}{dx^2}} = \frac{4\sqrt{Re_o}}{B}\, x^{3/2} \tag{31}$$

It should be noted here that the quantity Re_o, as defined on p. 3, has

the dimension $\frac{1}{cm}$.

We may use the criterion that a wave is considered weak if

$$C_b/D \geq 1$$

In our case, combining Equations (31) and (28),

$$\frac{C_b}{D} = \frac{\gamma+1}{2} \frac{M_1}{\left(1 - \frac{1}{M_1^2}\right)} \tag{32}$$

which is always greater than unity as long as $M_1 > 1$. The case for M_1 1 is irrelevant, since we are only concerned with a flow which is not only supersonic ahead of the shock, but behind as well.

With the validity of the zero feed-back assumption established, we may now proceed to find, for a practical case, the extent of the region in which there is measurable curvature of the shockwave.

Equation (A-18) gives the radius of curvature of the shockwave as a function of the radius of curvature of the boundary:

$$C_S = \left(\frac{4}{\gamma+1}\right)^2 \frac{(M_1^2-1)^2}{M_1^5} \frac{C_b}{\theta} \tag{A-18}$$

For the case of a wedge θ is the sum of the wedge angle, θ_o, and the slope of the boundary layer, $\frac{d\delta}{dx}$.

Combining Equations (A-18), (31) and (30), we have

$$C_S = \left(\frac{4}{\gamma+1}\right)^2 \frac{(M_1^2-1)^2}{M_1^5} \frac{4\sqrt{Re_o}\, x^{3/2}}{B\left(\theta_o + \frac{B}{2\sqrt{Re_o}} \frac{1}{\sqrt{x}}\right)} \tag{33}$$

The limiting radius of curvature must be taken relative to some characteristic length in the experiment. In the present case this is taken as a distance that can be measured with good accuracy. Specifically, this distance is taken as 10^{-1} cm. The limiting ratio C_s/x is taken to be 10^3, that is to say, a radius of curvature of 10^2 cm. is

considered measurable.

For the sake of estimate only, we may consider the limiting case of a flat plate at zero angle of attack, so that $\theta_o = 0$.

Then

$$\frac{c_s}{x} = \frac{8}{B^2}\left(\frac{4}{\gamma+1}\right)^2 \frac{(M_1^2-1)^2}{M_1^5} Re_o \, x \qquad (34)$$

From this we see that at a given distance from the leading-edge the curvature of the shockwave decreases with the Reynolds number. Therefore, to assure that there be measurable curvature within some easily measured distance from the leading-edge, we must impose an upper limit on Re_o for any given Mach number M_1.

The relationship that must be satisfied by Re_o and M_1 to produce sufficient curvature in the shockwave is then

$$\frac{(M_1^2-1)^2}{M_1^5} Re_o \leq \frac{B^2}{8}\left(\frac{\gamma+1}{4}\right)^2 \left(\frac{c_s}{x}\right)_m \frac{1}{x_m}$$

The following values may be assumed for our experiments:

$M_1 = 2$

$B = 3.3$*

$\gamma = 1.33$

$\left(\frac{c_s}{x}\right)_m = 10^3$

$x_m = 10^{-1}$ cm.

The upper limit on Re_o then becomes

$$Re_o \leq 16{,}000$$

8.12 The Sub-region

As we approach the leading-edge several considerations will

---

*See Section 10 for the derivation of B.

cause our arguments regarding the shockwave curvature to break down. Even if interaction effects were not strong the assumptions leading to the expressions for the slope and curvature of the boundary layer, Equations (30) and (31), become invalid as the Reynolds number becomes very low. On this basis we should limit the sub-region by a length that corresponds to a Reynolds number of, say, 100. With $Re_o = 5,000$, this means a distance of 2×10^{-2} cm.

Looking at the situation more realistically, however, we must define the sub-region in terms of the effects of interaction between the shockwave and the boundary layer very near the leading-edge. We will not attempt to solve this interaction problem, but, instead, will try to establish from experimental data the extent of the sub-region. However, as an approximate guide in the choice of configuration in the experiment, we may set the limit of the sub-region at, say, ten times the thickness of the shockwave. Near the leading-edge the effective slope of the boundary is increasing rapidly, so that the shockwave must become almost normal. Therefore we will use the approximate expression for the thickness of a normal shock given in Appendix A.

$$\tau = \frac{2 M_1}{Re_o (M_1 - 1)} \qquad \text{(A-8)}$$

The extent of the sub-region thus defined is then

$$x_\ell = \frac{20 M_1}{Re_o (M_1 - 1)}$$

In practice x_ℓ should be small compared to x_m, so that the extent of the region useful for measurements will be adequate. Setting an upper limit on x_ℓ then furnishes a lower limit on Re_o.

Suppose we set

$x_\ell \simeq 3 \times 10^{-2}$ cm.

Then we have as a lower limit on Re_o

$Re_o \geq 1,300$

Thus, by setting the limits on the extent of a usable influence region we are able to establish an upper and a lower limit on the Reynolds number for a flow at a Mach number of 2.

Using the actual operating Reynolds number of $Re_o = 5,000$ and $M_1 = 1.7$, we find that the limits of the outer-influence region are

$x_\ell = 10^{-2}$ cm.

$x_m = 3 \times 10^{-1}$ cm.

9. The Problem to be Investigated

The experiments which are to be described in the ensuing sections have been devised to verify the validity of the explanation given above regarding the nature of the shockwave curvature near the leading-edge of a wedge. The geometry of the shockwave is determined from schlieren photograph of the flow field about the wedge. We then deduce the shape of the effective boundary which would give rise to such a shockwave geometry, working under the assumption (as elucidated in the preceding sections) that the presence of the shockwave does not affect the structure of the boundary layer as it exists in a uniform flow over a flat plate. The study is carried as close to the leading-edge as is feasible with the experimental data, thus furnishing some measure of the extent of the sub-region in which the Prandtl boundary-layer assumptions are not valid, and where there are strong interaction effects between the shockwave and the boundary layer.

Since in the way we have formulated the problem the slope of the boundary, θ, is the significant factor in determining the slope of the shockwave, the comparison between experiment and theory may well be carried out at the boundary instead of at the shockwave. In other words, the slope of the effective boundary is deduced from the experimentally determined slope of the shockwave, and is then compared to the theoretically computed slope. As far as the thickness of the boundary layer is concerned, it is, by this method, indeterminate to the extent of a constant which would be zero if we were to carry the procedure to the leading-edge.

9.1 Other Investigations Relevant to the Present Work.

The conditions at a sharp leading edge in supersonic flow have in one case been investigated by Bardsley (Ref. 18), who studied the flow in the expansion region of a wedge at a sufficiently high angle of attack that one side of it is an expansion region. A shock wave was observed ahead of the expansion and this could be caused by one of three reasons: growth of the boundary layer near the leading edge, separation of the boundary layer, or bluntness of the leading edge. In Bardsley's experiments the distance from the leading edge at which the theoretical boundary-layer slope was sufficient to cause a shock-wave of the strength observed was approximately 8×10^{-4} cm., which was of the same order as the bluntness of the leading edge. The possibility of boundary-layer separation and reattachment (as observed by Liepmann, Ref. 19) was discounted because there was no shock-wave at the end of the expansion. The observed shockwave strength appeared to be constant over a wide range of expansion angles

(0° to 10°). Bardsley thus concluded on the basis of the experimental evidence that the condition of a shockwave preceding an expansion over a wedge was the result of the bluntness of the leading edge.

The Reynolds number of the experiments just mentioned was 1.34×10^{5} per cm., so that the influence of viscosity was not easily observable. In the present investigation the Reynolds number is lower by two orders of magnitude. It is expected that viscous effects will become more amenable to experimental perusal.

10. Procedure of the Investigation

If the slope, β, of the shockwave at a point is known, as well as the Mach number ahead, the Mach number behind the shockwave, and, consequently, the angle (referred to the direction of the undisturbed flow) of the Mach line there, β', can be determined from the shock polar. In our approximation of the flow field behind the shock there are no reflections of the Mach waves, so that the field can be regarded as consisting of a number of simple waves. Therefore, Mach lines can be drawn from points on the shockwave where the Mach numbers (behind the shock) are known, thus dividing the field into a number of uniform fields. The slope of the boundary at the point intersected by one of these Mach lines can be taken as that which causes a shock of such a strength to be formed as to produce a flow field corresponding to that behind this Mach line. This is illustrated in Fig. 14, in which the effective boundary is a number of polygonal segments, 1', 2', 3', etc. The slope of the shockwave at the point 1 is β_1. M_1 and β_1 determine the angle of the Mach line, β_1', and

the slope of the boundary at 1', θ_1. The angle of the wedge is θ_o. The slope of the boundary layer, measured from the wedge surface, is then $(\theta - \theta_o)$.

For comparison with theory the Howarth solution (Ref. 20) to the Prandtl boundary layer in a viscous, compressible flow is used, because it gives a simple expression for the thickness of the displacement boundary layer.

The displacement boundary layer thickness is defined as

$$\delta = \int_o^\infty \left(1 - \frac{\rho u}{\rho_\infty U}\right) dy \tag{35}$$

where u and U are the velocities (in the direction parallel to the free-stream), and ρ and ρ_∞ the densities in the boundary layer and in the free-stream respectively.

Under the following assumptions,

(a) zero pressure gradient,

(b) insulated wall,

(c) Prandtl number unity,

and (d) viscosity proportional to absolute temperature, proceeding from the Howarth solution, it can be shown that

$$\frac{\delta}{\delta^*} = 1 + \frac{\gamma - 1}{2} M^2 \left(1 + \frac{\theta^*}{\delta^*}\right) \tag{36}$$

where δ^* is the displacement thickness and θ^* the momentum thickness in incompressible flow, given by the Blasius solution (Ref. 21) as

$$\delta^* = 1.73 \frac{\sqrt{x}}{\sqrt{Re_o}} \quad , \quad \frac{\theta^*}{\delta^*} = 0.386$$

Hence

$$\delta = \frac{B\sqrt{x}}{\sqrt{Re_o}} \tag{37}$$

where

$$B = 1.73 \left[1 + 0.693 (\gamma - 1) M^2\right] \tag{38}$$

M in this expression is the free-stream Mach number, which in our case is the Mach number, M_2, behind the shockwave. Since we assume constant Mach number for the flow outside the boundary layer, and in reality the flow is non-uniform, we shall assign some fixed value of M_2 to the computation of the effective slope. This fixed M_2 will be taken as the average Mach number within the region covered by the experimental results. Strictly speaking, the Reynolds number should also be computed on the basis of the flow conditions behind the shockwave. But under the conditions prevailing in our experiments the change in Reynolds number in going through a shockwave is quite small. Therefore, in the expression for δ^* the Reynolds number is a constant, equal to that of the flow ahead of the shockwave.

The slope of the effective boundary is, finally,

$$\theta = \theta_o + \frac{B}{2} \frac{1}{\sqrt{Re_o x}} \tag{39}$$

11. Description of the Experiment

The experimental work undertaken to show the effect of the boundary layer on the shock wave slope consists essentially of measurements of the geometry of the shockwaves as shown on schlieren photographs. The shockwaves are produced by one of three wedges of total angles 7.0°, 14.6° and 19.8°. Fig. 15 shows the three wedges. The width of the wedge does not span the test section. It is arbitrarily chosen to be 0.26 cm. less than the test section width of 2.06 cm. in

order to approximate two-dimensional conditions by having the tips of the wedge out of the side-wall boundary layers. The struts serve also as pressure leads, with orifices on the wedge surfaces. The pins are placed near the tips and equidistant from the leading edge to aid in aligning the light path of the schlieren system parallel to the leading edge. The wedges are ground and lapped to nose radii of approximately 2×10^{-4} cm., which is considered sufficiently small since it is of the same order as the mean free path.

With the flow established, the wedge is turned until the two pressure taps show equal readings, indicating zero angle of attack. The Mach number is determined by measuring the total head just in front of the shock near the nose of the wedge and the static pressure on the nozzle wall. Space limitation does not allow another pressure probe near the total head probe to pick up the local static pressure. The effect of this on the accuracy of the Mach number determination will be discussed in Section 12.21.

Some typical results of the schlieren photography are shown in Fig. 10. These are enlarged about ten times. For actual measuring of the shockwave shape the film is placed in a viewer with a 20:1 magnification (Recordak) and the image on the screen traced onto translucent paper. A typical tracing is reproduced in Fig. 16.

12. Experimental Results

12.1 Test Configurations

The following configurations are executed:

Half-wedge angle $\theta_o = 3.5^o$

M_1	Re_o
1.58	4900
1.59	4800
1.63	4800
1.64	5100

Half-wedge angle $\theta_o = 7.3^o$

M_1	Re_o
1.64	4600
1.67	4500

Half-wedge angle $\theta_o = 9.9^o$

M_1	Re_o
1.84	5500
1.88	5500

12.2 Results and Discussion

Schlieren photographs of the above runs are shown in Figs. 17 - 20. Plots showing the slope of the boundary deduced from the shockwave geometry compared to the slopes computed from Equation (39) are given in Figs. 21 to 24. In each figure the solid line is the slope computed from Equation (39), using the average Mach number behind the shock. The dotted line is the incompressible solution. The parabolic increase of the effective slope of the boundary is evident in all the results. The scatter of the experimental points is considerable, though not so high as to preclude the drawing of some qualitative conclusions.

In discussing the results one must bear in mind that they are only qualitative. Many approximations enter into the solution leading to the computation of δ. Howarth (Ref. 19) indicates that the assumptions of $Pr = 1$ (for water vapor in our operation range $Pr = 0.73$)

and $\mu \sim T$ lead to an overestimate of the viscous effects, resulting in a thickness larger than the actual value; while the incompressible flow assumption underestimates the effects of viscosity. This does not seem to be borne out by the results presented in Figs. 21 to 24, where the experimental points lie mostly above the computed incompressible and compressible curves. The explanation for this is not yet evident.

12.21 Effects of Interaction between the Shockwave and the Tunnel Wall Boundary Layer

In addition to the discrepancies inherent in the manner of comparison discussed above, there are other factors in connection with the experimental methods. First of all, there are the questions of the uniformity of the flow ahead of the shockwave, and the accuracy of the Mach number determination. The uniformity of the flow in the test section without the wedge is demonstrated by the Mach number profiles in Fig. 11. Any changes in the flow upstream of the shockwave produced by the presence of the wedge must be due to shockwave, boundary-layer interaction (barring choking, of course). It is shown in Ref. 22 that when a shockwave intersects a laminar boundary layer there is a thickening of the latter upstream of the point of intersection, attended by a pressure rise in the boundary layer extending upstream many times the boundary-layer thickness (about 30 times in some instances). In the present low Reynolds number set-up, the boundary layer on the tunnel wall being quite thick, the influence of a shockwave hitting the tunnel wall may extend upstream by 5 or 6 cm. The result is a continuous compression

zone ahead of the point of intersection. The situation is illustrated in an approximate scale sketch in Fig. 25. With this compression zone the flow field ahead of the shockwave is no longer uniform, and the Mach number determined from a total-head measurement in the center of the test-section and a static pressure taken at the wall will be lower than the true value at the position of the total-head tube.

Some estimate of the extent of the interaction effects can be made from the results of some static pressure surveys by a probe through a shockwave. These results are shown in Fig. 26, in which p_1 is the lowest pressure measured ahead of the shock and p_2 the highest after the shock. It is seen that the pressure begins to rise about 0.75 cm. upstream of the intersection of the shockwave and the probe. The boundary-layer thickness, δ, on the probe at the point of intersection in this case is estimated to be about 0.08 cm. The upstream influence can therefore be considered to extend, very roughly, 10 times the boundary-layer thickness. On the tunnel wall the thickness of the boundary layer is about 0.2 cm. (see Fig. 11) so that the upstream pressure rise will begin about 2 cm. ahead of the intersection of the shockwave from the wedge and the wall boundary layer. On this basis the pressure on the wall 0.9 cm. ahead of the intersection is estimated to be about 8.4 mm. Hg. The actual reading taken at an orifice at this point is 8.6 mm.

Now we may examine the effects of shockwave, boundary layer interaction on the shockwave curvature we have undertaken to investigate. The effect of the compression zone is to cause the shockwave (if it were straight to begin with) to become concave in the upstream

direction, which is contrary to the observed curvature. But the curvature of the shock caused by the boundary layer on the wedge can be reduced if there is a compression zone ahead of the shock. However, the portion of the shockwave of which we have measured the slope is mostly outside the compression zone, as may be seen in Fig. 25.

The probable error in Mach number (as determined from total-head taken in free-stream and static pressure taken at wall) due to the pressure rise on the tunnel wall because of shockwave, boundary-layer interaction is estimated to be about $-5^{o}/o$. The subsequent error in the slope of the effective boundary is about -2 deg. in the range covered by our data.

12.22 Other Sources of Inaccuracy

The geometry of the shockwave cannot be determined very accurately, for it is quite thick and not well defined in the photographs. A theoretical estimate of the shockwave thickness indicates it to be of the order of 10^{-2} cm. A very rough estimate from the schlieren photographs shows that the thickness is about 10^{-2} cm. In the tracing the shockwave is drawn through the approximate center of the thickness. Near the nose the proper consideration of the shockwave geometry is especially difficult for the photographs all show the center of the shock to be slightly ahead of the leading edge, resulting in the question whether the shock is always detached. The distance separating the leading edge and the shock is estimated to be about 5×10^{-3} cm., which is ten times the mean free path. If

we pause here to recall that the theories considered so far dealing with gas dynamics treat the gas as a continuum, so that macroscopically it seems reasonable to consider as the ultimate in distance (zero distance) a dimension of at least the mean free path. In this sense a shockwave that starts apparently from within 10λ of the leading-edge may be considered attached to it.

Diffraction patterns (cf. Appendix C) at the leading-edge confuse the field considerably, so that it is not as easy to ascertain the shape of the shock there as it is some distance away from the leading-edge.

13. Concluding Remarks

Limitations of the small size of the tunnel preclude the possibility of deducing the boundary-layer slope farther than about 10^{-1} cm. from the leading-edge. As may be surmised from the discussions of Section 8.1 regarding the validity of our basic assumptions leading to the simple model of the phenomenon under study, the discrepancy between experiment and theory should increase with increasing wedge angle, θ_o. The general trend in our results, comparing Figs. 21 - 24, tends to verify this. In these results we also find that the discrepancy is no larger at a distance from the leading-edge of about 10^{-2} cm. than it is farther downstream, indicating that our estimate of the extent of the sub-region (cf. Section 8.12) is of the right order of magnitude. It should be noted that at this distance the Reynolds number is only about 50, which would place the flow in the slip-flow regime, invalidating the boundary-layer solution we have used

in the present study.

The difficulties attending the experiments have not permitted extensive measurements within the available time. However, taking account of all the heretofore-mentioned approximations and inaccuracies, the results of this study do indicate that it is possible for an attached shockwave on a wedge in uniform supersonic flow to display curvature as a result of the growth of the boundary layer on the wedge surface.

APPENDIX A

Shockwave Thickness and Curvature

1. Shockwave Thickness

1.1 Normal Shock

Consider a flow which is near sonic, so that we may write for the velocity

$$u = a^* + u_1 \tag{A-1}$$

where $u_1/a^* << 1$.

If a normal shock occurs in this flow, the velocity downstream of the shock, to the same approximation as above, is

$$u' = a^* - u_1 \tag{A-2}$$

If u_s is the perturbation velocity within the shock, we may define the thickness of the shockwave as

$$\tau = 2 \int_{-\infty}^{0} \left(1 - \frac{u_s}{u_1}\right) dx \tag{A-3}$$

It is shown in Ref. 23 that the thickness of this normal shock under the above restrictions is

$$\tau = 2 \log 4 \; \frac{\frac{4}{3} + (\gamma - 1) \frac{K^*}{c_p \mu^*}}{\gamma + 1} \; \frac{\nu^*}{u_1} \tag{A-4}$$

Using the transonic approximation

$$\frac{u_1}{a^*} = \frac{2}{\gamma + 1} (M_1 - 1) \tag{A-5}$$

where M_1 is the Mach number upstream of the shock, τ becomes

$$\tau = \log 4 \left[\frac{4}{3} + (\gamma - 1) \frac{K^*}{c_p \mu^*}\right] \frac{\nu^*}{a^* (M_1 - 1)} \tag{A-6}$$

This may be written approximately, assuming $K^*/c_p\mu^* = 1$ and

$\gamma = 1.33$,

$$\tau = \frac{2 v^*}{a^* (M_1 - 1)} \tag{A-7}$$

which is deemed a sufficient approximation for our purposes.

If we make the further approximation that

$$v^* \cong v$$

and

$$a^* \cong a$$

τ may be written in the dimensionless form

$$\frac{\tau}{\ell} = \frac{2 M_1}{Re_\ell (M_1 - 1)} \tag{A-8}$$

where ℓ is some characteristic length.

1.2 Oblique Shock

If, now, instead of a normal shock at $M_1 \cong 1$, we have an oblique shock caused by a deflection in the flow by a small angle θ, the Mach number normal to the shock is still nearly unity, while the Mach number in the direction of the flow is greater than one. In Equation (A-7) the Mach number M_1 should then be written as $M_1 \sin \beta$, where β is the angle the shockwave makes with the direction of the undisturbed flow. If $M_1 \cong 1$, v^* and a* can still be approximated by v and a.

The thickness (measured normal to the shock) of an oblique shock (for small θ) at angle β to the undisturbed flow may then be written as

$$\frac{\tau}{\ell} = \frac{2 M_1}{Re_\ell (M_1 \sin \beta - 1)} \tag{A-9}$$

In the above expressions the term sin β may be approximated

for small θ in the following manner, as developed in Ref. 24.

Referring to Fig. 13, let

$$\beta = \beta^* + \varepsilon$$

where $\sin \beta^* = 1/M_1$, and $\varepsilon/\beta^* << 1$.

It is shown in Ref. 24 that

$$\varepsilon = \frac{\gamma+1}{4} \frac{M_1^2 \theta}{M_1^2 - 1} \tag{A-10}$$

which is a good approximation for small θ and $\theta/\beta << 1$.

The conditions on θ and θ/β imply that the Mach number cannot be too much greater than one.

We can now write (A-9), by substituting (A-10), as

$$\frac{\tau}{\ell} = \frac{8\gamma}{\gamma+1} \frac{\sqrt{M_1^2 - 1}}{Re_\ell M_1 \theta} \tag{A-11}$$

If in the above equation the characteristic length is taken to be the thickness of the boundary layer, we have

$$\frac{\tau}{\delta} = \frac{8\gamma}{\gamma+1} \frac{\sqrt{M_1^2 - 1}}{Re_\delta M_1 \theta} \tag{A-12}$$

In a particular investigation one may be interested in the interaction of shockwave and boundary layer, in which case it would be convenient to consider the shockwave as a discontinuity while treating the boundary layer as a finite viscous region. This implies the restriction

$$\frac{\tau}{\delta} << 1$$

The Mach number and Reynolds number must then be limited by the relation

$$\frac{\sqrt{M_1^2 - 1}}{M_1 Re_\delta} << \frac{\gamma+1}{8\gamma} \theta \tag{A-13}$$

where θ is a small angle and M_1 is not much greater than unity.

2. Shockwave Curvature

Since, by our approximation,

$$\beta = \beta^* + \varepsilon$$

the use of Equation (A-10) yields

$$\frac{d\beta}{dx'} = \frac{\gamma+1}{4} \frac{M_1^2}{M_1^2-1} \frac{d\theta}{dx'} \tag{A-14}$$

where dx' is the differential distance along the shockwave.

If dx is the differential distance along the boundary, which in our approximation can be taken as being parallel to the undisturbed flow, it can be seen from Fig. 13 that

$$dx = dx' (\cos\beta - \sin\beta \cot\beta') \tag{A-15}$$

where $\beta' = \beta + \varepsilon'$ is the Mach angle (referred to the direction of the undisturbed flow) behind the shockwave.

It is shown in Ref. 24 that

$$\varepsilon' = \varepsilon$$

so that Equation (A-15) becomes, neglecting terms of orders higher than ε,

$$\frac{dx}{dx'} = \varepsilon M_1 \tag{A-16}$$

The curvature of the shockwave in terms of the curvature of the boundary is obtained by combining Equations (A-14) and (A-16):

$$\frac{d\beta}{dx'} = \left(\frac{\gamma+1}{4}\right)^2 \frac{M_1^5}{(M_1^2-1)^2} \theta \frac{d\theta}{dx} \tag{A-17}$$

If $C_s = \frac{1}{d\beta/dx'}$ and $C_b = \frac{1}{d\theta/dx}$ are the radii of curvature of the shockwave and the boundary respectively,

$$C_s = \left(\frac{4}{\gamma+1}\right)^2 \frac{(M_1^2-1)^2}{M_1^5} \frac{C_b}{\theta} \qquad \text{(A-18)}$$

It should be recalled that (A-17) or (A-18) is valid only for small θ and for M_1 not much greater than unity.

APPENDIX B

The Selection of a Working Fluid for a Wind Tunnel

1. General Considerations

To attempt a comprehensive analysis of wind tunnels it is necessary, among other things, to consider the performance requirements and the properties of a gas which govern its suitability in meeting these requirements. Paralleling these two sets of considerations are factors related to the mechanical and structural aspects of the equipment making up the total wind tunnel; these will not be dealt with in the present discussion, since the problems therein, such as nozzle design and power-plants, have been well covered in the literature.

The performance requirements of a wind tunnel are usually given in terms of the Mach number and the Reynolds number. Pertinent to the attainment of these are the considerations of stagnation pressure, stagnation temperature and power consumption. The range of Mach number used in research is about from 1 to 10, and Reynolds numbers (based on one centimeter) from 10 to 10^6. Theoretically there need be no limits on the maximum stagnation pressure and temperature, although in practice these have to be held to reasonable magnitudes which might be set at 500 atmospheres and 1000°K. A high stagnation temperature poses not only structural difficulties, but physical problems with the flow itself as well, which will be discussed in Section 2.

The properties of a gas which are pertinent to the consideration of its suitability for use as the working medium in a wind

tunnel are listed below:

Molecular weight
Specific heat
Ratio of specific heats
Boiling point
Critical point
Triple point
Heat of vaporization
Coefficient of viscosity
Thermal conductivity

2. Relationships Between the Properties and Thermodynamic State of Gas and Wind Tunnel Flow Parameters

The conversion of the thermal energy of random motion of the molecules of a perfect gas into kinetic energy of directed motion is governed by the equation

$$\frac{T_o}{T_1} = 1 + \frac{\gamma - 1}{2} M^2 \qquad \text{(B-1)}$$

in which T_o and T_1 are the stagnation and static temperatures, respectively*.

If this conversion of energy takes place isentropically, the stagnation and static pressures are related by the equation

$$\frac{p_o}{p_1} = \left(1 + \frac{\gamma - 1}{2} M^2\right)^{\gamma/\gamma-1} \qquad \text{(B-2)}$$

The Reynolds number (based on unit length) of the flow in the test-section is

$$Re_o = \sqrt{\frac{\gamma m}{R_o}} \frac{p_o M}{\mu \sqrt{T_o}} \left(1 + \frac{\gamma - 1}{2} M^2\right)^{-\frac{\gamma+1}{2(\gamma-1)}} \qquad \text{(B-3)}$$

where m is the molecular weight and R_o the gas constant for one mole.

The mass flow per unit test-section area is

---

*The subscripts correspond to those in Fig. 5.

$$Mf = \mu Re_o \tag{B-4}$$

The power consumption depends on the compression ratio, p_o/p_2 (where p_o is the stagnation pressure and p_2 the pressure at the exit of the diffuser) and the mass flow: (See Sect. 3)

$$P = Mf\ R\ Te\ \log \frac{p_o}{p_2} \tag{B-5}$$

At the present stage of development of fluid mechanics it is not yet possible to relate p_o/p_2 to the properties of the gas, the flow conditions and the geometry of the nozzle and diffuser, so that one can only find p_o/p_2 empirically. With this one exception, Equations (B-1) to (B-5) can be used (assuming a perfect gas) to relate the wind tunnel flow parameters to the properties and state of the working medium.

Before one can use these relationships there is one condition in addition which must be satisfied--that is, that there be no condensation of the working fluid in the nozzle. To deal with this we make use of the Clapeyron-Clausius equation

$$\frac{dp_s}{dT_s} = \frac{L}{T_s \Delta v} \tag{B-6}$$

In this expression L, the heat of vaporization, and Δv, the change in specific volume during evaporation, are not constants, and their dependence on p_S and T_S not explicitly known, so that it is not generally possible to give an integrated form relating the saturation pressure and temperature. However, to a first approximation, L may be assumed constant over a small range of pressure and temperature, and Δv may be considered equal to the specific volume of the gaseous phase, by which assumptions (B-6) can then be integrated,

giving

$$p_s = p_{cr}\, e^{-\frac{L}{R}\left(\frac{1}{T_s} - \frac{1}{T_{cr}}\right)} \tag{B-7}$$

Using (B-1), (B-2), (B-3) (with $\mu = \mu_1 T^{1/2}$) and (B-7) a relation is obtained for the minimum stagnation temperature (for condensation-free flow) as a function of Re_o and M:

$$T_o\, e^{\frac{L\alpha}{RT_o}} = p_{cr}\, e^{\frac{L}{RT_{cr}}} \sqrt{\frac{\gamma}{R}}\ \frac{1}{\mu_1}\ \frac{M\alpha^{3/2}}{Re_o} \tag{B-8}$$

where $\alpha = 1 + \frac{\gamma-1}{2} M^2$. With (B-8), (B-3) then gives the minimum stagnation pressure.

Thus it is seen that the minimum stagnation pressure and temperature depend not only on the boiling point but also on γ and R (or m) for given M and Re. The dependence of T_o/T_1, p_o/p_1 on γ is shown in Figs. 27 and 28. It follows that, in general, in the determination of the stagnation temperature boiling point is not the sole consideration. Substances with low boiling points are made up of molecules which have very little polarity in their external fields so that intermolecular attraction is very small compared to the forces due to thermal agitation. This means that low boiling substances have symmetrical, and in most cases, simple molecular structure. Simple structure results in a small number of degrees of freedom, and, according to the equipartition of energy, has a large value of γ, since $\gamma = n+2/n$, where n is the number of degrees of freedom of the molecule. A high value of γ means high T_o/T_1, according to Equation (B-1). In practice this is not a drawback, because the lowering of the saturation temperature outweighs the increase in T_o/T_1, and the resulting T_o in using a low boiling substance of high γ will, in

general, be lower than that of a higher boiling substance with a lower γ. The influence of γ on the pressure ratio p_o/p_1 is much greater, as is evident in Fig. 28.

2.1 Departure from a Perfect Gas

So far it has been taken for granted in using Equations (B-1) - (B-4) that the specific heats, and therefore γ, are constant for a particular gas. This is not strictly correct if the temperature of the gas varies over a wide range during the flow through a nozzle. The specific heat of a gas is a function of the temperature which determines the energy states of the molecules. Transitions between energy levels take place when the temperature is varied over sufficiently wide ranges. If the relaxation time of transition between energy levels is much smaller than the transit time of the molecules through the temperature gradients, the specific heat of the gas may be considered to be changing instantaneously and continuously. If, however, the relaxation time is relatively large, the specific heat may well be considered constant and equal to stagnation condition when the transit time of the molecules through the tunnel is very small. The relaxation times of gases vary considerably, depending on the kind of gas and the amount of impurities present. For instance, Kantrowitz (Ref. 25) finds that the vibrational relaxation time of steam without impurities is as small as 2×10^{-8} sec. and that of nitrogen with 0.05 per cent water is of the order of 10^{-3} sec.; while the rotational relaxation time of nitrogen, according to Griffith (Ref. 26), is less than 2×10^{-9} sec.

The scope of the present work does not allow any elaboration on the theory of molecular spectra and associated problems. However, introductory information may be found in such standard texts as

Richtmeyer and Kennard (Ref. 27) and Herzberg (Ref. 28). Suffice it here to mention that the error in the computed static temperature of a high-speed air flow (Equation (B-1)) as a result of varying γ, according to the work of Kestin (Ref. 29) is as high as 90°K. at a stagnation temperature of 1700°K. The effect of a varying γ on the static pressure is still larger, because γ appears in the exponent of Equation (B-2). Schetzer (Ref. 30) finds the error in the ratio p_o/p_1 to be 26 per cent at M = 6 when a constant value of 1.4 is used for γ.

3. Selection of the Working Fluid

For a specified Mach number the Reynolds number is proportional to the square root of the molecular weight and inversely proportional to the viscosity. The power consumption is inversely proportional to the square root of the molecular weight. Therefore, from the standpoint of attaining high Reynolds number with low power consumption, one should choose a substance with a large molecular weight. The decrease in the value of γ in case the heavy molecule is polyatomic has but slight effect on the Reynolds number, since γ can vary only between 5/3 and 1.

The importance of γ as a basis for choosing the working fluid does not become significant until the Mach number gets high, say above 5. Then from the power consumption viewpoint the selection should be a gas with high γ, since p_o/p_2 is in some way related to p_o/p_1 which depends on γ by Equation (B-2). A high γ, however, results in a high ratio T_o/T_1, which means that to avoid condensation a high T_o may be necessary, unless the substance has a very low boiling point. Such a favorable combination of properties--low boiling

point to give low T_o and high γ to give low p_o/p_1--does actually occur, as has been pointed out in the preceding section. (Cf. p65). Neon, for example, has a γ of 1.64 and a boiling point (at 1 atm.) of 27°K. Helium has a γ of 1.66 and boiling point (at 1 atm.) of 3°K.

Whereas for hypersonic operation the property affecting the choice of the working medium is the boiling point, one has wider choices if only medium Mach numbers are needed. If the tunnel is operated on a two-phase cycle one should take into account the critical and triple points of the working fluid. The pressure p_2 after the non-isentropic recompression must be higher than the triple point, p_{tr}, and lower than the critical pressure, p_{cr}, for, below the former, the vapor sublimates to a solid upon cooling, making the transfer back to the boiler difficult, and, above the latter, the gas cannot be liquefied by isobaric cooling.

4. Selection of the Working Fluid for a Two-phase Low Reynolds Number Supersonic Tunnel

With a design Mach number of 2 condensation presents no difficulty. Since the working fluid has to be liquefied, it is advantageous to choose a substance with a fairly high boiling point in order to simplify the cooling and refrigeration processes. The low Reynolds number requires operation at low pressure. A cursory survey of suitable substances shows that most of the low order alcohols, the low paraffins and their chloro and fluoro derivatives have boiling points not far from atmospheric at pressures of the order of 10 cm. Hg, fairly high molecular weights (from about 40 to 200) and thermal stability. Many of these substances--principally the chloro and fluoro derivatives

of methane and ethane (known commercially as Freons)--are non-inflammable and non-toxic. The latent heats of these are mostly under 100 cal/gm. Therefore, on the basis of low power consumption, reasonable operating pressures and temperatures, and safety, the Freons appear to be the best suited for our particular tunnel.

There is, however, another substance which is comparable to the Freons in all respects except power consumption. This is water, which has a latent heat of about 580 cal/gm. Because of the small size of the tunnel the absolute magnitude of the power consumption is quite small, so that the high latent heat of water does not pose any serious problem, while its ease of handling in other respects makes it quite desirable for use as the working fluid. The properties of water vapor pertinent to our considerations here are listed below:

Molecular weight	18
Specific heat at constant pressure	0.44 cal/gm. ^{o}C.
Ratio of specific heats	1.33
Latent heat of vaporization	580 cal/gm.
Coefficient of viscosity	1.4×10^{-4} poise
Thermal conductivity	5.2×10^{-5} cal/sec. cm. ^{o}C.
Critical pressure	218 atm.
Critical temperature	647^{o}K.
Triple point pressure	4.6 mm. Hg.
Triple point temperature	273^{o}K.

APPENDIX C

Analysis and Critical Design of a Schlieren System for Low Density Flow Visualization

1. Summary of Flow Visualization Methods

Under conditions of low density and small density gradient, when the use of the schlieren technique becomes rather ineffective for flow visualization, several other methods appear to be feasible, though possessing varying degrees of difficulty in execution. These are mentioned briefly here, with references to the literature for detail treatment.

The nitrogen after-glow technique is probably the best developed to date. When nitrogen is excited sufficiently a radiation in the visible spectrum persists for an appreciable period. The intensity of this radiation depends, aside from other factors, upon the density of the nitrogen. It is evident then that a sharp change in density can be detected visually by the change in intensity of the glow. Refs. 31, 32 and 33 describe details of the after-glow theory and technique. In physical mechanism opposite to the after-glow technique are methods of density measurement by absorption of radiation. X-ray absorption by high-speed air flow at normal densities has been explored by Winkler (Refs. 34 and 35) and Weltman (Ref. 36). At low densities the absorption by oxygen of radiation at 1450 $\mathring{A}$ may be useful for density measurement, as indicated by the work of Evans (Refs. 37 and 38). In the case of water vapor at low density the absorption of infra-red radiation appears to be a good method, since water vapor has very strong absorption bands at 1.4, 1.9, 2.8 micron. Infra-red spectroscopy work has been highly developed

in chemistry, so that the basic techniques can well be adapted to flow measurements. The chief problems that need be tackled in using infra-red absorption for density measurement are: (a) a strong source of monochromatic radiation in the range 1 - 3 μ ; (b) high resolving power (which is inherently difficult to achieve with a low frequency radiation) to make point measurements; (c) a highly sensitive detector of infra-red radiation. The scope of the present investigation has not allowed more than just some literature survey in this matter, and no experiments have been attempted to explore the feasibility of the technique. However, the limited study shows that problems (a) and (c) can be solved; while the solution of (b) awaits further study. The combination of a carbon arc and a monochromator should solve (a); and lead sulphide (PbS) cells appear to be very promising as detectors.

Refs. 39 to 42 give some of the background material on the infra-red bands of water vapor. Early work on the production of infra-red radiation by the Nernst glower and Welsbach mantle is described in Refs. 43 to 45, while more recent work on the subject may be found in Refs. 46 to 48. The detection of infra-red by thermocouple is the most commonly used, but is not sensitive enough for our use in flow measurements. The "thermophone", which measures infra-red radiation by the pressure it produces in a gas, is far more sensitive than thermocouples (Refs. 49 and 50), but is somewhat more complicated in the associated equipment. The lead sulphide cell seems to be the best detector, and its application is still being developed (Refs. 51 to 53).

2. Development of a Sensitive Schlieren System

The limitations of time and equipment preclude the use of any but the schlieren method. It is then necessary to resort to a critical design of the optical system in order to obtain a high degree of sensitivity. In the experimental study of shockwave curvature the schlieren method is of prime importance. Therefore, some discussion is included here on the pertinent factors in attempting to use the schlieren method on low density flows. Such factors affecting the ultimate performance of the system as the focal lengths of the lenses and mirrors, width and length of the light source slit, aperture of the system, light source, and finally, photographic technique, are included in the discussion. It is evident, of course, that all these must enter into the design of any schlieren system, regardless of the conditions under which it is to be used. However, these factors reach critical proportions when the disturbance to be measured becomes extremely small, as in the present case of low density flow, wherein the deflection of the light beam after passage through the tunnel is about 5 to 6 orders of magnitude below those encountered in conventional tunnels.

Toepler first proposed the striation method in 1864 (Ref. 54). Mach first adapted the system to the visualization of shockwaves on bullets. A comprehensive treatise on the theory and application of the Toepler schlieren system is by Schardin (Ref. 55). Barnes and Bellinger (Ref. 56) give a helpful consideration of the practical aspects in setting up a schlieren system, as well as a very extensive bibliography.

2.1 Fundamental Relations and Sensitivity Considerations

The refraction of light in passing through a non-homogeneous

medium can be expressed by the relation

$$\frac{1}{R} = \frac{\text{GRAD } n}{n} \sin \varphi \qquad \text{(C-1)}$$

where

R = radius of curvature of the light beam

n = index of refraction

φ = angle between light beam and grad n

The index of refraction n is a function of the density of the transmitting medium

$$n = 1 + k\rho \qquad \text{(C-2)}$$

where k is a constant depending on the nature of the medium and the wave length of the light.

The total deflection of the light in passing a distance a through a medium is (Fig. 29)

$$\varepsilon = \int_0^a \frac{1}{R}\, ds \qquad \text{(C-3)}$$

Fig. 30 shows one way of setting up an optical system to detect this deflection ε. The light from a source A is collimated by lens B, and refocused by C to an image at K. If now some disturbance is introduced between B and C, the light is deflected by an angle ε, so that, after focusing by C, arrives at K displaced from the original position by an amount εf, where f is the focal length of C. If now a stop is placed at K, and another lens D is placed so as to form an image on G of the plane S where the disturbance occurs, there will be a change of image intensity when the light suffers a deflection at S and falls towards or away from the stop at K. The source A is usually in the

form of a uniformly illuminated slit of width d and length ℓ. The image of A formed at K is of width ad and length a ℓ where a is the amplification factor. For simplicity, and without losing generality in the discussion, let a = 1. If a stop in the form of an opaque body with a straight edge is placed across the image so that the straight edge is parallel to the long sides of the slit, the amount of light passing to D and G will be diminished by an amount proportional to ℓ(d-h) as seen in Fig. 31. If the light is deflected away from the stop, the illumination on the screen at G increases and vice versa. It is evident from the geometry shown in Figs. 30 and 31 that the change of illumination at G is proportional to ε f.

Before continuing it will be useful to define the following terms:

Φ = light flux or amount of energy per unit time

I = illumination, energy falling on a unit area in unit time

$\mathcal{J} = \frac{\Delta I}{I}$ = variation in illumination

It can easily be seen then that the variation of intensity at the screen G due to the disturbance S can be expressed as

$$\frac{\Delta I}{I} = \frac{\Delta h}{h} = \frac{\varepsilon f}{h} \qquad \text{(C-4)}$$

where h is the uncut portion of the slit image. If $\mathcal{J}_m$ is the minimum variation detectable (either by eye or by photographic film), the minimum deflection detectable becomes, using Equation (C-4)

$$\varepsilon_m = \frac{\mathcal{J}_m h}{f} \qquad \text{(C-5)}$$

Thus, it is seen that if the sensitivity of the schlieren system is defined as the minimum deflection of the light beam measurable it is proportional to h and inversely proportional to the focal length f.

It should be noted here that f is only the focal length of the focusing lens C and not the total distance from S to K, as it is sometimes mistaken to be.

Equation (C-4), which relates the variation of intensity to the strength of the disturbance, holds only when $\varepsilon f < h$ or $\varepsilon f < d-h$, for if $\varepsilon f = h$ or d-h there is total darkening or brightening of the field and further increase of the disturbance causes no more change in illumination. Thus, in addition to sensitivity, the range of the system should be considered. This is discussed by Mair (Ref. 57). For the present investigation, however, range will not be considered, since the disturbances are so weak that the problem of range does not enter.

It would appear from Equation (C-5) that the sensitivity can be increased indefinitely by decreasing h and increasing f. In practice, unfortunately, there are limitations.

(a) Limitations on h

The illumination of the field at G depends on the amount of light let past the stop at K, so that as h is decreased the intensity also drops. Another factor limiting h is diffraction. When the light passes an obstruction diffraction takes place and is pronounced when the obstruction is a sharp edge. The result of diffraction in this case is to cause dark shadows on the objects in the light path to appear on the screen G. These dark shadows appear as apparent reflections of the objects, and extend from the objects with decreasing darkness in a direction perpendicular to the edge of the stop at K. This effect is clearly discernible in the schlieren photographs in Figs. 10 and 17-20. There is also diffraction at the edges of the objects causing bright fringes. But this does not depend on the conditions at K. The dark

shadows become more pronounced as the illumination is decreased by decreasing h. This effect therefore sets a practical lower limit on the width of the slit image, even if sufficiently strong light source is available for adequate intensity on the screen with smaller widths.

(b) Limitations on f

Space is perhaps the major factor limiting the focal length of the focusing lens or mirrors. By using a series of mirrors the light beam can be turned back and forth to fit in a small space; but this has the disadvantages of attenuation of the light and added sources of vibrations as a result of several surfaces of reflection. An aluminum coated first surface mirror reflects about 85 per cent of the incident light so that three reflections will reduce the original light by 40 per cent. With a highly sensitive system spurious disturbances outside the wind tunnel, even though they occur away from the focal plane of the image formation lens D, will cause distortions in the image field. This is the usual noise problem with any highly sensitive detecting device. If the light path is lengthened, the noise problem becomes aggravated.

The minimum detectable intensity variation $\mathcal{I}_m$, whether visually or photographically, is not a constant but depends on the absolute level of intensity and the color of the light. The intensity of illumination at the screen cannot be decreased indefinitely without raising $\mathcal{I}_m$.

By substituting some practical values into Equation (C-5) it may be seen that ε_m can be extremely small. For example, let

$\mathcal{I}_m = 0.10$

$h = 0.02$ cm.

$f = 150$ cm.

Then $\varepsilon_m = 1.3 \times 10^{-5}$ radian

In practice, however, it will be found that such a sensitivity cannot be attained with the above configuration because of the detrimental circumstances already described.

Up to this point the optics has been based on idealized conditions tacitly assumed, these being: light source slit of uniform intensity, perfect collimation into parallel rays, perfect formation of image. Actually, all these can only be approximated. The treatment of aberrations may be found in any standard treatise on geometric optics, such as Hardy and Perrin, Monk, and Martin (Refs. 58 to 60). The simplified geometric optics in Fig. 30 has A as a point, while actually it is a rectangular area. Perfect image formation is hampered by various aberrations. With lenses, spherical and chromatic aberrations are important. Astigmatism and coma are not as serious since the elements of the optics can be arranged on the center lines of the lenses. With mirrors chromatic aberration is absent; but spherical aberration and astigmatism are present unless special off-center parabolic reflectors are used, and the cost of these is certainly prohibitive. In general, it is preferable to use spherical mirrors instead of lenses in a schlieren system because it is easier to produce larger focal length mirrors than lenses, and there is no chromatic aberration.

2.2 The Arrangement of a Two-Mirror System

A system using only mirrors is shown in Fig. 32. Since it is

not co-linear, there are coma and astigmatism. The mirrors also cause spherical aberration. The finite dimensions of the light slit cause further astigmatism and coma. All these distortions can be held to very low values by certain restrictions on the geometry of the setup. By keeping the angles θ_1 and θ_2 small and making the system symmetrical, $\theta_1 = \theta_2$, and coplanar (A, B, C, K coplanar) astigmatism and coma can be reduced. Spherical aberration and astigmatism due to the finite size of the slit can be kept low by using a very small aperture (ratio of mirror radius to focal length) and large mirror diameter compared to the length of the slit. A large mirror diameter requires even larger focal length in order to give a small aperture. It is therefore an advantage to keep the length of the slit small, though at the expense of reduced flux in most cases. The finite size of the slit not only causes distortion of the image but non-uniformity of the illumination at the image as well. This illumination decreases with distance away from the optical axis and can be shown to be proportional to $\cos^4 w$, where w is the angle subtended by the half-length of the slit at the center of the mirror or lens, as shown in Fig. 33, or $w \simeq \frac{\ell}{2f}$, for very small angles. To keep the image illumination uniform to within 1 per cent w must be no greater than 4 degrees, which means $\ell/2f \leq 0.07$.

The deviation from parallel of the light rays when a spherical mirror is used for collimation depends on the aperture of the mirror. In Fig. 34 δ denotes the maximum deviation from parallel of the light ray reflected from the edge of the mirror. It can be shown that when $\frac{f}{r_o} >> 1$, $\delta \simeq \left(\frac{r_o}{2f}\right)^3$. Therefore, if $\frac{r_o}{2f} = \frac{1}{100}$, $\delta \simeq 10^{-6}$ RAD.

The off-set, θ, (Fig. 32) causes no additional error so long as the second mirror is of the same focal length and is offset by the same amount.

The various quantities determining the geometry of the system and their inter-relationships as affecting the amount of aberrations may now be summarized below.

(a) Focal Length, f: For minimum distortions the two mirrors should have the same focal length. The sensitivity of the schlieren system increases with f. But space and noise level considerations place an upper limit on f.

(b) Radius of Mirror, r_o: The aperture, r_o/f, gives a measure of the spherical aberration, so that, to keep the latter at a low level, r_o/f should be made small, of the order of 10^{-2}.

(c) Light Source Slit: The width of the slit enters in the determination of the sensitivity. With a given light source the area of the slit, ℓ d, determines, up to some fixed value, the amount of light let through which then determines the illumination of the viewing screen or the exposure of the photographic film. Small width gives high sensitivity, but increases diffraction effects, and reduces illumination. The length of the slit is limited by the relation $\ell = 0.14f$ in order to maintain uniformity of illumination at the slit image.

2.3 Light Source

With f, r_o, ℓ and d determined, the next step is to consider the light source. The requirement here is to have a small rectangular area with high and uniform light emission. It is usually not possible to achieve this directly with an emitter because the area of an emitter is larger than the size of the required slit. The usual

practice is to pick an emitter which is as small as possible, yet producing a large amount of luminous energy, and gather the light with a lens or mirror which then focuses the light onto a slit of the proper dimensions. Fig. 35 shows such an arrangement. Regarding the lamp as a point, the amount of power arriving at A is proportional to the solid angle ω. Defining E, the intensity, as the amount of energy issuing from L per unit solid angle per unit time, the luminous power at A is

$$\mathcal{L} = E\omega = 2\pi E\ (1 - \cos a) = 2\pi E \left(1 - \cos \frac{r_o}{f}\right)$$

If

W = luminous power of lamp

E = $W/4\pi$

so that

$$\mathcal{L} = \frac{W}{2}\left(1 - \cos \frac{r_o}{f}\right) \qquad \text{(C-6)}$$

It becomes immediately obvious now that the requirement of small aperture makes $\mathcal{L}$ a very small portion of the total power of the lamp. For an aperture, r_o/f of 0.05, $\mathcal{L}/W$ only amounts to 0.0006. It should be noted here that once the aperture is specified $\mathcal{L}/W$ is fixed, regardless of the arrangement of the collecting lens. The collecting lens N can be so chosen as to reduce the image of L to dimensions somewhat greater than the desired slit at A, so that the slit opening masks off the outer portions of the image that are usually non-uniform in intensity. After masking by the slit the amount of luminous power admitted into the schlieren system is probably no greater than 0.0001 of the total power of the lamp. Even this amount admitted is not all useful, because the eye or the photographic film is sensitive to

only certain wave length ranges of the total spectral output of the lamp.

2.4 The Schlieren Image and Photographic Technique

The image of the disturbance S (Fig. 32) is focused on the screen at G. Visual observation of the image is not sufficient to detect all that may be taking place at S, because the eye cannot detect small variations in illumination nor can it stop a rapidly moving image. Photographs must therefore be taken not only as records but to render visible to the eye more information than the eye alone can see.

The density of an exposed and developed film is defined as

$$d = \log_{10} \left(\frac{\text{incident illumination}}{\text{transmitted illumination}}\right)$$

This density is a function of the type of emulsion on the film, the exposure and the developing process. Exposure is defined as the amount of energy falling on a unit area of the film and is expressed in meter-candle-seconds (the meter-candle being equal to 1 lumen per square meter). A typical group of curves of film characteristics is shown in Fig. 36. The slope of the curve is the contrast and is called gamma in photographic nomenclature. The speed of the film expresses its sensitivity to light, so that films with higher speeds have characteristic curves lying to the left of ones with lower speeds as seen in Fig. 36.

The selection of film depends first of all on how much detail information of the flow is desired. In cases where the phenomena to be examined are spread out (such as expansion zones and gradual

compression zones) it would be best to use a film with medium contrast that allows gradation of film density. But if the effects to be measured are very weak (as in the case of shock waves in very low density flow) high contrast film must be used in order to show anything at all. The graininess of the film should be considered when enlargements are necessary, although low graininess usually means low film speed. Where very fine details are important the resolving power of a film should be considered. This is expressed in terms of the number of lines per millimeter that can be distinguished by the film. The highest resolving power attainable is about 160 lines per mm. As with the case of graininess, high resolving power results in low film speed.

The sensitivity of the film depends on the wave length of the energy. Thus, the energy from a light source cannot be effective over the whole spectral range in exposing the film. Therefore, in computing the exposure only the energy in the spectral bands the film is sensitive to can be included. Fig. 37 shows the spectral distribution of emission power of a high-pressure mercury vapor lamp (General Electric BH-6). Knowing this and the characteristics of a film (Fig. 36) the proper exposure can then be computed. In practice it must be remembered that a shutter to let through light for a given interval can only be used with a continuous light source, unless it is properly synchronized with a non-continuous source. Any A.C. lamp gives forth periodic emission. This is the reason consistent exposures cannot be obtained with a BH-6 lamp operating on a 60-cycle A.C. if the shutter speed is higher than 1/120 sec.

Strong emission for a very short duration can be produced by the discharge of a capacitor through an air gap or a gap enclosed in some other gas. The analysis, design, and adaptation to flow visualization of discharge light source techniques have been treated by Melton (Ref. 62), Kovasznay (Ref. 63), Whelan (Ref. 64) and Drosd (Ref. 65).

2.5 Description of the Schlieren System for the Low Reynolds Number Tunnel

The setup adopted in the light of the considerations elucidated above is shown schematically in Fig. 38. The system is so arranged as to have a minimum number of lenses and mirrors, and, for a given focal length, the shortest overall optical path length. The slit is adjusted to about 0.75 cm. by 0.03 cm. With such a small slit the alignment of the system is fairly critical so that a minimum of surfaces not only reduces losses of light but makes the alignment much easier too. The spark gap and the mercury lamp are placed so that neither one need be moved when the other is being used. The spark gap is connected through a thyratron trigger-switch to a 1.75 μf capacitor charged to 20,000 volts. A diagram of the circuit is shown in Fig. 39. The original circuit had 0.25 μf capacity; but the additional illumination needed to expose the slow film used necessitated an increase to 1.75 μf.

Blackened tubes are placed at both sides of the test section over the light path to cut down the level of noise in the system. Actually, the full sensitivity cannot be used, due to noise, even with these tubes in place; while, without them, it is nearly impossible to get any useful photographs.

2.6 Sensitivity

Using Equation (C-5) and assuming $\mathcal{J}_m = 0.1$ and h = 0.02 the minimum deflection detectable is

$$\varepsilon_m = 1.4 \times 10^{-5} \text{ RAD.}$$

This is the sensitivity attainable under ideal conditions: uniform illumination, perfect alignment of slit and knife-edge, no noise, and no vibrations. The actual sensitivity is probably one order lower.

The actual deflection of the light beam by refraction through the density gradient in the flow (Equations (C-1) and (C-3) will now be estimated.

If the light beam is parallel to the plane of the shock wave, $\sin\varphi$ in Equation (C-1) becomes unity. Taking the direction of the gradient parallel to the flow Equation (C-1) may be written as

$$\frac{1}{R} = \frac{1}{n}\frac{dn}{dx} \simeq \frac{dn}{dx} \qquad \text{(C-7)}$$

since n is very nearly equal to unity.

If the flow is two-dimensional $\frac{1}{R}$ is constant throughout the width of the tunnel, and if the light beam does not diffract so far that it leaves the thickness of the shockwave (this case is discussed by Liepmann and Puckett (Ref. 66) and Mair (Ref. 57), Equation (C-3) becomes

$$\varepsilon = s\frac{dn}{dx} \qquad \text{(C-8)}$$

where s is the width of the tunnel.

Writing Equation (C-2) in the form

$$n-1 = (n_1-1)\frac{\rho}{\rho_1} \qquad \text{(C-9)}$$

where n_1 and ρ_1 are the index of refraction and density of the gas ahead of the shockwave, Equation (C-8) may be written as

$$\varepsilon = \frac{s(n_1 - 1)}{\rho_1} \frac{d\rho}{dx} \qquad \text{(C-10)}$$

In Equation (C-10) $d\rho/dx$ will be approximated by $\Delta\rho/\Delta x$, where $\Delta\rho$ is the change in density through the shockwave and Δx its thickness. If the subscripts 1 and 2 denote conditions ahead and behind the shockwave respectively

$$\Delta\rho = \rho_2 - \rho_1 = \frac{\rho_1}{u_2}(u_1 - u_2) \qquad \text{(C-11)}$$

The shockwave thickness, Δx, may be estimated by the method of Taylor and Maccoll (Ref. 67)

$$\Delta x = 4.4 \frac{D}{u_1 - u_2} \qquad \text{(C-12)}$$

and

$$D = \left[\frac{K}{R}\left(1 - \frac{1}{\gamma}\right) + \frac{4}{3}\frac{\mu}{\gamma - 1}\right] \frac{2(\gamma - 1)}{\rho_1(\gamma + 1)} \qquad \text{(C-13)}$$

Using Equations (C-11) and (C-12), Equation (C-10) becomes

$$\varepsilon = \frac{s(n_1 - 1)}{4.4D} \frac{(u_1 - u_2)^2}{u_2} \qquad \text{(C-14)}$$

The calculations of ε will be based on a normal shockwave under the following conditions, which are typical for this tunnel:

M	$= 1.5$	R	$= 4.61 \times 10^6$ ergs./gm°C
p_1	$= 8.4$ mm.	γ	$= 1.33$
T_1	$= 310$°K	μ_1	$= 9.4 \times 10^{-5}$ poise
ρ_1	$= 7.84 \times 10^{-6}$ gm./cm.^{3}	K_1	$= 5.6 \times 10^{-5}$ cal./cm. sec.°C
u_1	$= 6.54 \times 10^4$ cm./sec.	$n_1 - 1$	$= 1.78 \times 10^{-6}$
u_2	$= 3.44 \times 10^4$ cm./sec.	s	$= 2.06$ cm.

Then

$$D = 1.85$$

and $$\varepsilon = 1.26 \times 10^{-3} \text{ rad.}$$

This compares favorably with the estimated sensitivity of 1.4×10^{-4} radian, so that a normal shock wave at M = 1.5 in this tunnel should be visible in the schlieren screen. If the shockwave is inclined at 45°, by the same method as above, ε is estimated to be 10^{-5} radian, and the shockwave is probably just barely visible. As a comparison, it may be noted that in the Galcit Transonic Tunnel ε is of the order of 1 radian.

2.7 Actual Performance of the Schlieren System

Under actual operating conditions the shockwaves are barely discernible to the eye. Several reasons may account for this. On the one hand, the sensitivity of the system may be lower than the estimate, due to many imperfections, chief among which seem to be diffraction and noise. On the other hand, the actual deflection of the light is probably less than estimated due to the very diffuse formation of the shockwaves. Photographic technique must then be depended upon to produce useful results.

The demands are for high contrast (so that the shockwaves can be distinguishable) and low graininess (so that enlargements can be made to study conditions near the leading edge of the wedge). The film meeting such demands is a high-contrast positive type film, Kodak Fine-Grain Positive, with a gamma of over 3, very low graininess, and a resolving power of 100 lines per millimeter. The serious drawback of such a film is the low speed, only about 0.5 on

the A.S.A. (American Standards Association) rating, as compared to 100 for the Super-XX film. Nevertheless, an estimate of the exposure indicates that even at such low speeds this film can be properly exposed with the present setup.

Using Equation (C-6), with $r_o/f = 0.027$

$$\mathcal{L} = 2 \times 10^{-4} \, W$$

Assume that the masking by the slit cuts the light by half, and that the lens, two mirrors, and two windows reduce the light again by half. Then

$$\mathcal{L} = 5 \times 10^{-5} \, W$$

The BH-6 lamp emits 80 watts in the blue band (4350 Å), and the film is sensitive to the same band. Therefore, the amount of luminous power reaching the film, after another cut in half by the knife-edge, is

$$\mathcal{L} = 2 \times 10^{-3} \text{ watts} = 1.3 \text{ lumens}$$

With an illuminated film area of 20 $cm.^2$ and an equivalent shutter speed of 0.005 sec., the exposure E is equal to 3 meter-candle-seconds. Reference to Fig. 36 shows that sufficient density will result from this exposure.

A photograph taken with the BH-6 lamp is shown in Fig. 10. No estimate of the exposure with the spark has been made, for lack of information as to the spectral distribution of energy of the spark. However, successful results have been obtained, and one is shown in Fig. 10.

REFERENCES

1. Dushman, S.: Scientific Foundation of Vacuum Technique. John Wiley and Sons, New York (1949).

2. Strong, J.: Procedures in Experimental Physics. Prentice Hall, New York (1946).

3. Hawthorne, Kaye, Keenan, Shapiro, and Wadleigh: Analysis of Various Systems for Supersonic Wind Tunnels. Rept. UAC-23, Proj. Meteor, United Aircraft Corp. (1948).

4. Ackeret, J.: High Speed Wind Tunnels. Fifth Volta Congress, Italy (1935). Translated as NACA T.M. 808 (1936).

5. Tolman, R. C. and Fine, P. C.: On the Irreversible Production of Entropy. Rev. Mod. Phys. 20, 51 (1948).

6. Crocco, L.: High Speed Wind Tunnels. L'Aerotecnica No. 3 (1935). Translated as Ae. Tech. 962, Air Ministry (1935), also Translation 366, Air Mat. Command (1946).

7. Ruptash, J.: Supersonic Windtunnels - Theory, Design and Performance. UTIA Rev. No. 5, Institute of Aerophysics, Univ. of Toronto.

8. DuMond, J. W. M. and Pickels, W. M.: Superiority of a Kundsen Type Vacuum Gage for Large Metal Systems with Organic Vapor Pumps; Its Design and Operation. Rev. Sci. Inst. 6, 362 (1935).

9. Glazebrook, R.: A Dictionary of Applied Physics. Vol. III, Peter Smith, New York (1950).

10. Maslach, G. J.: A Precision Manometer for Low Pressures. Eng. Proj. Rept. HE-150-75, Univ. of Calif. (1950).

11. Dow-Corning Catalog, Data Sheet 2001 La.

12. Dhawan, S.: Direct Measurement of Skin Friction. NACA T.N. 2567 (1952).

13. Horning, D. O.: Vacuum Vessel Construction Techniques and Sealing Methods. Eng. Proj. Rept. HE-150-84, Univ. of Calif. (1951).

14. Handbook of Design and Installation, Linear Moulded Seals. Linear Incorp., Philadelphia.

15. Guthrie, A.: Leak Detectors for Industrial Vacuum Systems. Electronics 23, 96 (1950).

16. Van Dyke, Milton D.: Impulsive Motion of an Infinite Plate in a Viscous Compressible Fluid. Zeits. f. Ang. Math. u. Physik, Vol. III, 343 (1952).

17. Chu, B. T.: On Weak Interaction of Strong Shock and Mach Waves Generated Downstream of the Shock. Jour. Aeron. Sci., 19, 433 (1952).

18. Bardsley, O.: The Conditions at a Sharp Leading Edge in Supersonic Flow. Phil. Mag., Ser. 7, Vol. XLII, 255 (1951).

19. Liepmann, H. W. Boundary Layer - Shock Wave Interaction. Symposium on Experimental Compressible Flow, Naval Ordnance Laboratory, Rept. 1133 (1949).

20. Howarth, L.: Concerning the Effect of Compressibility on Laminar Boundary Layers and Their Separation. Proc. Roy. Soc., Ser. A, 195, 16 (1948).

21. Blasius, H.: Grenzschichten in Flüssigkeiten mit Kleiner Reibung. Zeits. f. Math. u. Phys., 56, 1 (1908), also Durand Aerodynamic Theory, Vol. IV.

22. Liepmann, H. W., Roshko, A., and Dhawan, S.: On the Reflection of Shock Waves from Boundary Layers. NACA T.N. 2334 (1951).

23. Liepmann, H. W., Ashkenas, H., and Cole, J. D.: Experiments on Transonic Flow. U.S. Air Force Tech. Rept. 5667 (1948).

24. Liepmann, H. W.: On the Relation Between Wave Drag and Entropy Increase. Douglas Aircraft Co. Rept. SM-13726 (1950).

25. Kantrowitz, A. and Huber, P. W.: Heat-Capacity Lag in Turbine-Working Fluids. NACA R.B. L4E29 (War Time Rept. L-21) (1944).

26. Griffith, Wayland: Vibration Relaxation Time in Gases. Jour. Appl. Phys., 21, 1319 (1950).

27. Richtmyer, F. K. and Kennard, E. H.: Introduction to Modern Physics. McGraw-Hill, 4th ed., New York (1947).

28. Herzberg, G.: Molecular Spectra and Molecular Structure. Van Nostrard, New York, Vol. I, 2nd ed. (1950).

29. Kestin, J.: Influence of Variable Specific Heats on the High-Speed Flow of Air. C.P. No. 3, Tech. Rept., A.R.C. London (1950).

30. Schetzer, J. D.: Aerodynamic Relations with Variable Specific Heat. Jour. Aeron. Sci., 16, 190 (1949).

31. Williams, T. W. and Benson, J. M.: Preliminary Investigation of the Use of Afterglow for Visualizing Low-Density Compressible Flows. NACA T.N. 1900 (1949).

32. Kaplan, J.: The Preparation and Properties of Auroral Afterglows. Phy. Rev. 54, 176, 2nd Ser. (1938).

33. Rayleigh: New Studies on Active Nitrogen. I. Brightness of the After-Glow Under Varied Conditions of Concentration and Temperature. Proc. Roy. Soc., Ser. A, 176, 1 (1940).

34. Winkler, E.: Characteristics Required of X-ray Equipment with Ionization Chamber for Air-Density Measurements. N.O.L. M 9883 (1948).

35. Winkler, E.: Density Measurements by Means of the X-ray Absorption Method. N.O.L. M 10118 (1949).

36. Weltmann, Fairweather, and Papke: Application of X-ray Absorption to Measurements of Small Air-Density Gradients. NACA T.N. 2406 (1951).

37. Evans, R. A.: Progress Report on Design and Operation of a Source of 1470 Å Radiation. Engineering Projects Report HE-150-60, Univ. of Calif. (1949).

38. Evans, R. A.: Progress Report on Design of an Optical System for the Oxygen Absorption Flow Visualization Method. Engineering Projects Report HE-150-61, Univ. of Calif. (1949).

39. Forsythe, W. E. and Christison, F. L.: The Absorption of Radiation from Different Sources by Water and by Body Tissue. J. Opt. Soc. Am. 20, 693 (1930).

40. Hettner, G.: Über das ultrarote Absorptionsspektrum des Wasserdämpfes. Ann. d. Phys. 55, 476 (1918).

41. Dreisch, Th.: Die Absorptionskoeffizienten einiger Flüssigkeiten und ihrer Dämpfe im Ultraroten unterhalb 3μ. Zeits. f. Phys. 30, 200 (1924).

42. Collins, J. R.: Change in Infrared Absorption of Water with Temperature. Phys. Rev. 26, 771 (1925).

43. Pfund, A. W.: The Electric Welsbach Lamp. J. Opt. Soc. Am. 26, 439 (1936).

44. Ritzow, G.: Die Temperaturstrahlung glühender Oxyde und Oxygemische im ultraroten Spektralgebiet. Ann. d. Phys. 19, 769 (1934).

45. Rubens, H.: Über das Emissionsspektrum des Auerbrenners. Ann. d. Phys. 18,725 (1905).

46. Clark, W.: Photography by Infrared. John Wiley and Sons, New York (1946).

47. Koller, L. R.: Infrared - Production and Transmission - Reflection and Measurement. General Electric Ref. 44, 167 (1941).

48. Dushman, S.: The Search for High Efficiency Light Sources. J. Opt. Soc. Am. 27, 1 (1937).

49. Hayes, H.: A New Receiver of Radiant Energy. Rev. Sci. Inst. 7, 202 (1936).

50. Weber, P. E.: Das Membranradiometer. Optik 6, 152 (1950).

51. Lee, E. and Parker, R. C.: Use of PbS Cells for High-Speed Pyrometry. Nature 158, 518 (1946).

52. Sosnowski, Starkiewiez, and Simpson. Lead Sulphide Photoconductive Cells. Nature 159, 818 (1947).

53. Moss, T. S.: The Ultimate Limit of Sensitivity of PbS and PbTe Photo-conductive Detectors. J. Opt. Soc. Am. 40, 603 (1950).

54. Toepler, A.: Beobachtungen nach einer neuen optische Methode. Bonn (1864).

55. Schardin, H.: Toepler's Striation Method. Principles for its Application and Quantitative Evaluation. Forschung. 367 (1934). Translated as No. 249, A.R.C. (Britain) (1935).

56. Barnes, N. F. and Bellinger, S. L.: Schlieren and Shadowgraph Equipment for Air Flow Analysis. J. Opt. Soc. Am. 35, 497 (1945).

57. Mair, W. A.: The Sensitivity and Range Required in a Toepler Schlieren Apparatus for Photography of High-Speed Air Flow. Aero. Quart., Vol. IV, 19 (1952).

58. Hardy, A. C. and Perrin, F. H.: The Principles of Optics. McGraw-Hill, New York (1932).

59. Monk, G. S.: Light, Principles and Experiment. McGraw-Hill, New York, 4th ed. (1937).

60. Martin, L. C.: Technical Optics. Pitman, New York (1950).

61. Kodak Reference Handbook. Eastman Kodak Co., Rochester, New York.

62. Melton, Prescott and Gayhart: A Working Manual for Spark Shadowgraph Photography. Bubmlebee Series Rept. 90, Johns Hopkins Univ. (1948).

63. Kovasznay, L. S. G.: High Power Short Duration Spark Discharge. Rev. Sci. Inst. 20, 696 (1949).

64. Whelan, W. T. and White, E. L.: Circuit Considerations for Electronic Flashlamp Operation. N.O.L. M 10428 (1950).

65. Drosd, R. D. and Liddiard, T. P.: Commercial Flash Tubes; Adaptation for Use as Light Sources in Photography of Detonation. N.O.L. M 10960 (1950).

66. Liepmann, H. W. and Puckett, A. E.: Aerodynamics of a Compressible Fluid. John Wiley and Sons (1947) p. 96.

67. Taylor, G. I. and Maccoll, J. W.: The Mechanics of Compressible Fluids. Durand Aerodynamic Theory, Vol. IV, p. 218.

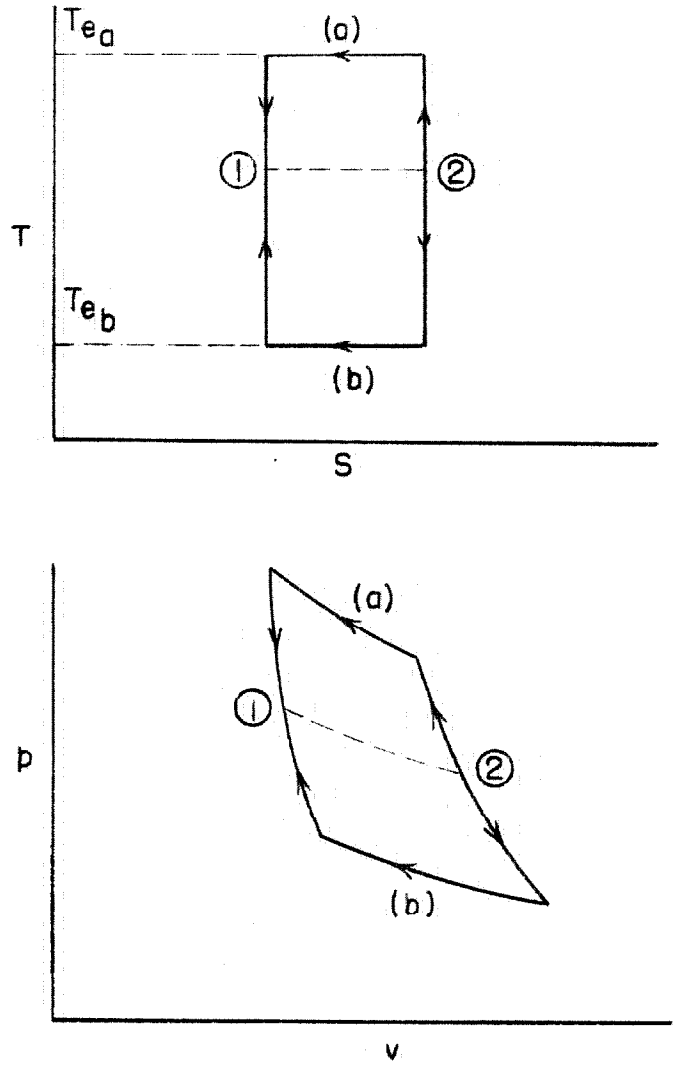

Fig. 1

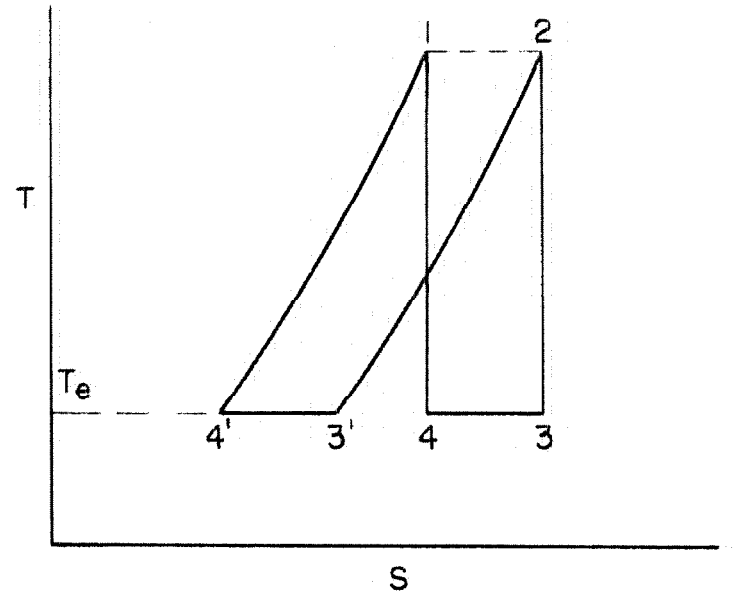

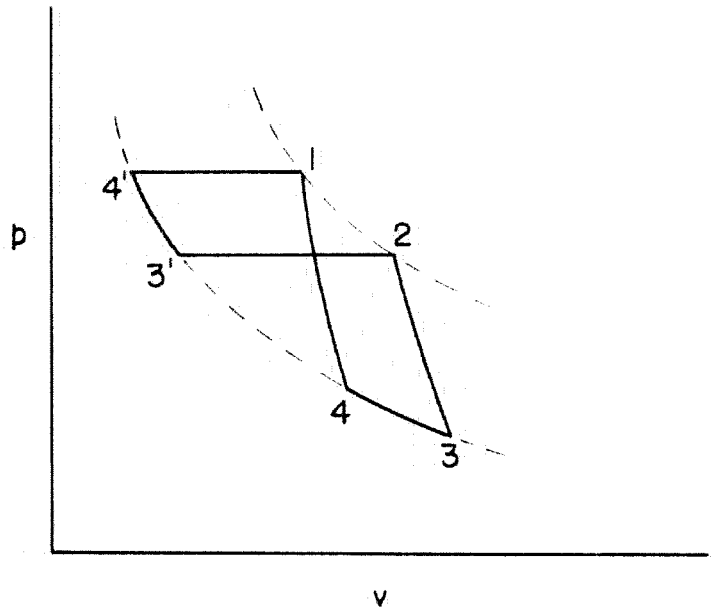

Fig. 2

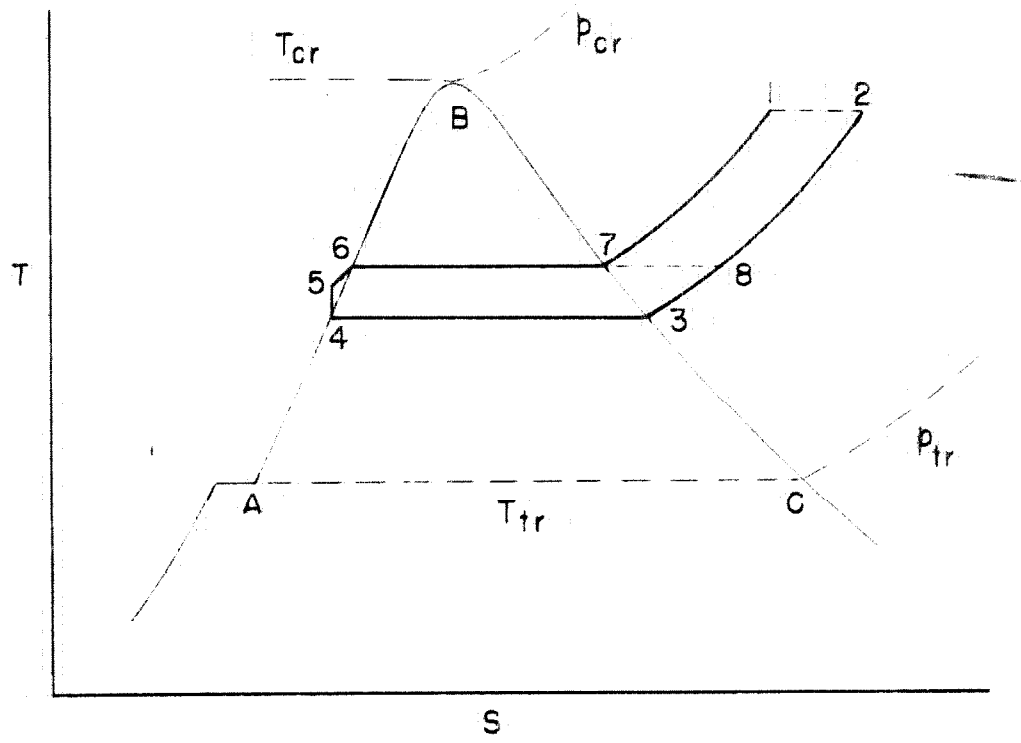

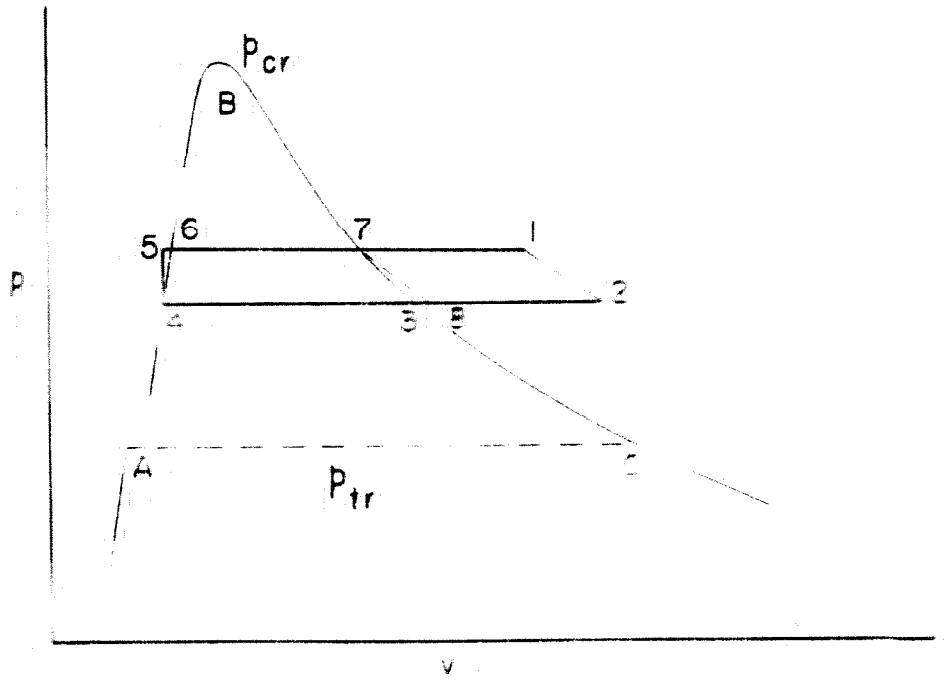

Fig. 3

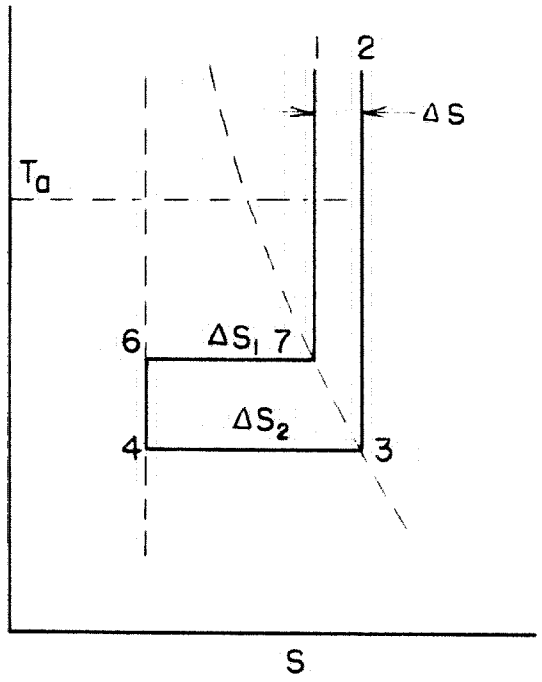

Fig. 4

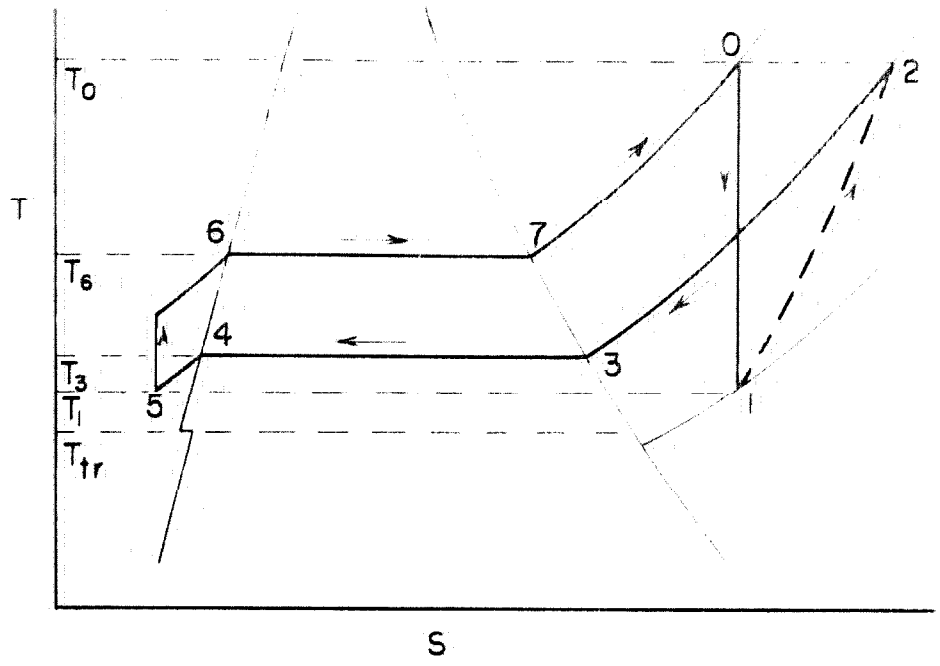

Stage	p mm.Hg.	T °C	q cal./gm.
0	21.9	191	
1	3.0	10.0	
2	12.5	191	
			-83
3	12.5	14.6	
			-588
4	12.5	14.6	
			-9.6
5	12.5	10.0	
			+9.0
6	21.9	23.6	
			+583
7	21.9	23.6	
			79
0	21.9	191	

The pressure at 2 is estimated on the basis of 50 per cent pressure recovery from the test section to the end of the diffuser.

Fig. 5

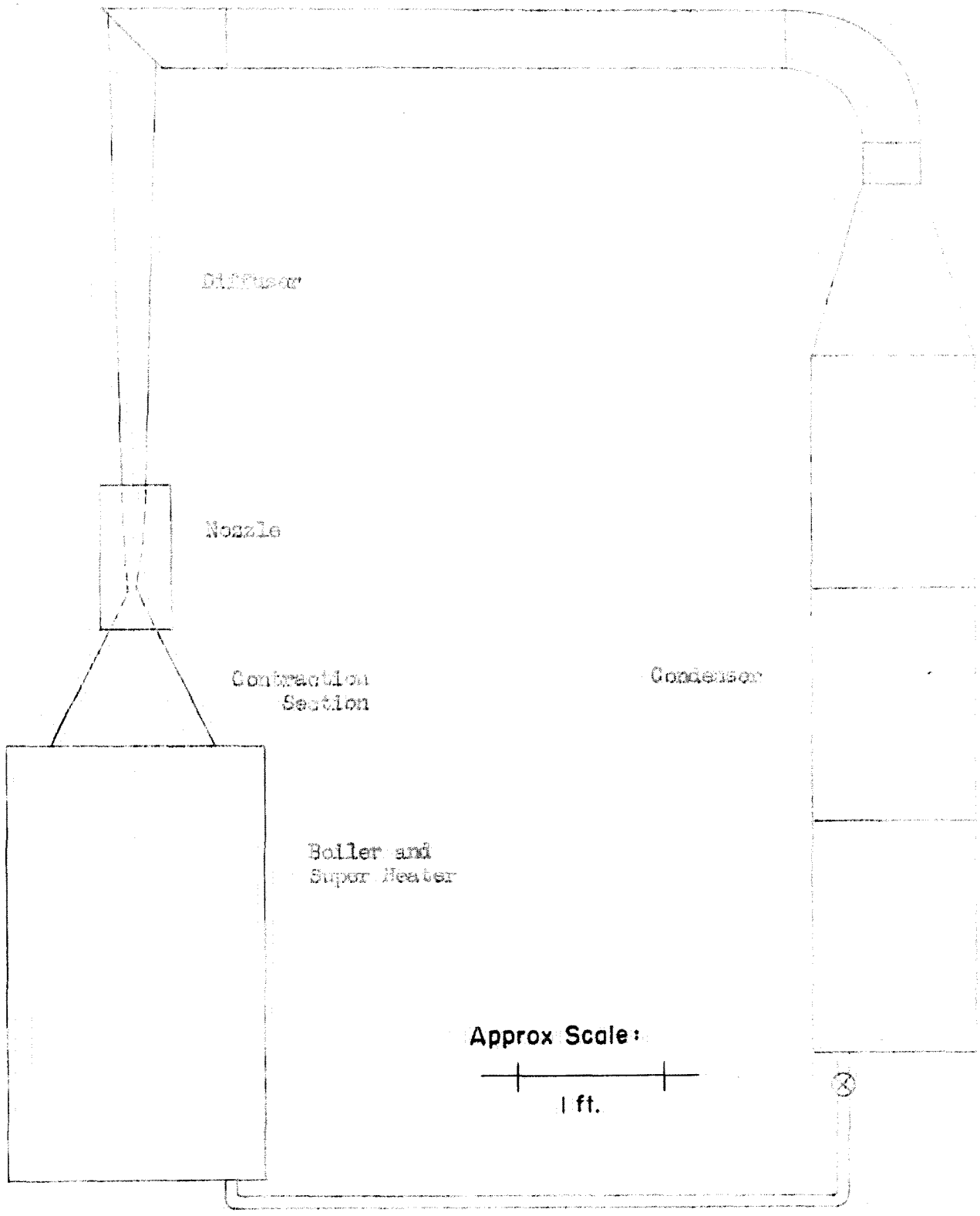
Diffuser
Nozzle
Combustion Section
Condenser
Boiler and Super Heater
Approx Scale:
1 ft.

Fig. 6

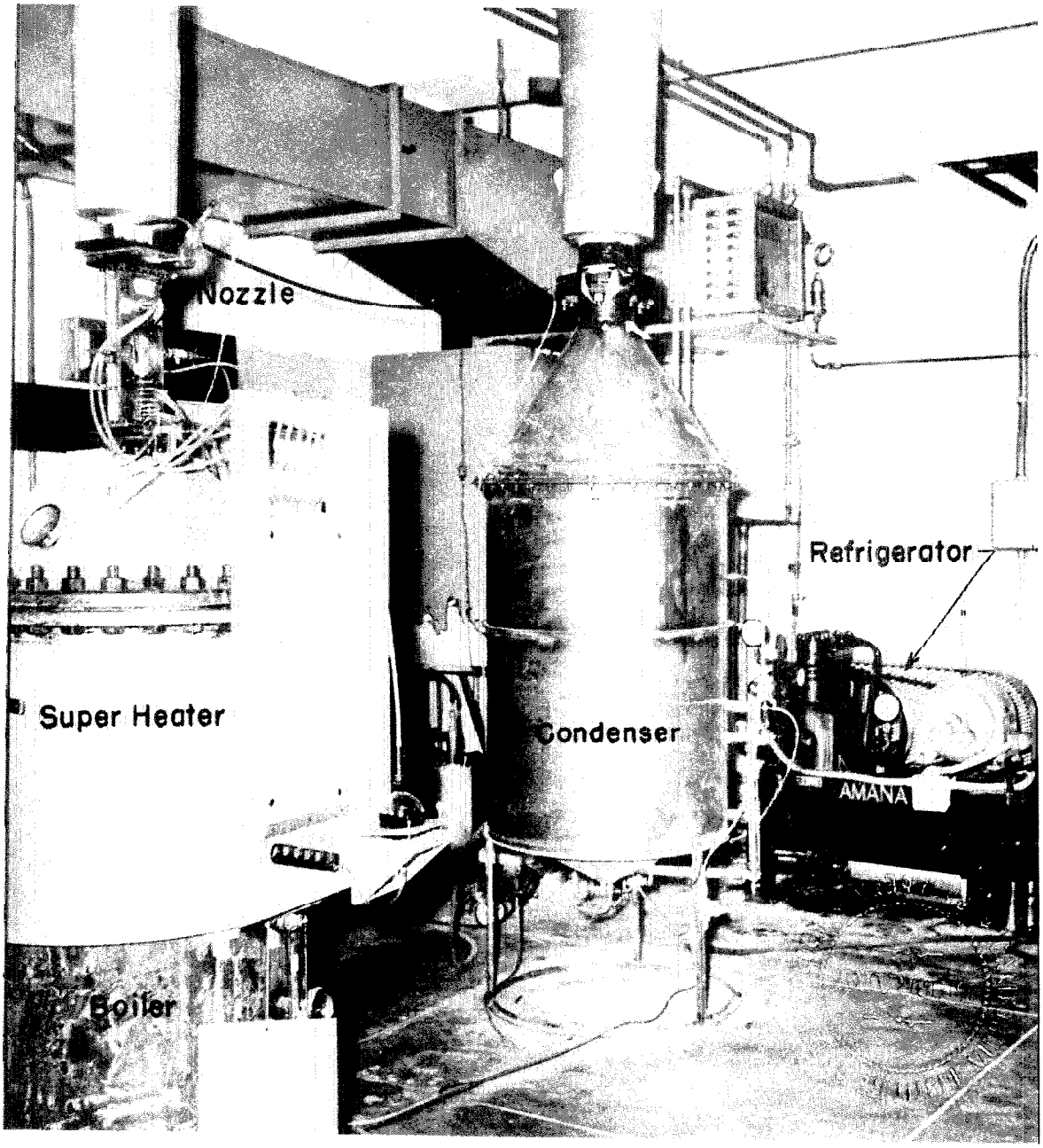

Fig. 7

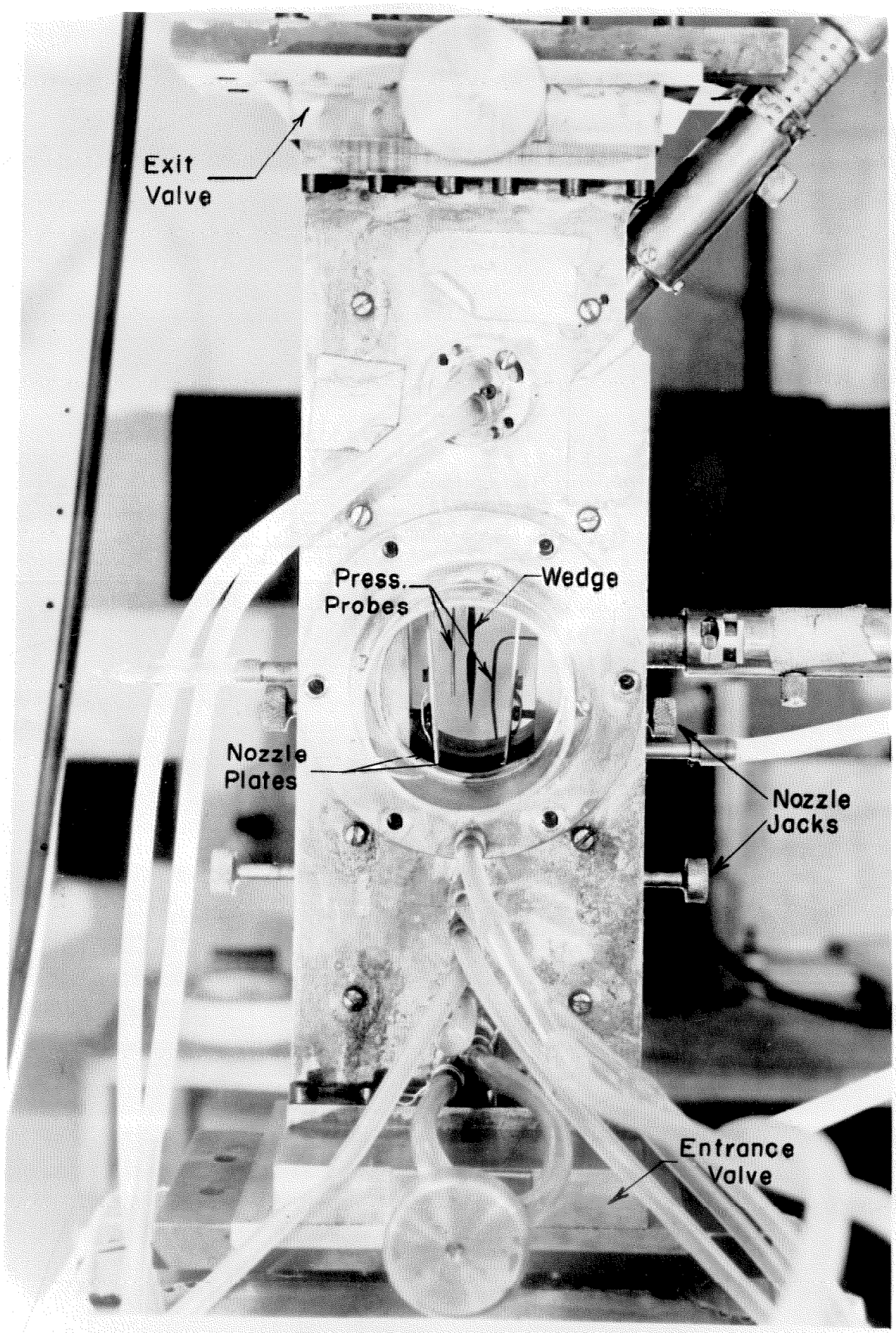
Exit
Valve
Press.
Probes
Wedge
Nozzle
Plates
Nozzle
Jacks
Entrance
Valve

Fig. 8

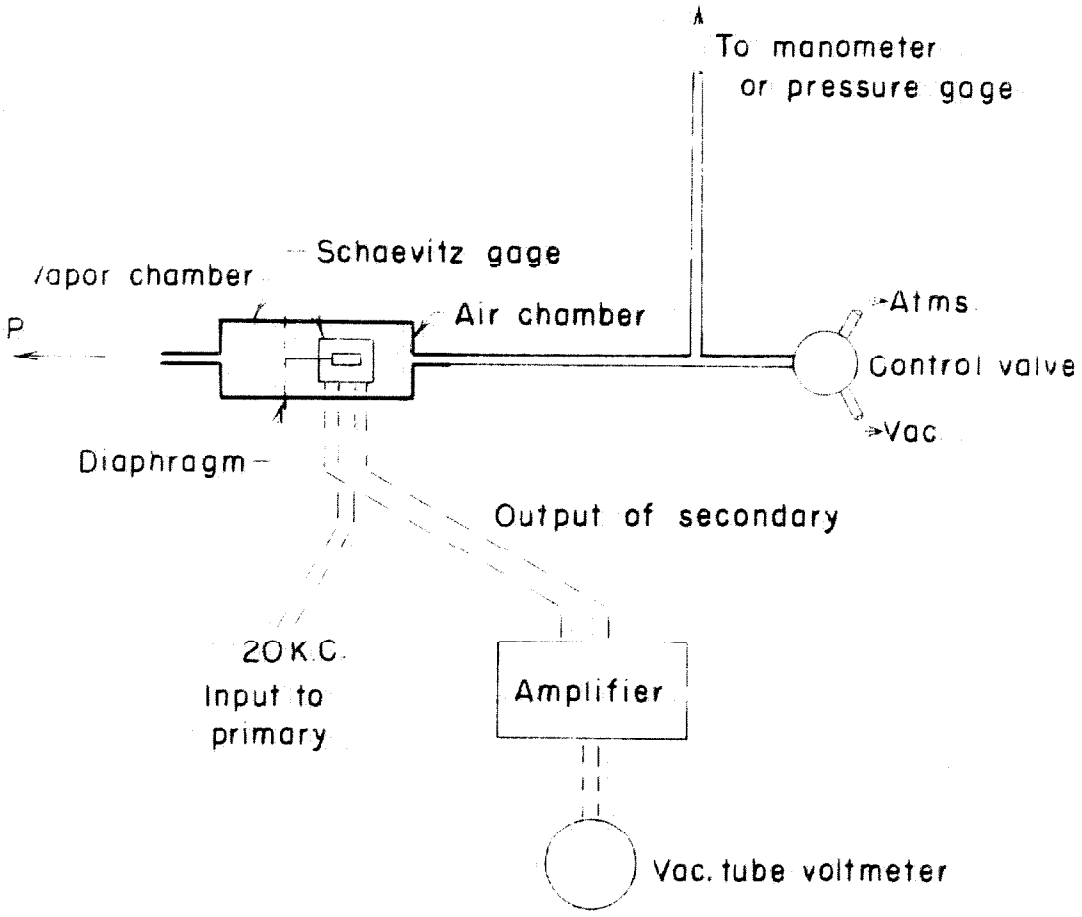

Pressure Transducer

Fig. 9

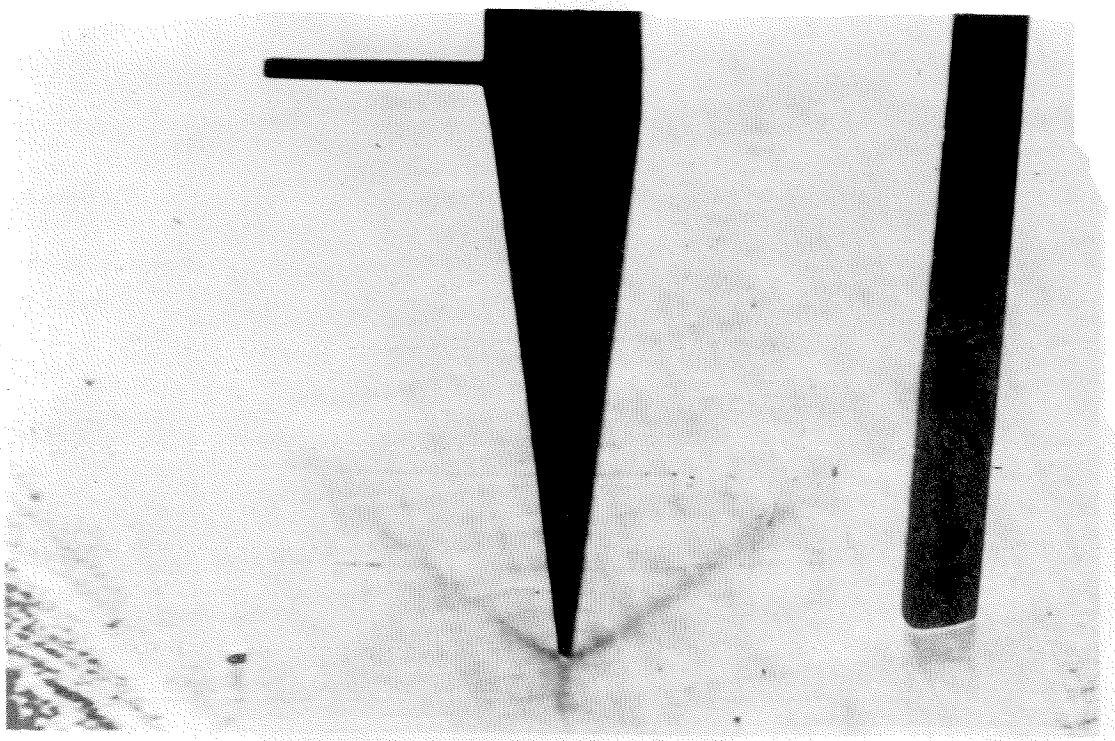

(a)

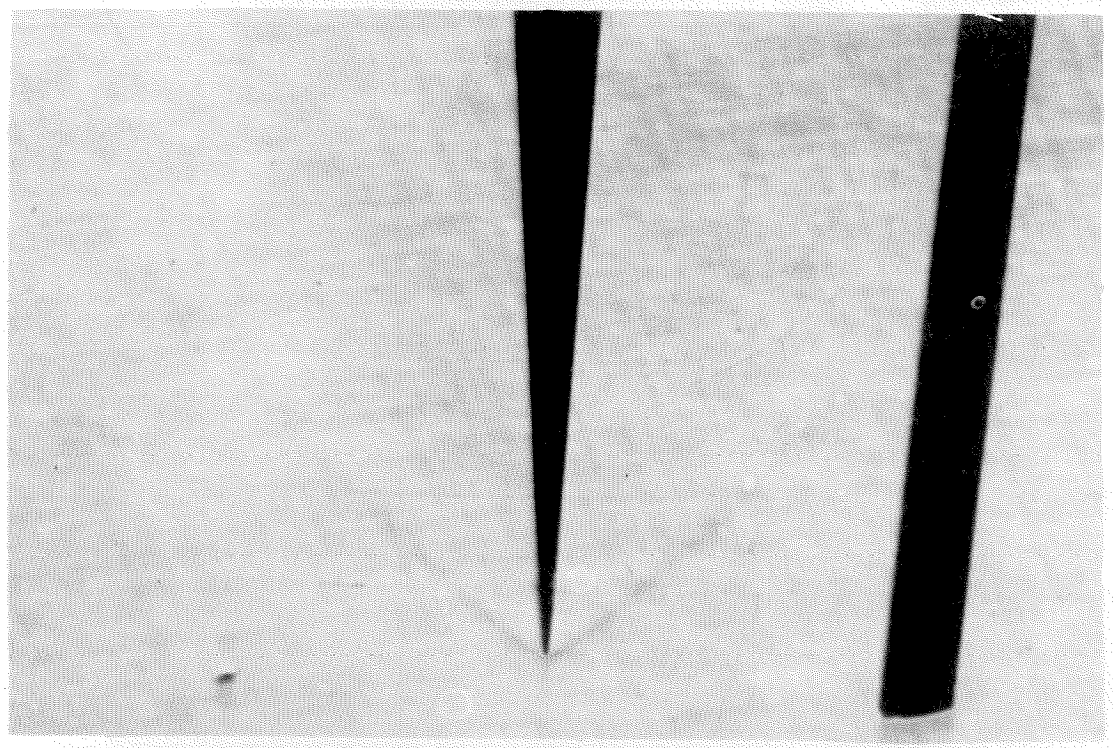

(b)

(a) BH-6 Schlieren $\theta_0 = 7.3$ $M_1 = 1.56$
(b) Spark Schlieren $\theta_0 = 3.5$ $M_1 = 1.64$

Fig. 10

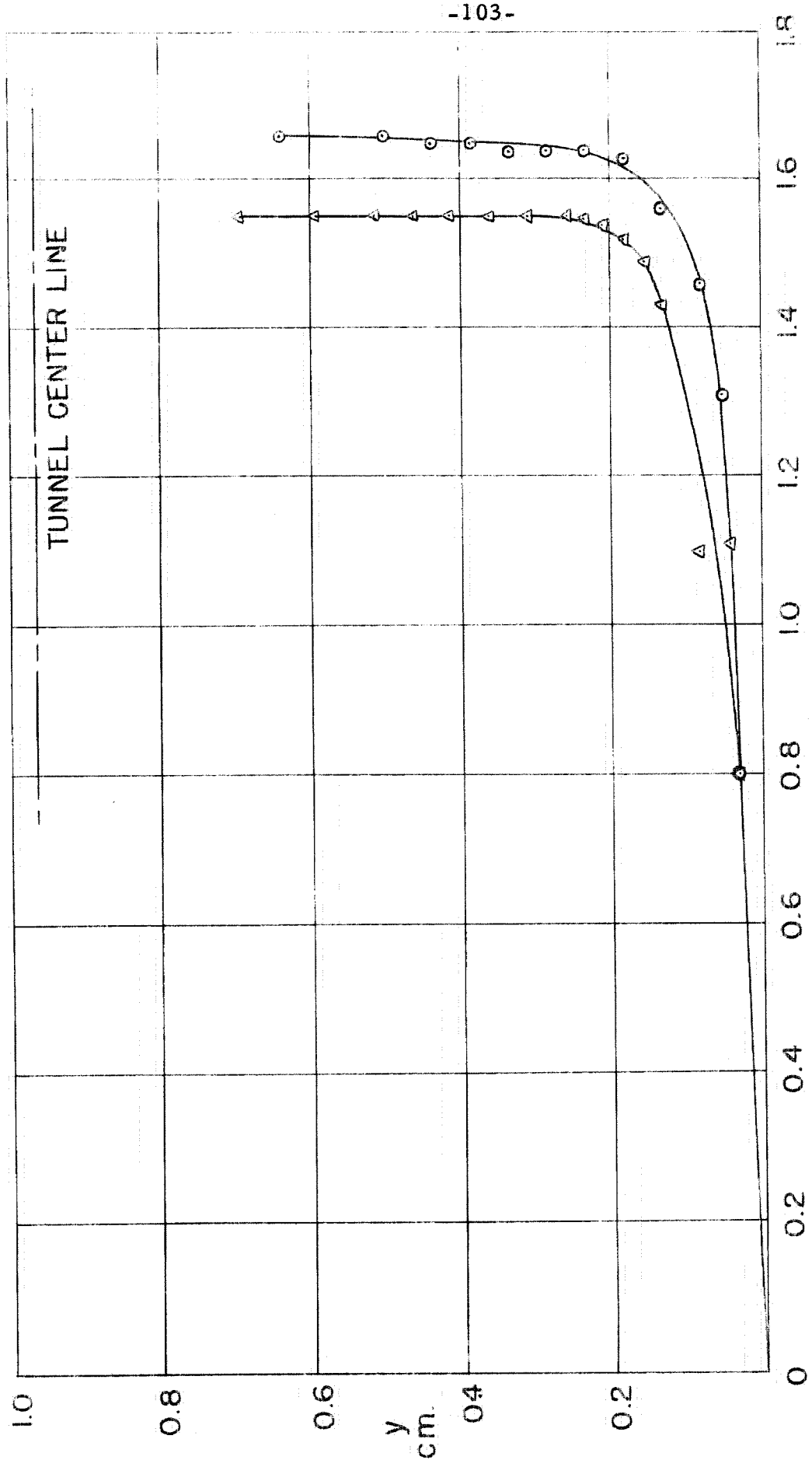

FIG. 11

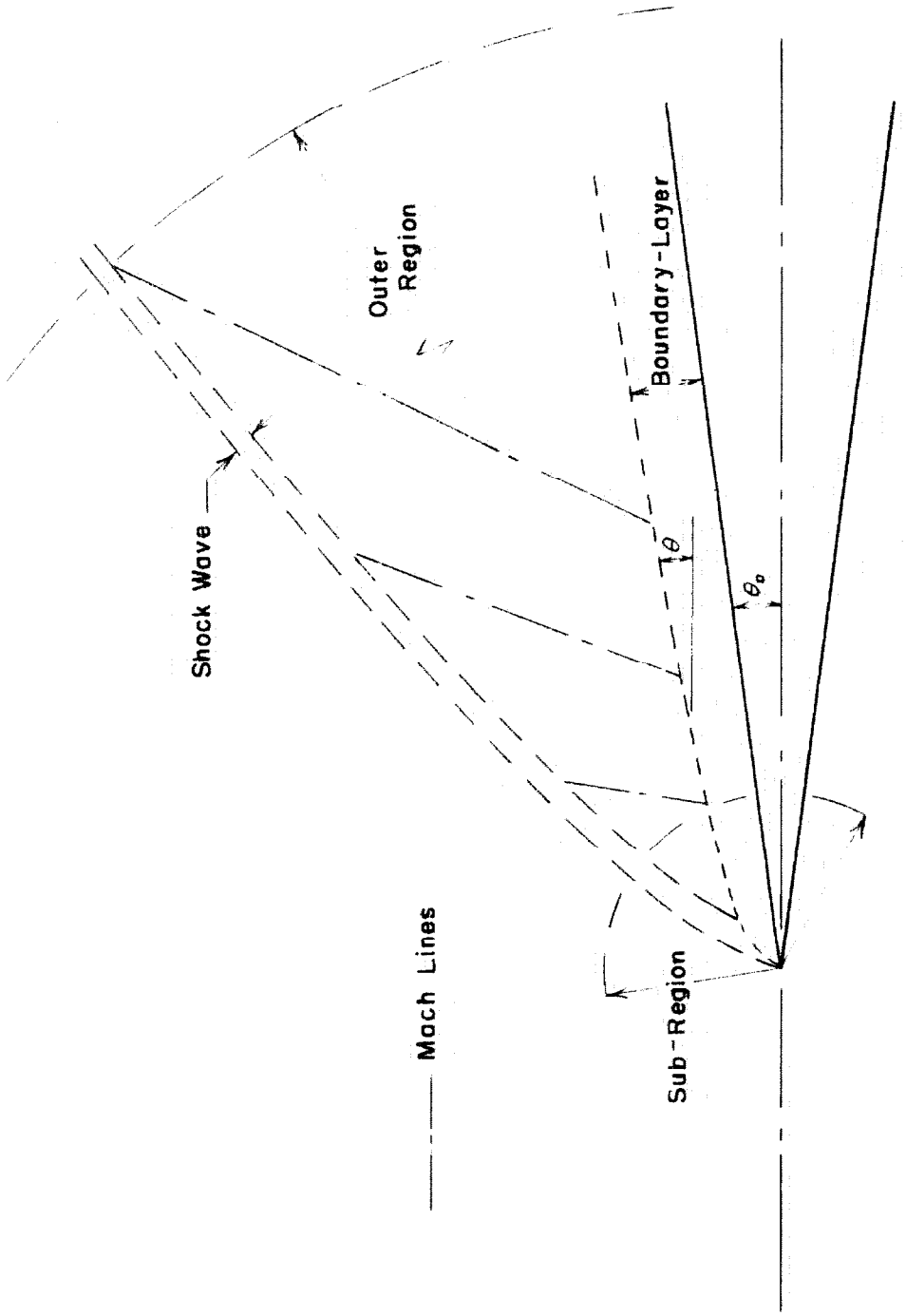
Outer
Region
Boundary-Layer
Shock Wave
θ
θ₀
Mach Lines
Sub-Region

Fig. 12

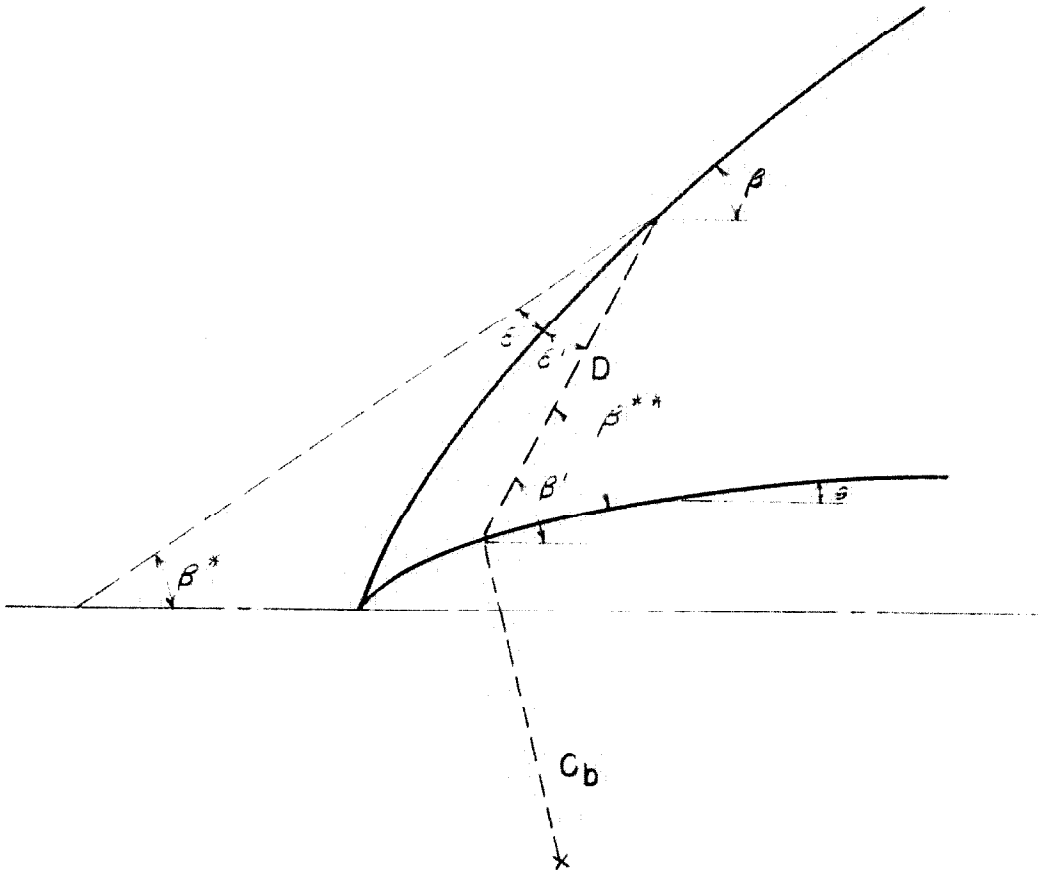

Fig. 13

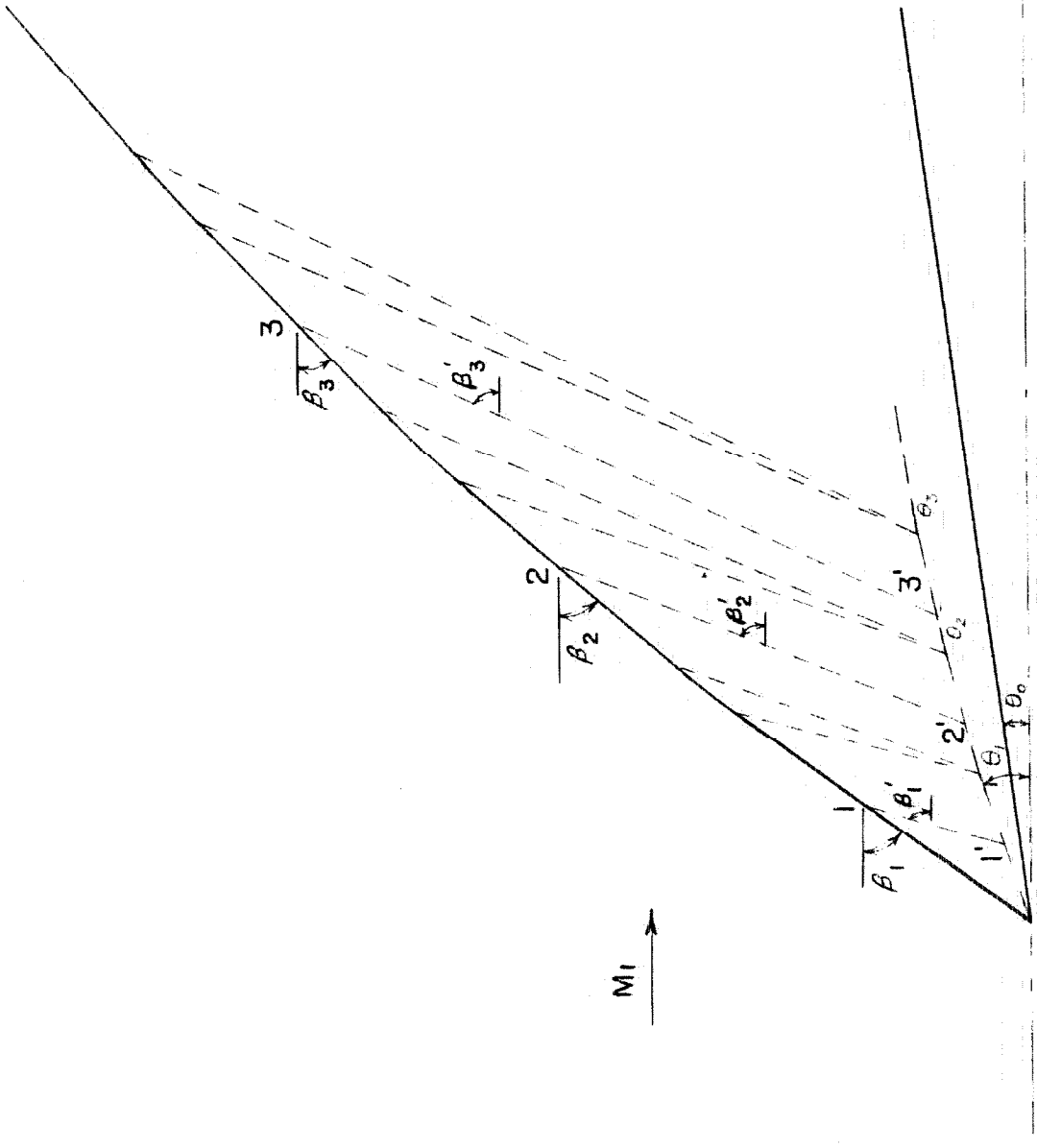
3
β_3
β_3'
2
β_2
β_2'
1
β_1
β_1'
1'
2'
3'
θ_0
θ_1
θ_2
θ_3
M1

Fig. 14

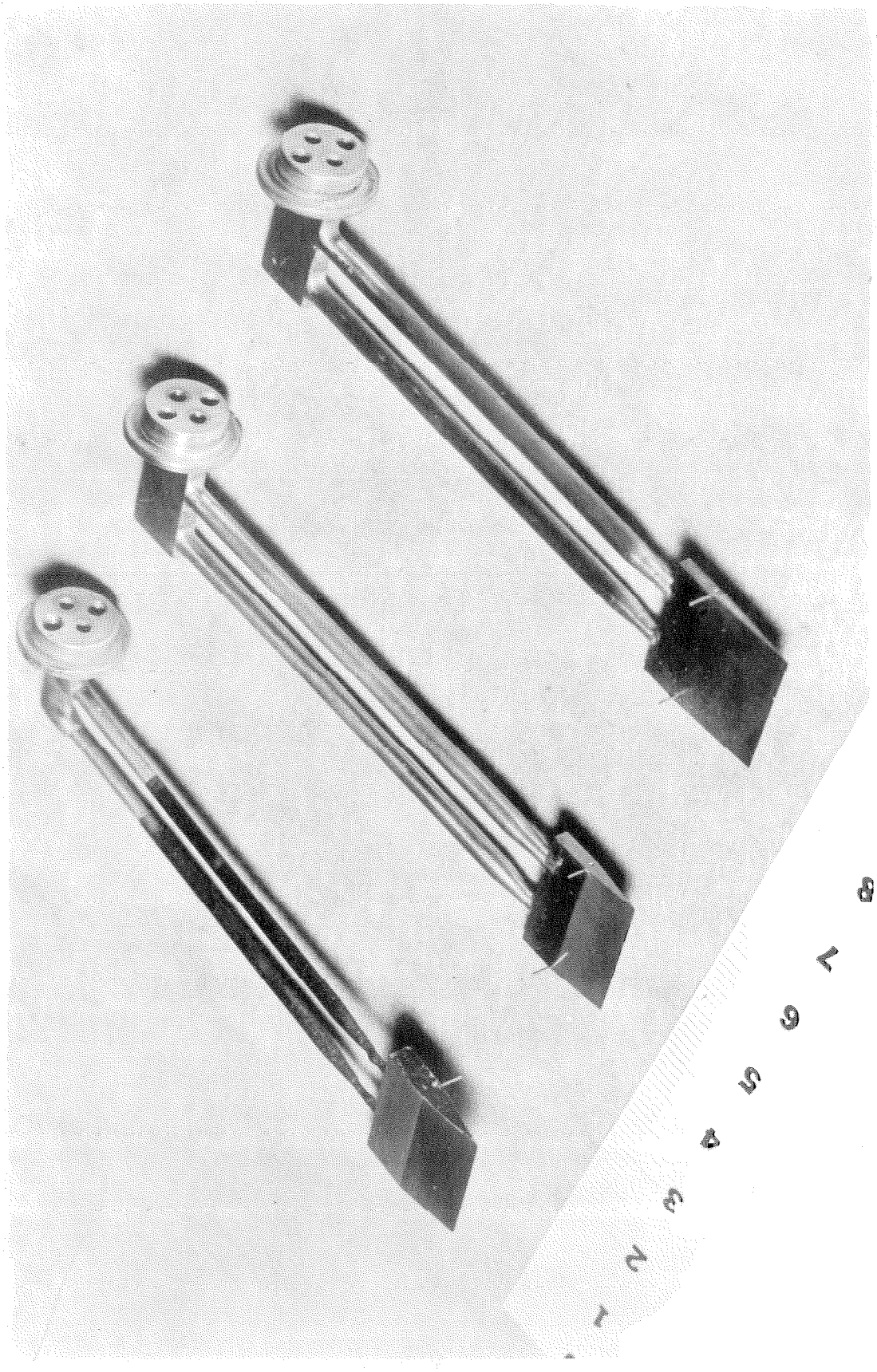

Fig. 15

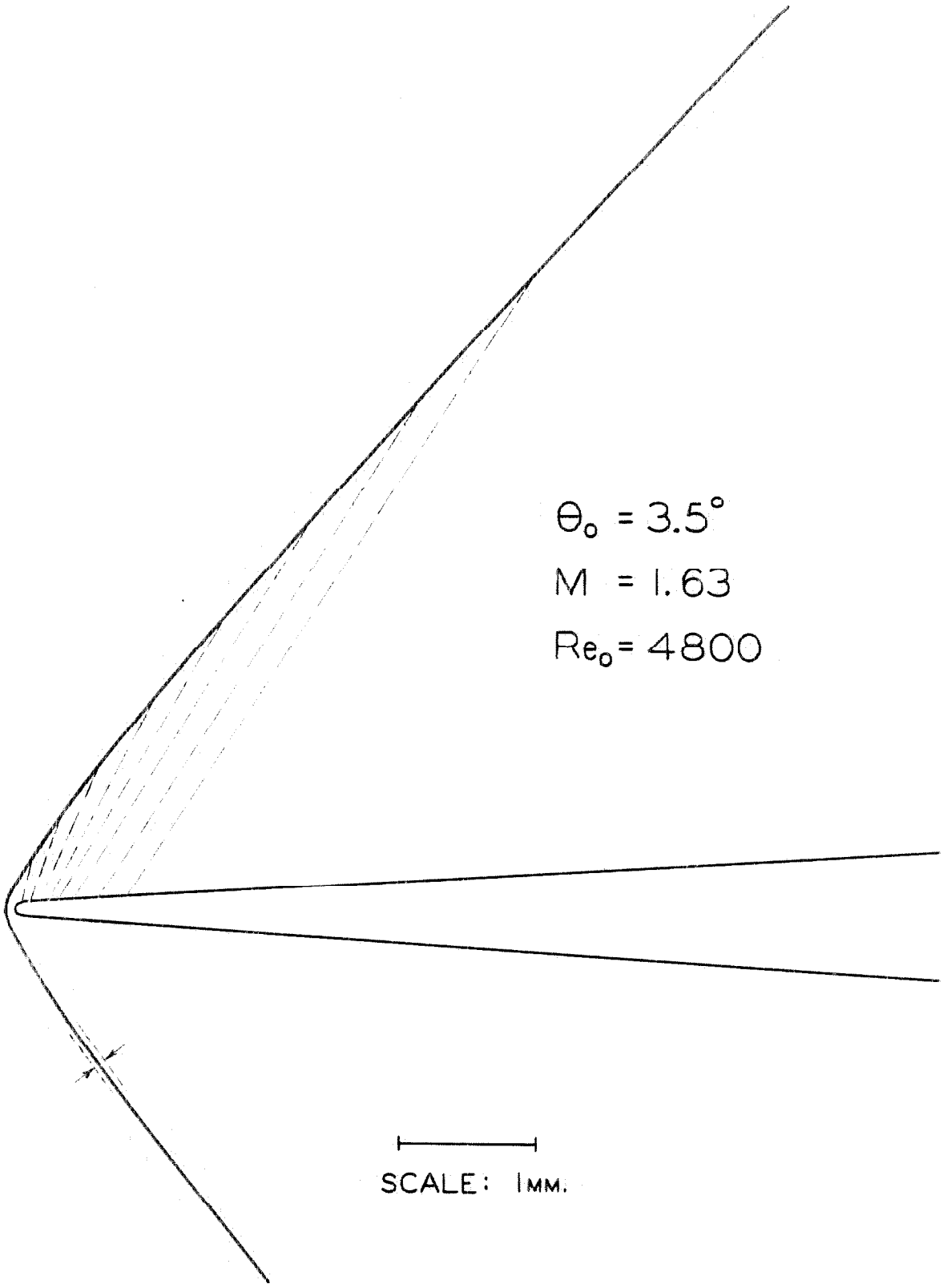

Fig. 16

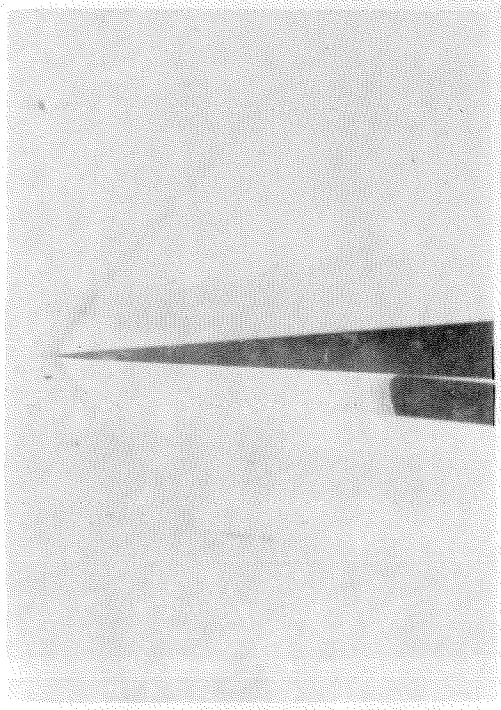

$M_1 = 1.58$
$Re_0 = 5300$

$\theta_0 = 3.5$

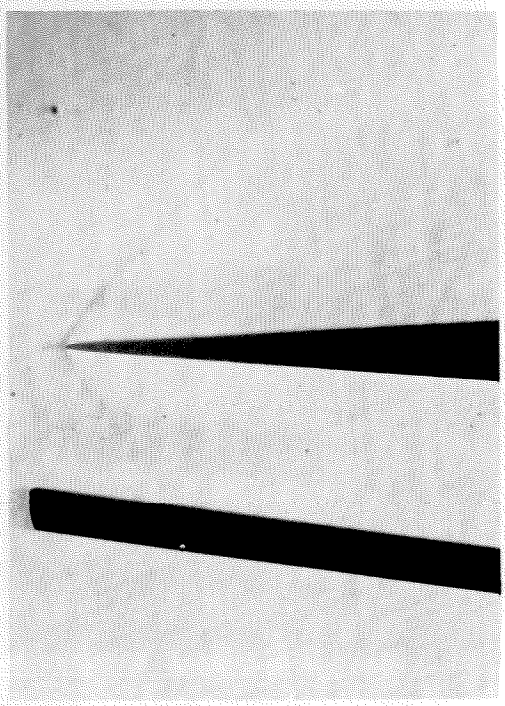

$M_1 = 1.59$
$Re_0 = 4800$

Fig. 17

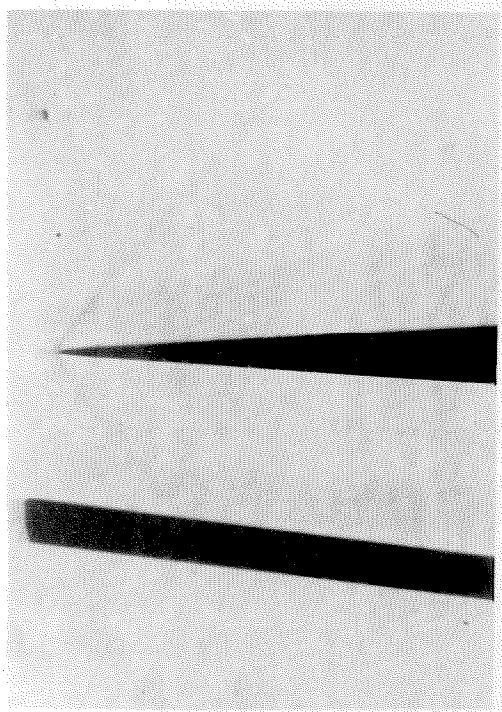

$M_1 = 1.63$
$Re_0 = 4800$

$\theta_0 = 3.5$

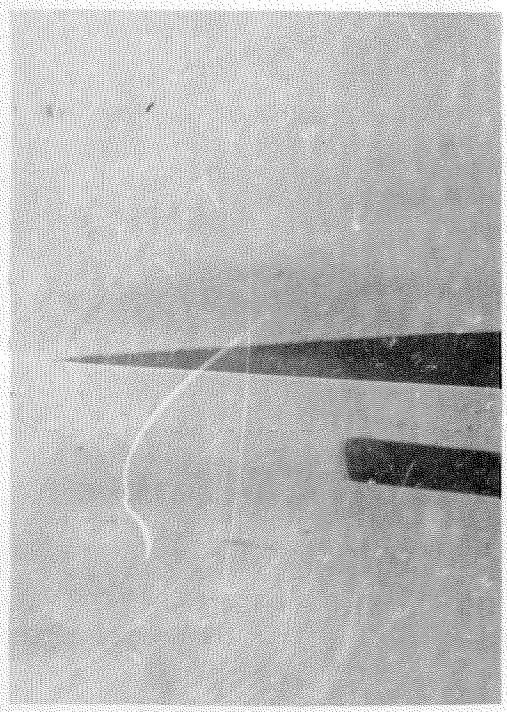

$M_1 = 1.64$
$Re_0 = 5100$

Fig. 18

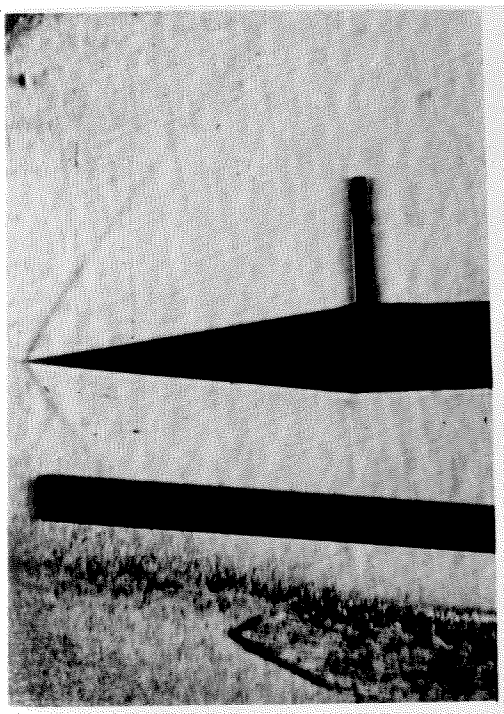

$M_1 = 1.64$
$Re_0 = 4600$

$\theta_0 = 7.3$

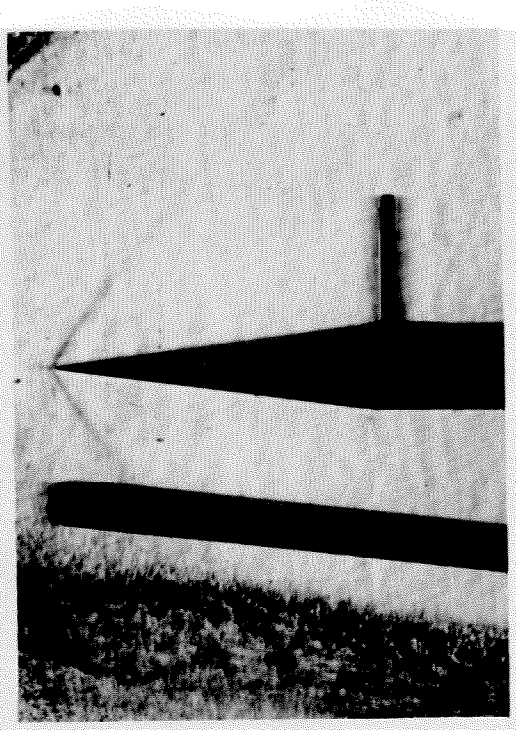

$M_1 = 1.67$
$Re_0 = 4500$

Fig. 19

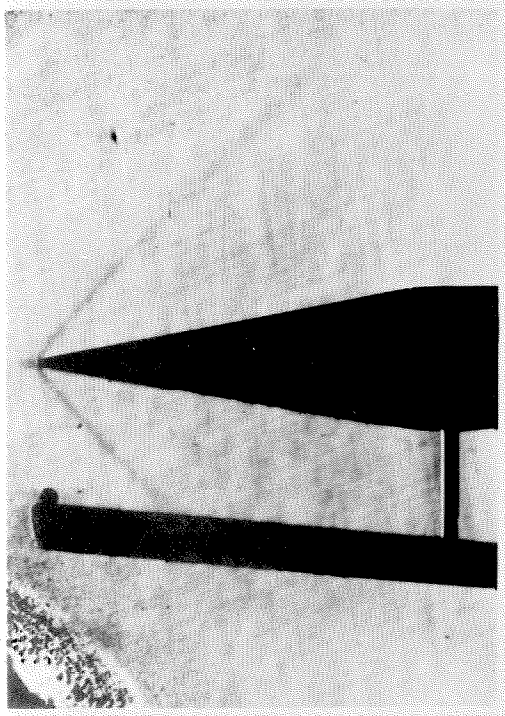

$M_1 = 1.84$
$Re_0 = 5500$

$\theta_0 = 9.9$

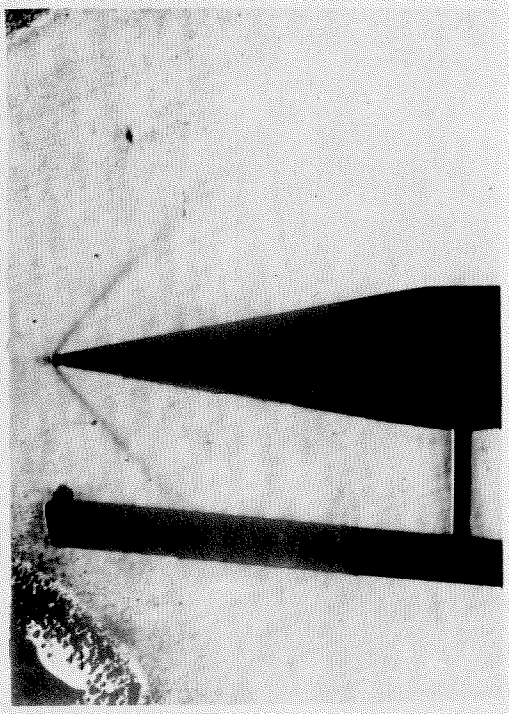

$M_1 = 1.88$
$Re_0 = 5500$

Fig. 20

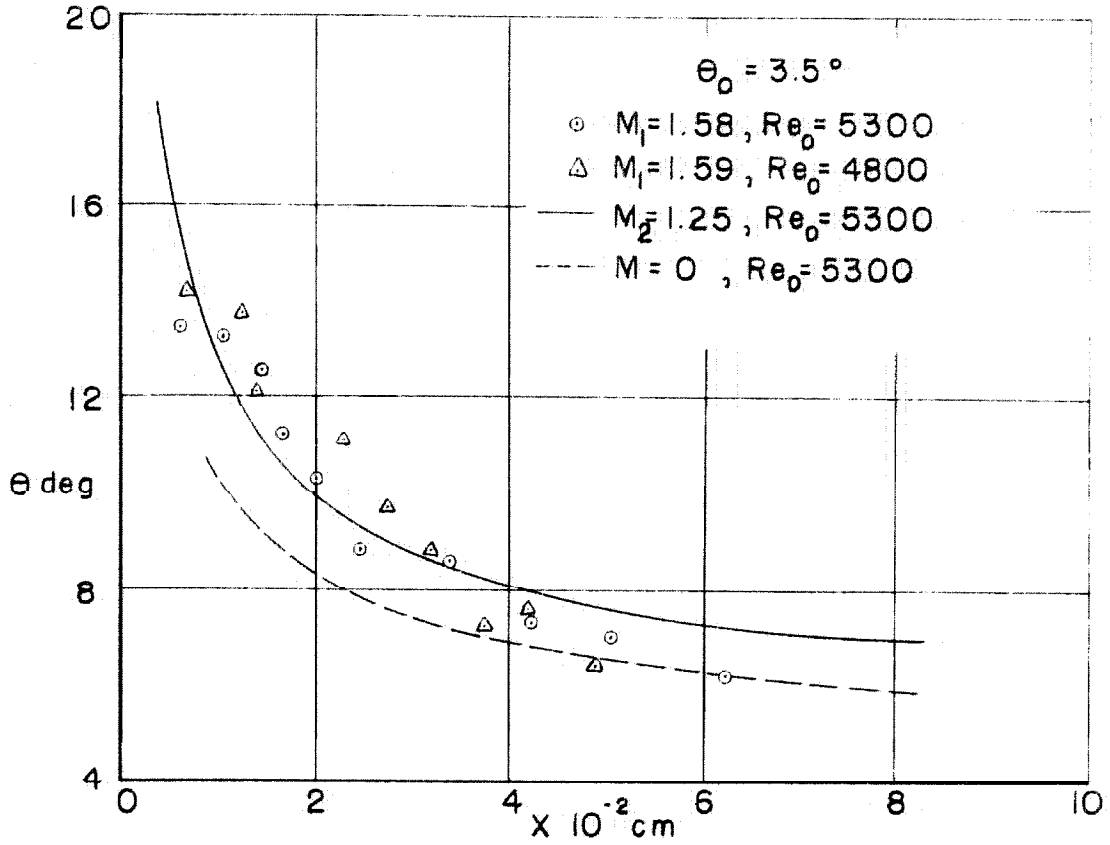
$\theta_0 = 3.5°$
$M_1 = 1.58$, $Re_0 = 5300$
$M_1 = 1.59$, $Re_0 = 4800$
$M_2 = 1.25$, $Re_0 = 5300$
$M = 0$, $Re_0 = 5300$
θ deg
20
16
12
8
4
0
2
4
6
8
10
X 10^{-2} cm

Fig. 21

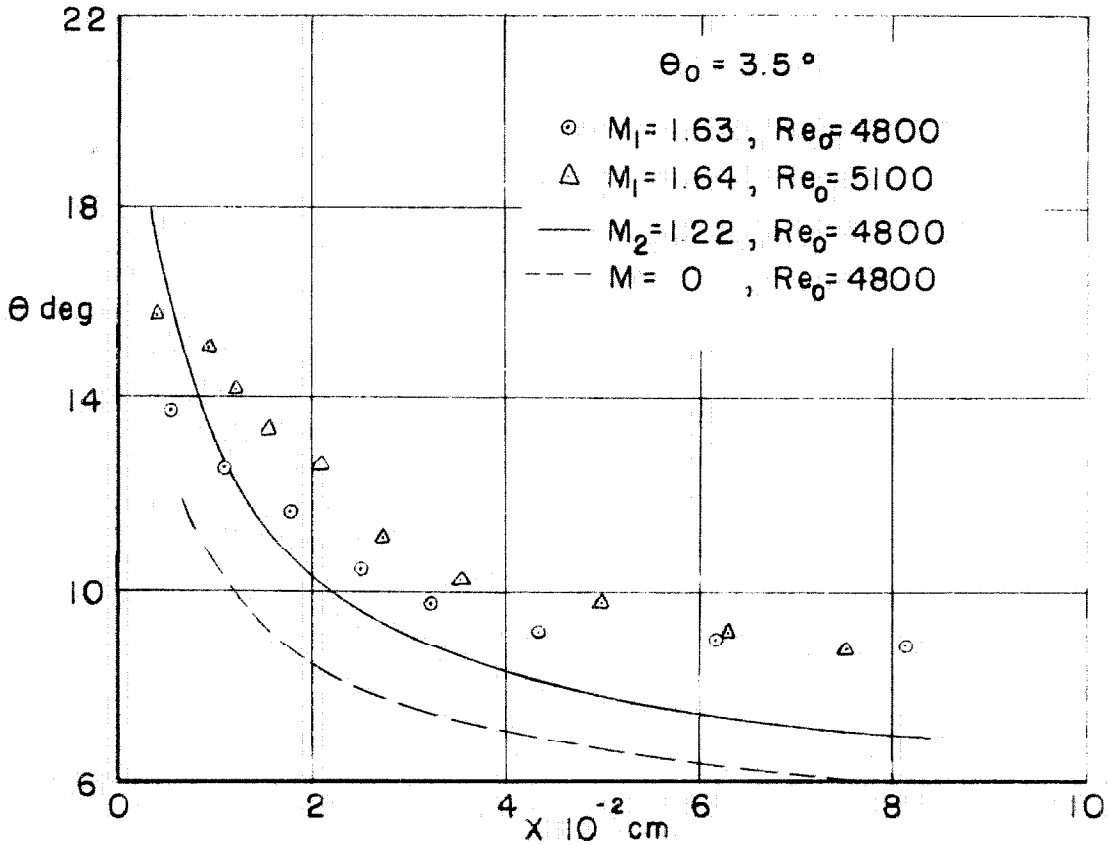
$\theta_0 = 3.5°$
$M_1 = 1.63$, $Re_0 = 4800$
$M_1 = 1.64$, $Re_0 = 5100$
$M_2 = 1.22$, $Re_0 = 4800$
$M = 0$, $Re_0 = 4800$
θ deg
22
18
14
10
6
0
2
4
6
8
10
X 10^{-2} cm

Fig. 22

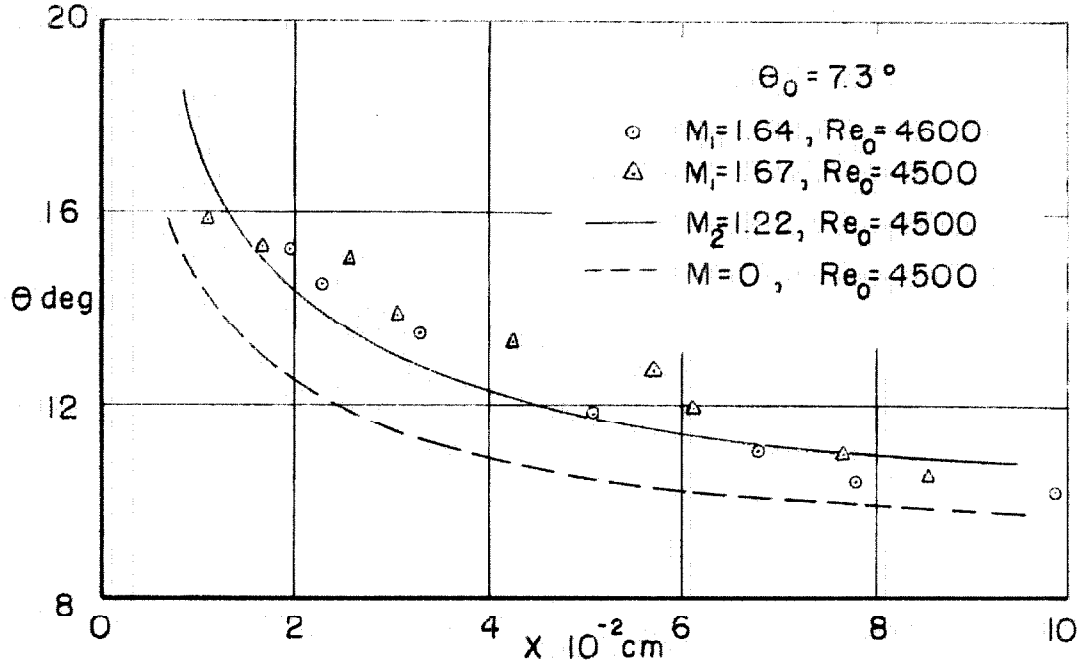
20
16
12
8
θ deg
0
2
4
6
8
10
X 10⁻² cm
θ₀ = 7.3°
M₁ = 1.64, Re₀ = 4600
M₁ = 1.67, Re₀ = 4500
M₂ = 1.22, Re₀ = 4500
M = 0, Re₀ = 4500

Fig. 23

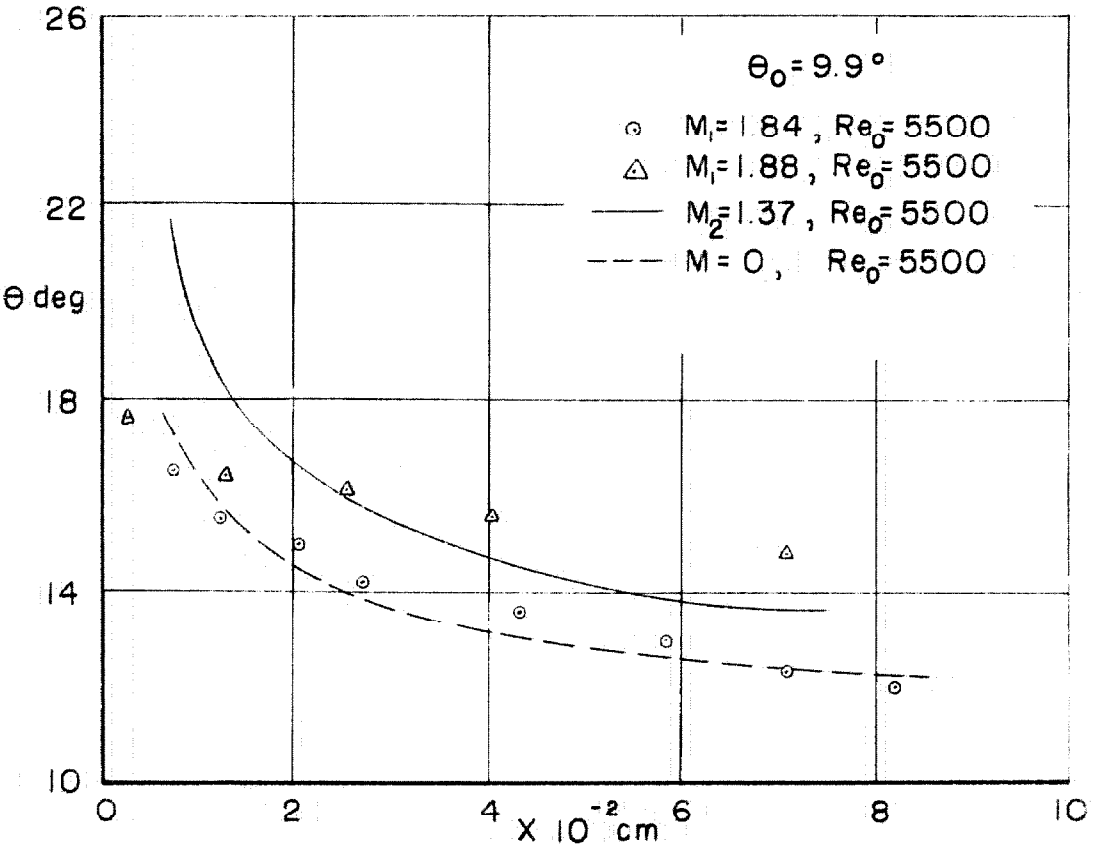
26
22
18
14
10
θ deg
0
2
4
6
8
10
X 10⁻² cm
θ₀ = 9.9°
M₁ = 1.84, Re₀ = 5500
M₁ = 1.88, Re₀ = 5500
M₂ = 1.37, Re₀ = 5500
M = 0, Re₀ = 5500

Fig. 24

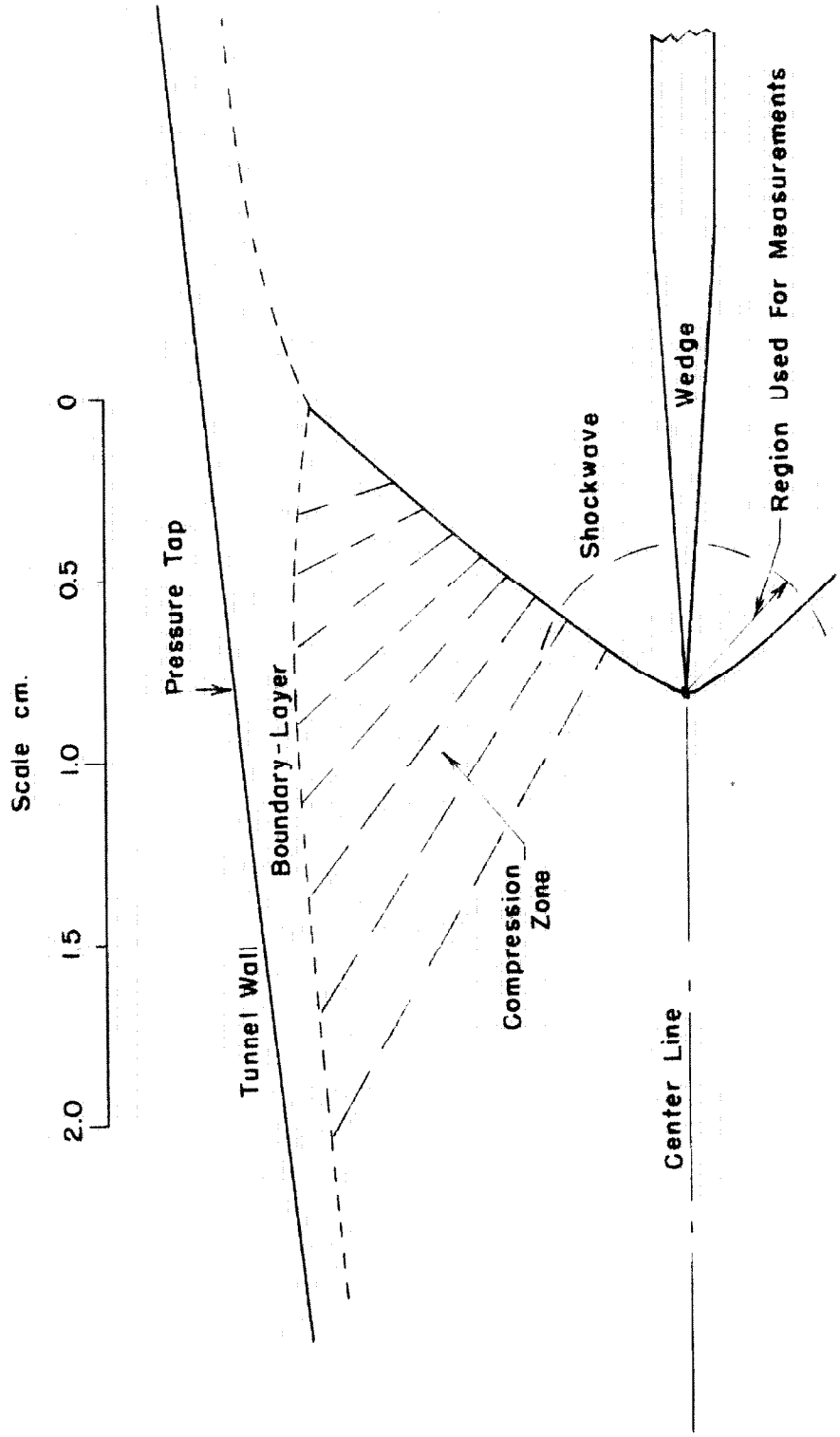
Scale cm.
0
0.5
1.0
1.5
2.0
Pressure Tap
Boundary-Layer
Tunnel Wall
Compression Zone
Shockwave
Wedge
Region Used For Measurements
Center Line

Fig. 25

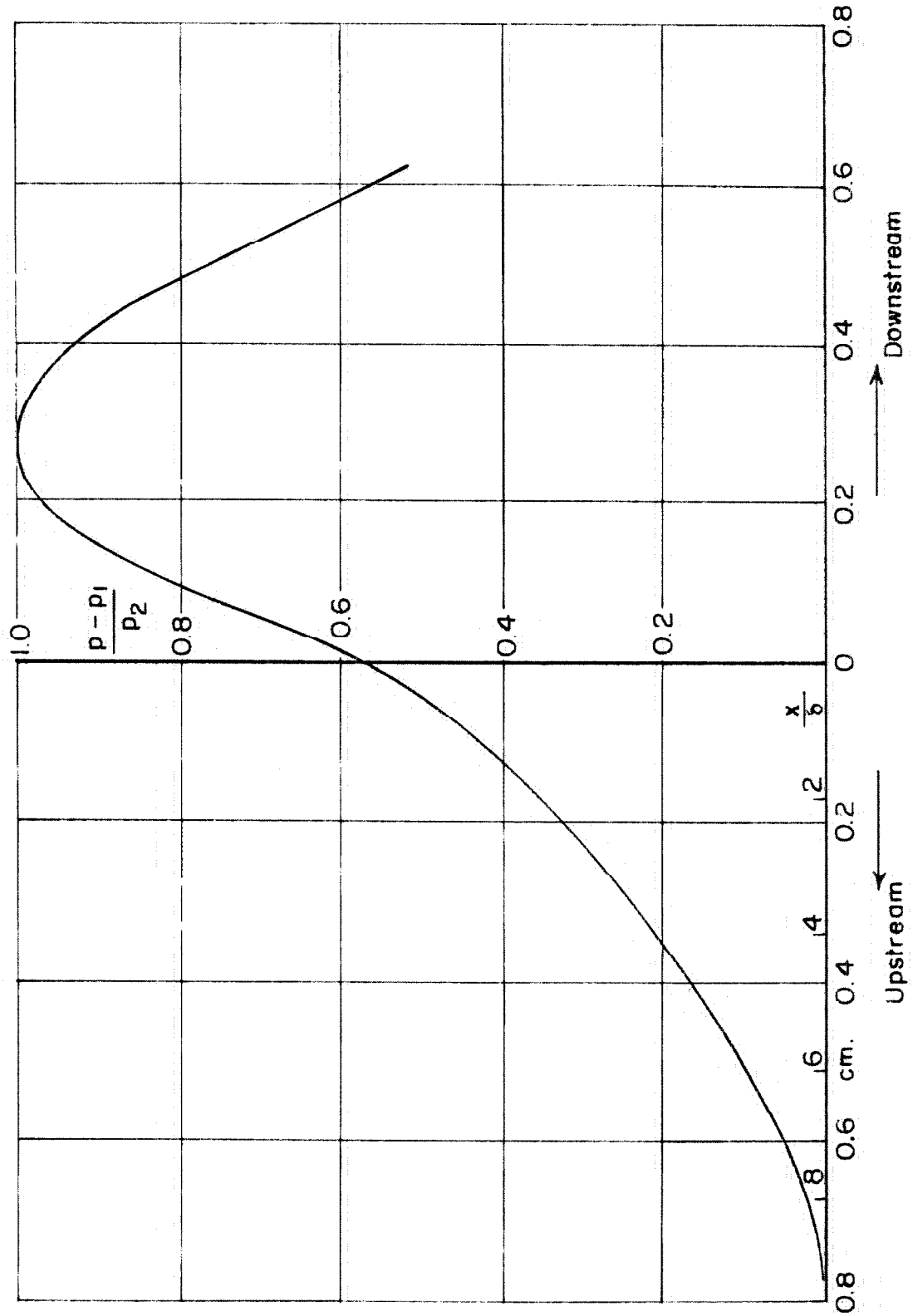
1.0
0.8
0.6
0.4
0.2
0
$\frac{p - p_1}{p_2}$
$\frac{x}{b}$
0.8
0.6
0.4
0.2
0
0.2
0.4
0.6
0.8
cm.
Downstream
Upstream

FIG. 26

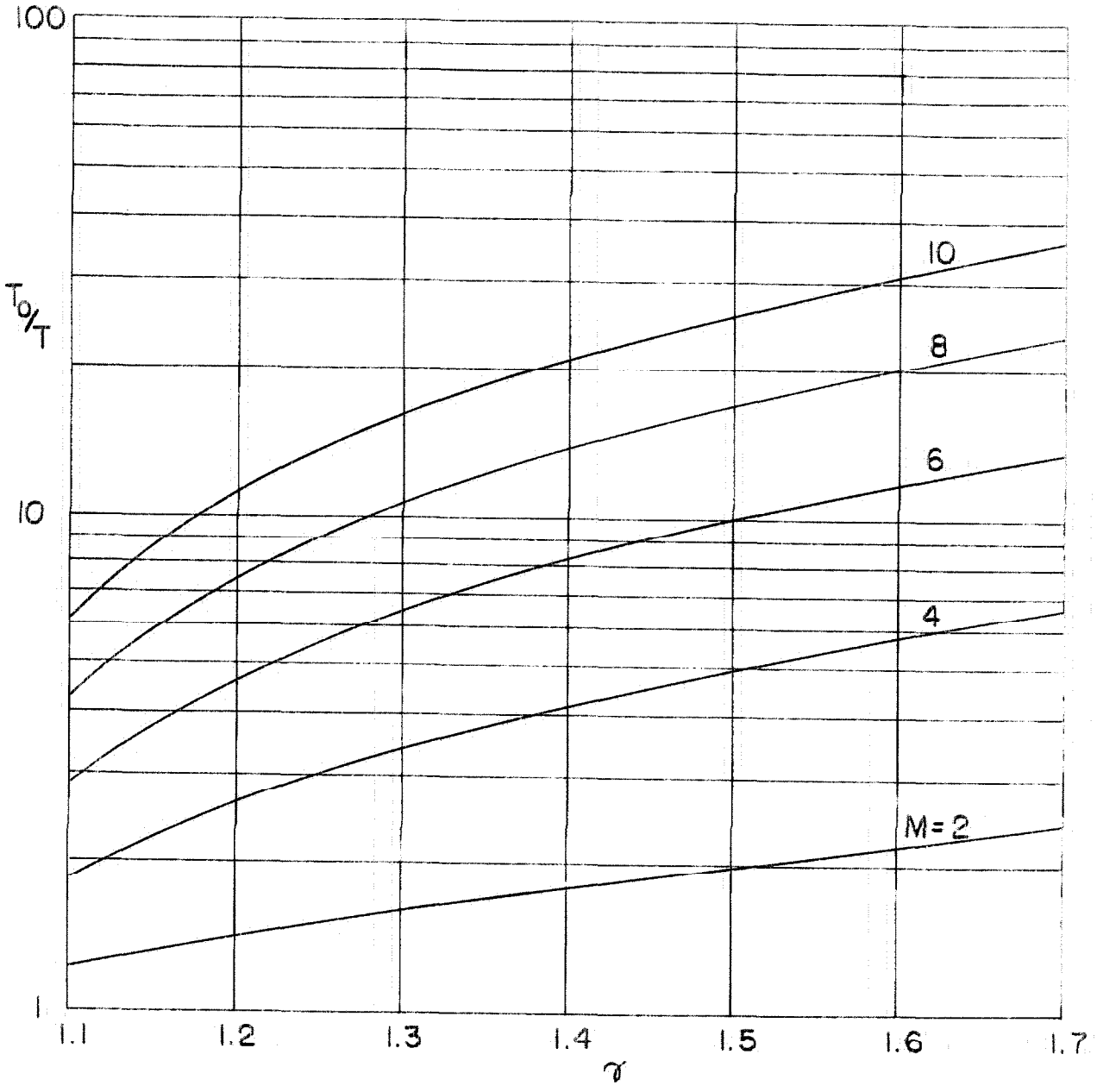

FIG. 27

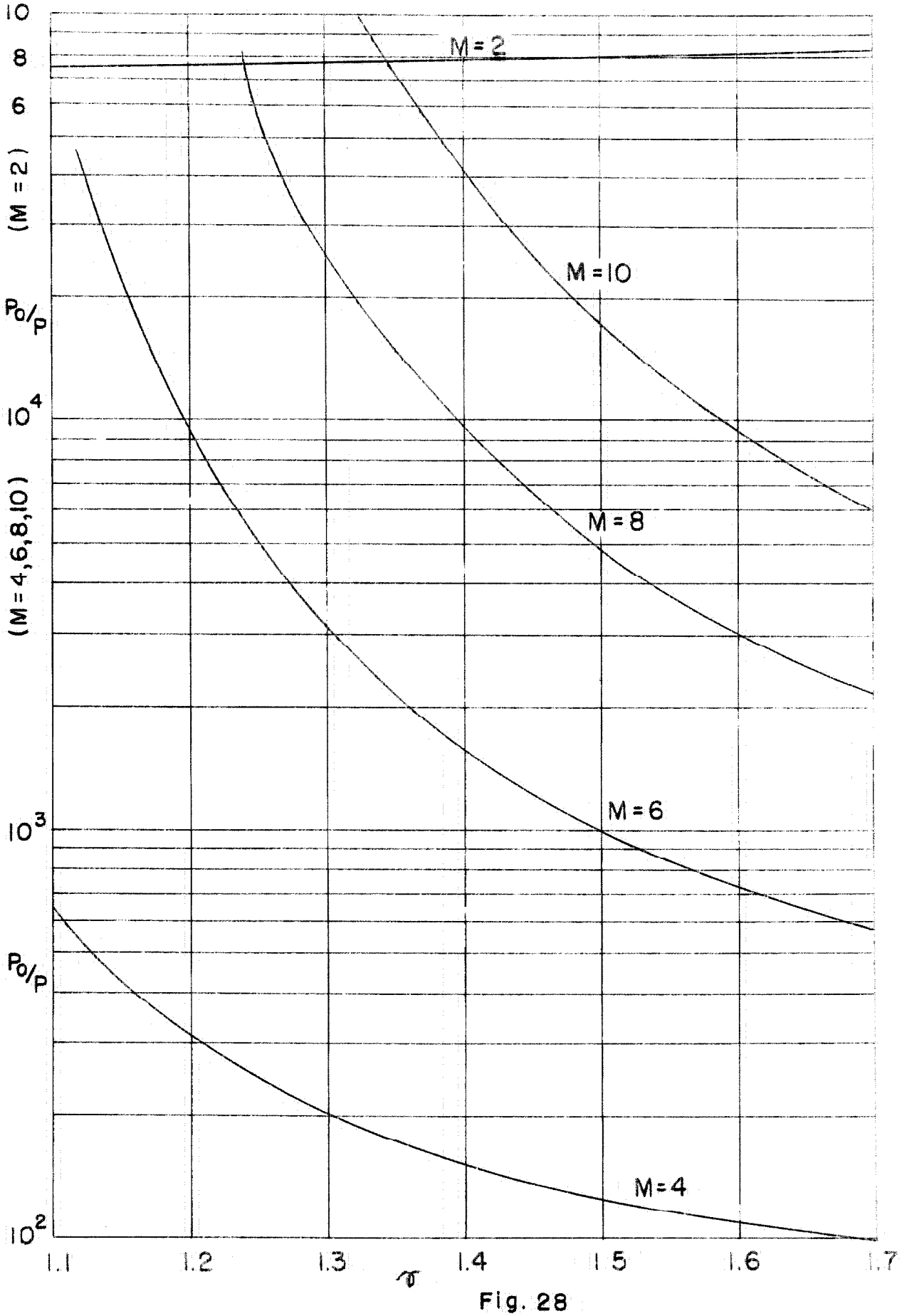
10
8
6
(M = 2)
P_0/P
10^4
(M = 4,6,8,10)
10^3
P_0/P
10^2
M = 2
M = 10
M = 8
M = 6
M = 4
1.1
1.2
1.3
1.4
1.5
1.6
1.7
σ

Fig. 28

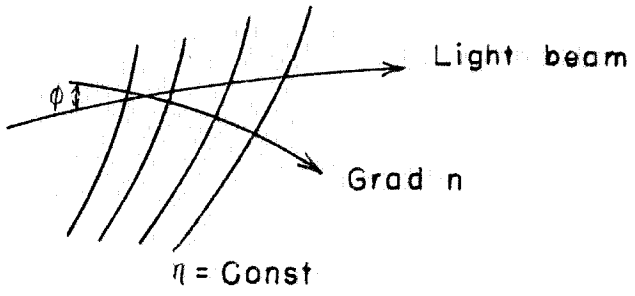

Fig. 29

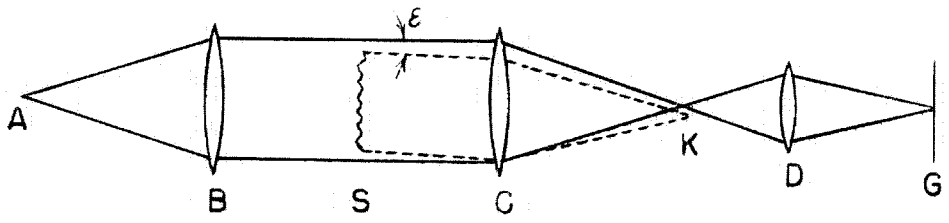

Fig. 30

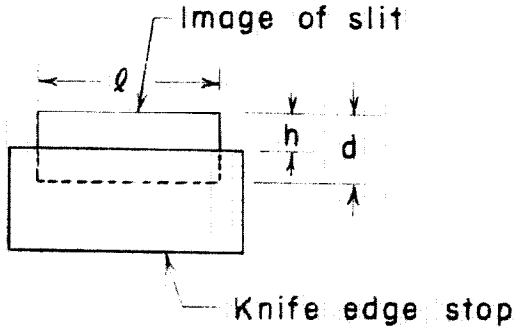

Fig. 31

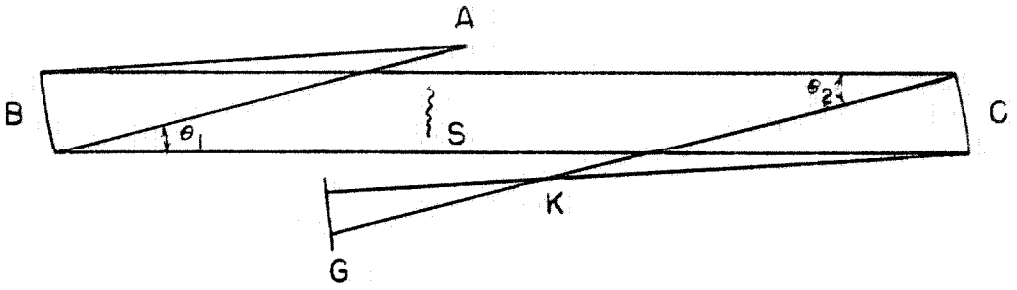

Fig. 32

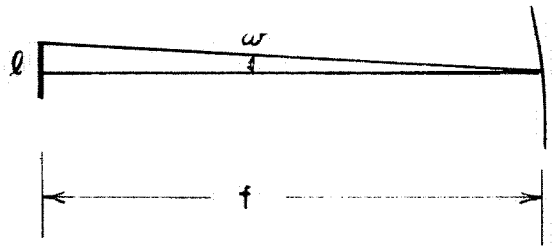

Fig. 33

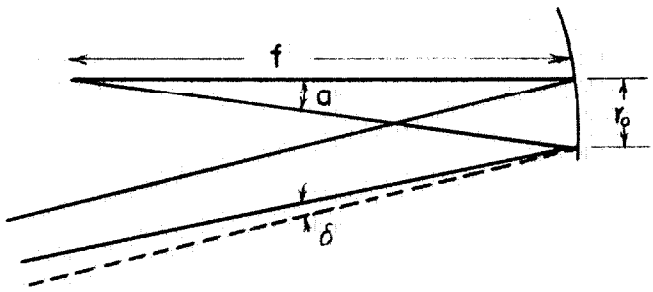

Fig. 34

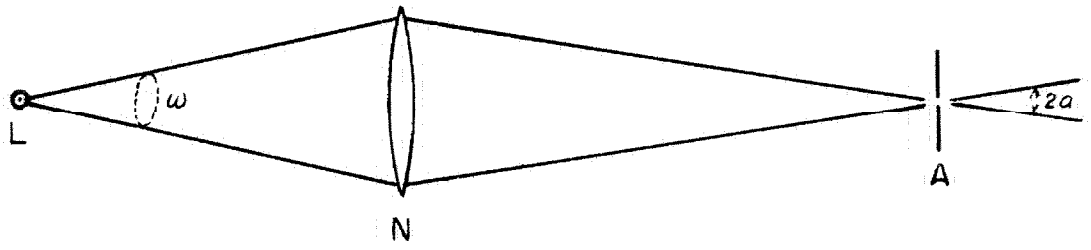

Fig. 35

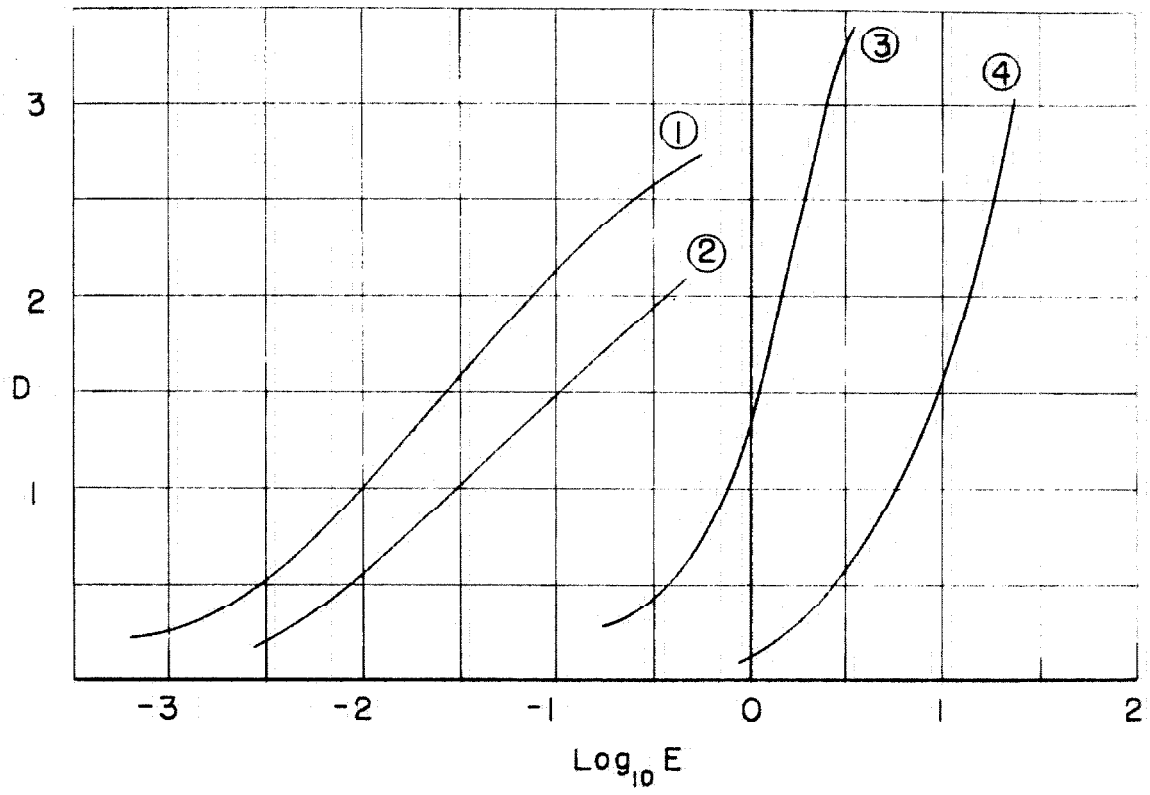

Film Type	Contrast	Resolving Power	Speed	Color Sensitivity
① Super Pan Press	1.1	35	250	Panchromatic
② Super XX	1.2	45	100	Panchromatic
③ Micro File	4.4	175	5	Blue-Green
④ Fine Grain Pos.	3.0	165	0.5	Blue

Film Characteristics (from Kodak Handbook, Ref. 61)

Fig. 36

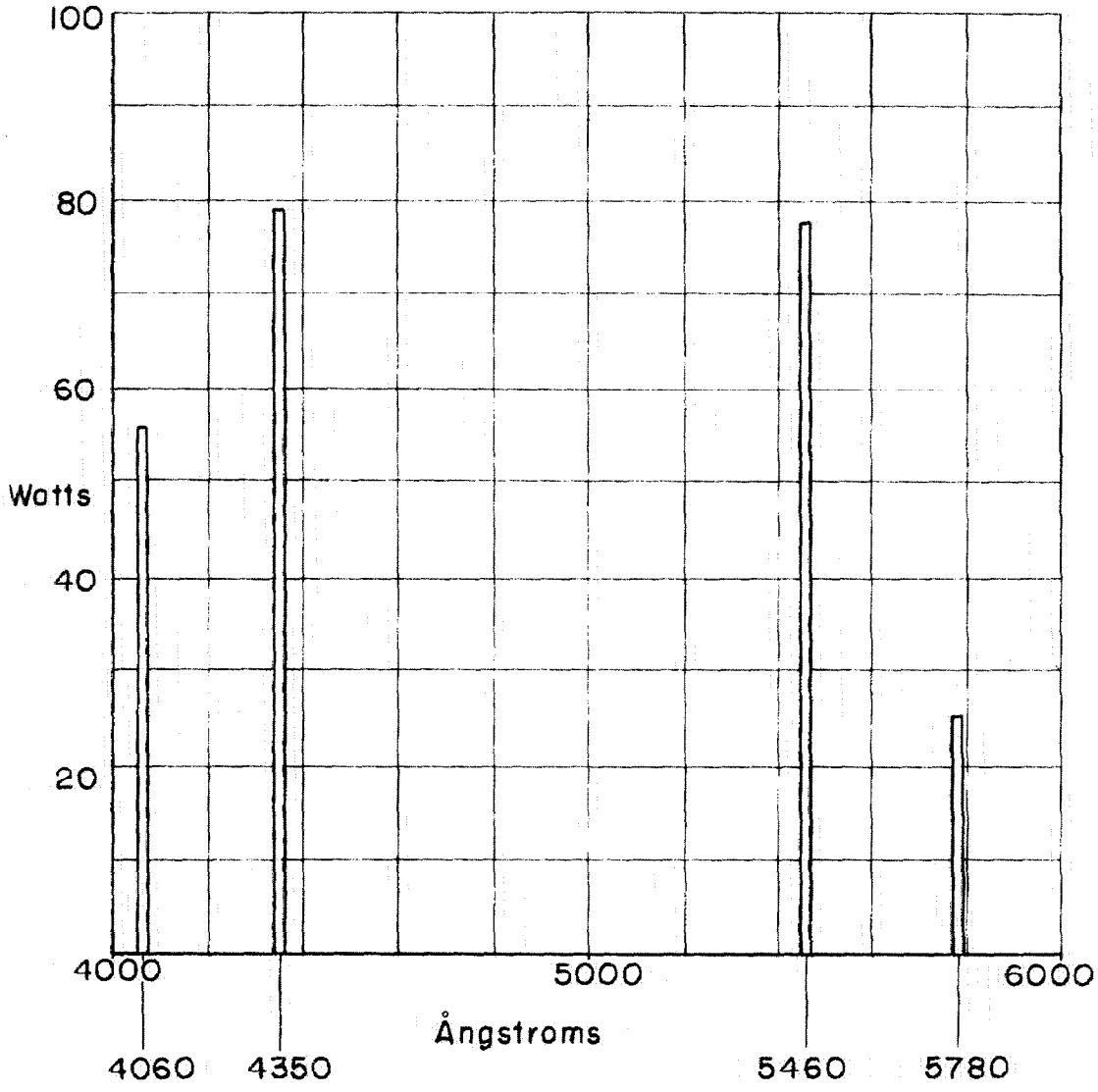

Emission of type BH-6 Mercury Vapor Lamp

Fig. 37

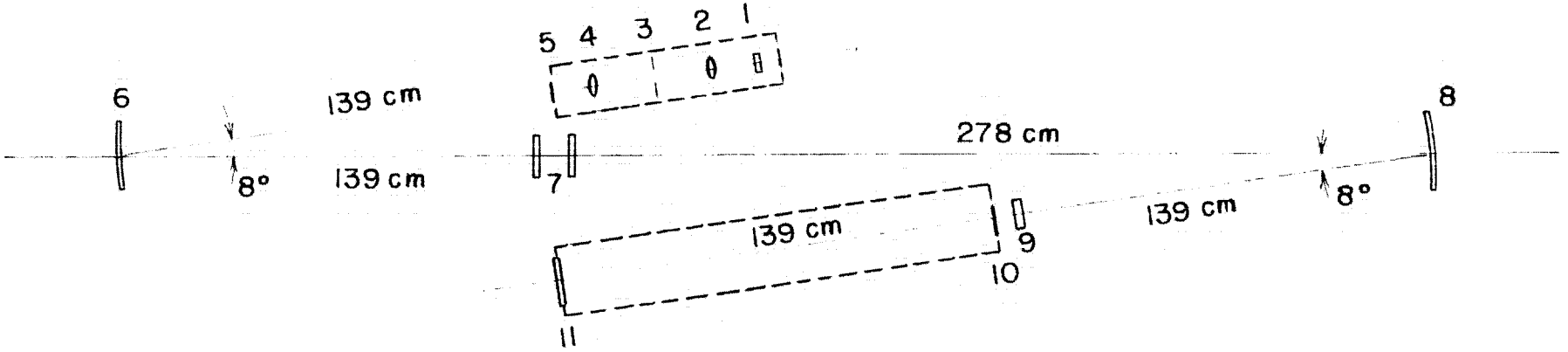

1 BH – 6 lamp

2 Condenser lens f = 6.5 cm

3 Spark gap

4 Condenser lens f = 6.5 cm

5 Adjustable slit

6 Collimating mirror f = 139 cm.

7 Test section of tunnel

8 Focusing mirror, same as 6

9 Shutter

10 Knife edge

11 View screen and film holder

Fig. 38

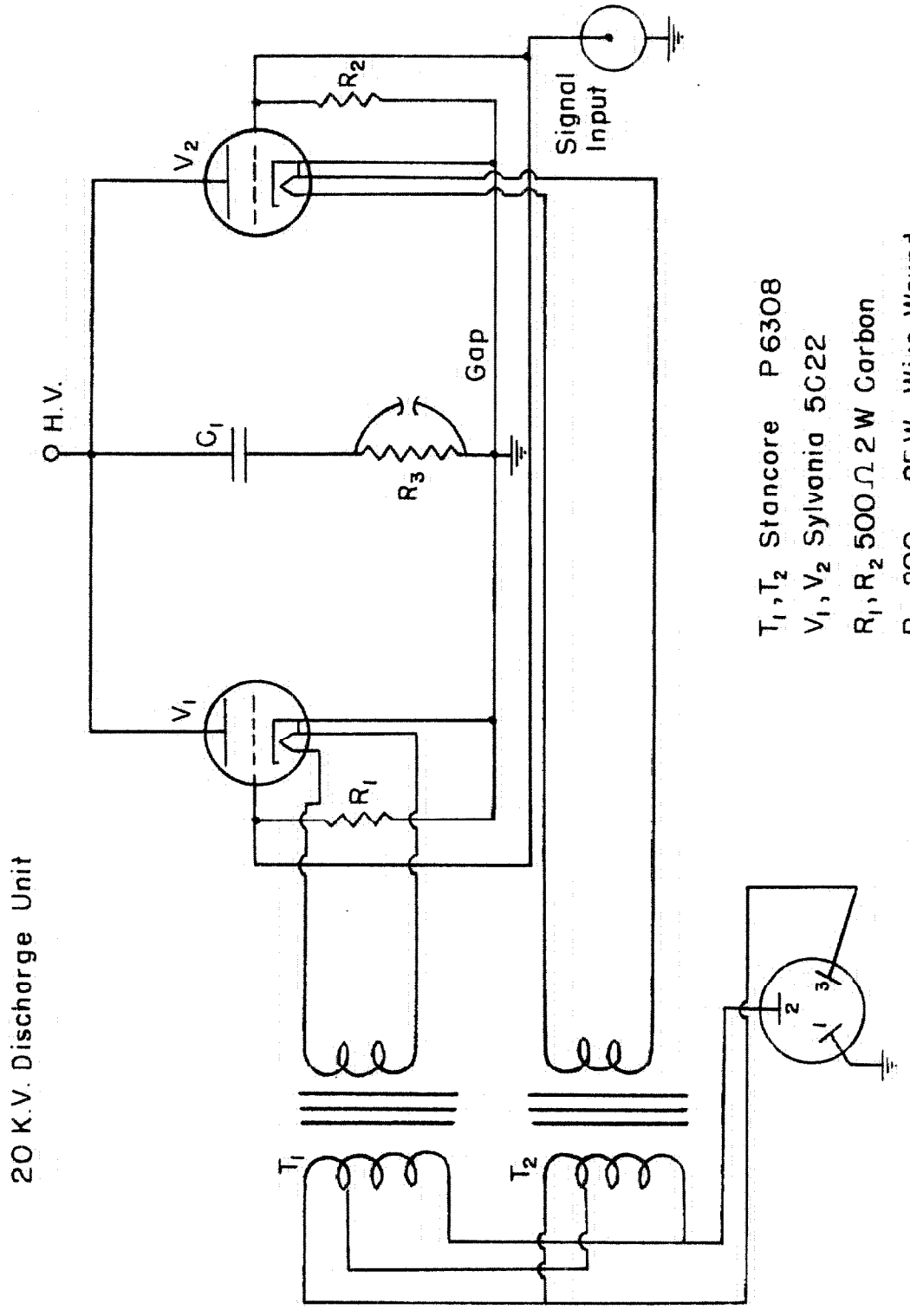

T_1, T_2 Stancore P6308
V_1, V_2 Sylvania 5C22
R_1, R_2 500Ω 2W Carbon
R_3 200 25W Wire Wound
C_1 Cornell Dublier Type T.K. 20002 .25MFD. 20K.V.

Fig. 39